Master’s Thesis

A Study on the Coordination Chemistry of the Lanthanoid Series with Pertechnetates and the Separation of ^{147}Pm from its Decay Product ^{147}Sm

Faculty of Mathematics and Natural Sciences
University of Cologne

Supervisors: PD Dr. Erik Strub
Prof. Dr. Matthias S. Wickleder

Submitted by:
Clarence Shanbei Yong

Cologne, July 2024

Eidesstattliche Erklärung

Hiermit versichere ich, Clarence Shanbei Yong, an Eides statt, dass ich die vorliegende Arbeit mit dem Thema

"A Study on the Coordination Chemistry of the Lanthanoid Series with Pertechnetates and the Separation of ^{147}Pm from its Decay Product ^{147}Sm"

selbstständig und ohne die Benutzung anderer als der angegebenen Hilfsmittel angefertigt habe.

Alle Stellen, die wörtlich oder sinngemäß aus veröffentlichten oder nicht veröffentlichten Schriften entnommen wurden, sind als solche kenntlich gemacht.
Die Arbeit ist in gleicher oder ähnlicher Form oder auszugsweise im Rahmen einer anderen Prüfung noch nicht vorgelegt worden.
Ich versichere, dass die eingereichte elektronische Fassung der eingereichten Druckfassung vollständig entspricht.

Köln, 22.07.2024______________
(Ort, Datum)

____
(Unterschrift)

Acknowledgement

Before all else, I would like to thank PD Dr. *E. Strub* for supervising and giving me the precious opportunity to work on this extraordinary topic during my research here at the university. His unwavering support has been instrumental in the completion of this thesis. I thank Prof. Dr. *M. Wickleder* for generously agreeing to take on the second appraisal, as well as sharing his invaluable knowledge and insight on the topic.

The completion of this thesis is the culmination of efforts from various individuals who in one way or another contributed and extended their valuable assistance, whom I like to express my sincerest appreciation. In particular, I would like to thank *Dennis Grödler* and Dr. *Markus Zegke* for introducing me to this technetium group, as well as helping me to analyse XRD data and taking the time to proofread this work. I would also like to give special thanks and recognition to *Lisa Dünnebier* for helping me in the difficult task of purifying and studying promethium. Further thanks extend to *Daniele Zaratti*, *Sonja Bazhenova* and *Simon Obrusnik* for assisting me in literature review, synthesis and crystallisation throughout this research. I thank *Dominik Elchine* for helping me with LSC measurements. A huge thanks goes to the rest of the working group for their warm welcome and sharing their expertise and time.

I would also like to thank PD Dr. *F. Wombacher*, Dr. *E. Hasenstab* and *Timo Lange* at the Institute of Geology and Mineralogy for their advice on lanthanoid separation and for measuring ICP-MS. I thank Dr. *J. Bruns* for helping me in describing solid state chemistry.

The team at Helmholtz-Zentrum Dresden-Rossendorf has kindly helped me in this collaborative effort to study promethium. I thank Dr. *N. Mayordomo-Herranz,* Dr. *R. Gericke* and *Stephan Weiß* for their help in organising my stay in HZDR, and analysing XRD data.

Finally and above all, I thank my family for their continuous support in spurring me on to research in this field of studies.

"Acknowledging the limitations of our knowledge is the first step towards true understanding and innovation." – Otto Hahn

Abbreviations

a	activity
A	mass number
α	alpha
Å	Ångström
β	beta
Bq	Becquerel
°C	degree Celsius
CCDC	Cambridge Crystallographic Database Centre
cpm	counts per minute
cps	counts per second
d	days
eV	electronvolt
g	gram
γ	gamma
h	hours
HDEHP	di(2-ethylhexyl)phosphoric acid
ICP-MS	inductively coupled plasma mass spectroscopy
IE	ionisation energies
J	joule
K	Kelvin
Ln	lanthanoid
LSC	liquid scintillation counting
λ	wavelength
µg	microgram
µL	microlitre
µmol	micromole
mg	milligram
mL	millilitre
mM	millimolar
mmol	millimole
M	molar
N	neutron number
ppm	parts per million
REE	rare-earth elements
rt	room temperature
$\mathbf{t_{1/2}}$	half-life
SC-XRD	single crystal X-ray diffraction (analysis)
UV	ultraviolet
Vis	visible
y	years
Z	atomic number

Tables of Contents

Abstract

Technetium-99 (^{99}Tc) is a long-lived ($t_{1/2}$ = 2.14·10^{5} y) fission product and is a major component of nuclear waste. Its most common form is the pertechnetate anion TcO_4^-, which is water-soluble and able to migrate readily into the environment. While little has been known regarding pertechnetates, recent achievements in obtaining $HTcO_4$ from NH_4TcO_4 *via* an acid cation exchange have now allowed facile synthesis of pertechnetate salts, allowing further studies on the pertechnetates. Investigating pertechnetate salts enables a better understanding of its solution chemistry and its solid state structure, and may point at strategies of its immobilisation or chemical modification for long-term storage. Like ^{99}Tc, promethium-147 (^{147}Pm) is also a fission product and is a component in nuclear waste. The decay of ^{147}Pm to ^{147}Sm requires purification and this difficulty in purification in addition to its radioactivity and short half-life ($t_{1/2}$= 2.62 y) have led to very few studies on this element.

In this work, by reacting lanthanoids with pertechnetic acid, lanthanoid pertechnetates were synthesised and structurally characterised *via* single crystal X-ray diffraction (SC-XRD). This data allowed the systematic study of the lanthanoid series' coordination geometry around the metal centre with pertechnetato ligands, their coordination number and degree of hydration. Comparisons between the lanthanoid pertechnetates and known lanthanoid perrhenates confirm their similarities as well as subtle differences. Further, a replicable miniaturised gravimetric lanthanoid separation column was successfully engineered and enabled the effective purification of ^{147}Pm from its decay product ^{147}Sm.

1. Introduction

1.1 Technetium and its Radioactivity

Technetium (Tc), a transitional metal element in the fifth period with atomic number 43, is the lightest element with no stable isotopes. Its history begins in 1869 when Mendeleev arranged the approximately 60 elements, known at the time, into the first periodic table of elements. He was able to predict the existence and likely properties of the elements that had yet to be discovered.[1] One of his predictions was the element of technetium, then named eka-manganese, which filled the gap underneath manganese with a predicted atomic weight of 100 and was expected to have similar chemical properties. In 1913, British physicist Henry Moseley used an X-ray spectrometer to measure the X-ray spectra of chemical elements.[2] In his observation, he discovered that there was a relationship between the wavelengths of the X-rays produced and the atomic numbers of the elements that were measured. This relationship, Moseley's law, is the foundation of the concept of atomic numbers. He helped predict the missing element for $Z = 43$.[2] The discovery of element 43 was made with the invention of the cyclotron by Ernest Lawrence in Berkeley, California. The cyclotron facilitated the synthesis of new elements and isotopes by bombarding targets with high-energy charged particles.[3] In collaboration, Emilio Segrè and Carlo Perrier took the irradiated molybdenum foil from Lawrence and isolated element $Z = 43$.[4] The new element was chemically similar to manganese, and even chemically closer to rhenium.[5] The element was later named technetium from the Greek word for artificial (τεχνητοζ).[6]

Isotopes from ^{85}Tc to ^{120}Tc are known, where the most stable isotopes are ^{97}Tc ($t_{1/2} = 4.2 \times 10^6$ years), ^{98}Tc ($t_{1/2} = 4.2 \times 10^6$ years), and ^{99}Tc ($t_{1/2} = 2.1 \times 10^5$ years). Though commonly referred to as an artificial element, Tc is naturally occurring; yet it is formed in ultra-trace quantities from the spontaneous fission of natural ^{238}U.[7] Almost all of the technetium that exists on Earth is a result of nuclear energy production in uranium-fuelled reactors and of atomic bomb tests. Because of the relatively high fission yield of 6%, ^{99}Tc is obtained almost exclusively from uranium fission products.[8] Approximately 2.5 g of ^{99}Tc are produced from uranium-fuelled reactor for every 100 MW of thermal energy released per day.[9]

Technetium's radioactivity is due to the fact that Tc has an odd Z of 43, therefore, it is unable to take an odd N to achieve a stable even A. This is because the odd Z and odd N configuration is not favourable and found only in elements with low atomic numbers (i.e., ^{2}H, ^{6}Li, ^{10}B and ^{14}N). Therefore, technetium would have to take an odd Z and even N configuration, narrowing down the isotopes to ^{97}Tc and ^{99}Tc.[10] Yet both are not stable.[7]

Mattauch's isobar rule can provide insights into why technetium lacks stable isotopes. The empirical isobar rule states that two adjacent isobars cannot both be stable.[11] Therefore, for ^{97}Tc and ^{99}Tc isotopes to be stable, adjacent molybdenum and ruthenium must lack stable isotopes with identical atomic mass numbers. However, Mo and Ru possess six and seven isotopes respectively, from A = 92 to A = 104. Even though ^{100}Mo is radioactive, it has a longer half-life of 7.3×10^{18} years and decays by double β- decay, which is "almost" a stable isotope. Moreover, consecutive stable isotopes of molybdenum and ruthenium above and below technetium indicate that the isotopes ^{97}Tc and ^{99}Tc cannot be stable in accordance with Mattauch's rule as depicted in Figure 1.[7,11,12]

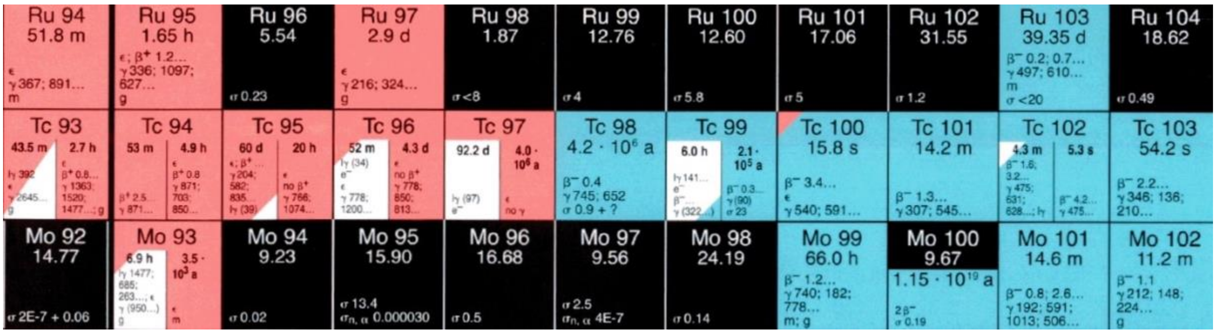

Figure 1: An excerpt of the Karlsruhe Nuclide Chart, showing a plot of proton number (Z) against neutron number (N) of isotopes of Mo (Z = 42), Tc (Z = 43) and Ru (Z = 44). Stable or very long-lived (i.e., ^{100}Mo) isotopes are shaded in black.[7,11,12]

A quantitative way to explain the radioactivity of technetium is by discussing its binding energy. Binding energy, or mass excess, is the amount of energy required to dissociate the nucleus into its constituent nucleons. Stable isotopes will occupy the lowest possible energy state while unstable isotopes undergoing radioactive decay to reach this minimum.[7] Unstable neutron-rich nuclides will β^- decay and unstable proton-rich nuclides will β^+ decay or electron capture to reach the stable lower-energy nuclide. Table 1 lists the mass excess values for molybdenum, technetium, and ruthenium isotopes with A = 97–101, with the most stable nuclei (lowest mass excess, i.e., largest binding energy), highlighted in bold. For A = 97, the stable nuclide is ^{97}Mo, and for A = 99, the stable nuclide is ^{99}Ru. For A = 98, while ^{98}Tc is unstable to both β^- decay and β^+ decay or electron capture, ^{98}Tc is only reported to β^- decay to ^{98}Ru with no observable β^+ decay to ^{98}Mo yet.[13] It can also be inferred that ^{97}Tc and ^{99}Tc are relatively more stable than ^{98}Tc. In conclusion, the absence of stable technetium isotopes is due to the relative stability of the neighbouring elements.

Table 1: Mass excess values for molybdenum, technetium, and ruthenium isotopes. The most stable nuclei, indicated by the lowest mass excess or largest binding energy, are highlighted in bold.[7]

Atomic Weight, A	$_{42}Mo$, MeV	$_{43}Tc$, MeV	$_{44}Ru$, MeV
97	**–87.54**	–87.22	–86.11
98	**–88.11**	–86.43	**–88.22**
99	–85.97	–87.32	**–87.62**
100	–86.18	–86.02	**–89.22**
101	–83.51	–86.34	**–87.95**

Other than the wide-spread and safe use as a medical diagnostic tool (^{99m}Tc, a metastable nuclear isomer of ^{99}Tc),[14–16] the other isotopes of technetium are rather limited in their application. One such use for ^{99}Tc is, for example, the equipment calibration for stand beta emitters.[17]

1.2 Pertechnetates

Technetium, a group 7 transitional metal, exhibits all oxidation states between –1 to +7, with +4, +5 and +7 being the most common. The most prevalent form is the Tc(VII) as a pertechnetate ion (TcO_4^-), a tetrahedral oxoanion that is isostructural and isoelectronic to permanganate $[MnO_4]^-$, perrhenate $[ReO_4]^-$, perchlorate $[ClO_4]^-$, perbromate $[BrO_4]^-$, metaperiodate $[IO_4]^-$, chromate $[CrO_4]^{2-}$, molybdate $[MoO_4]^{2-}$, tungstate $[WO_4]^{2-}$, ruthenium tetroxide RuO_4 and osmium tetroxide OsO_4. Its conjugate acid is the pertechnetic acid, described short-hand as $HTcO_4$ as there has not been an unambiguous characterisation of what is probably an oxonium pertechnetate and hydronium pertechnetate in solid state and aqueous state respectively.[18,19] $HTcO_4$ can be obtained by dissolving its anhydride Tc_2O_7 in water or by passing NH_4TcO_4 or $MTcO_4$ (M = Na or K) through an acidic cation exchanger column. Pertechnetic acid can be concentrated by evaporating off the water; first taking on a yellow colour before deepening to a dark orange as shown in Figure 2.[19]

Figure 2: Colour of pertechnetic acid where (a) is 5.7 M TcO_4H, (b) is 7.6 M TcO_4H, and (c) is 9.9 M TcO_4H.[19]

Upon further evaporation, or if allowed to stand, a highly-reactive red substance is formed at high acid concentration. When this red substance is redissolved in water, it forms a colourless solution with brown precipitate of TcO_2.[19] The nature of this red solid has been long debated as either a polymeric heptavalent hydrated species (i.e., $Tc_2O_7{\cdot}H_2O$) or a binary Tc(V) or Tc(IV) oxide (i.e., TcO_3 or Tc_2O_5) until German and co-workers were able to unambiguously establish the red compound as $[H_7O_3]_4[Tc_{20}O_{68}]{\cdot}4H_2O$, which contains the first example of a Tc polyanionic species, $[Tc_{20}O_{68}]^{4-}$. The technetium polyoxometalate (POM) consists of a centre of four Tc(V) octahedra surrounded by 16 $[TcO_4]^-$. It involves the formation of Tc(V) *via* the reduction and decomposition of TcO_4^- to TcO^{3+} (Equation 1).[20]

$$TcO_4^- + 4H^+ \rightarrow \tfrac{1}{2}\, O_2 + 2H_2O + TcO^{3+} \tag{1}$$

The first hypothesis of German and co-workers was that four TcO^{3+} polymerise to form a $[Tc_4O_4]^{12+}$ ring (Equation 2).[20] Sixteen pertechnetates are then complexed on to the $[Tc_4O_4]^{12+}$ centre unit (Equation 3).[20]

$$4\, TcO^{3+} \rightarrow [Tc_4O_4]^{12+} \tag{2}$$

$$[Tc_4O_4]^{12+} + 16\, TcO_4^- \rightarrow [Tc_{20}O_{68}]^{4-} \tag{3}$$

The second hypothesis of German and co-workers was the formation of a polyanionic species $[TcO(OH)(TcO_4)_4]^{2-}$ followed by condensation of these four identical anions (Equation 4).[20]

$$4\, [TcO(OH)(TcO_4)_4]^{2-} + 4H^+ \rightarrow [Tc_{20}O_{68}]^{4-} + 4H_2O \tag{4}$$

The structure of the polyoxometalate by German and co-workers are as shown in Figure 3.

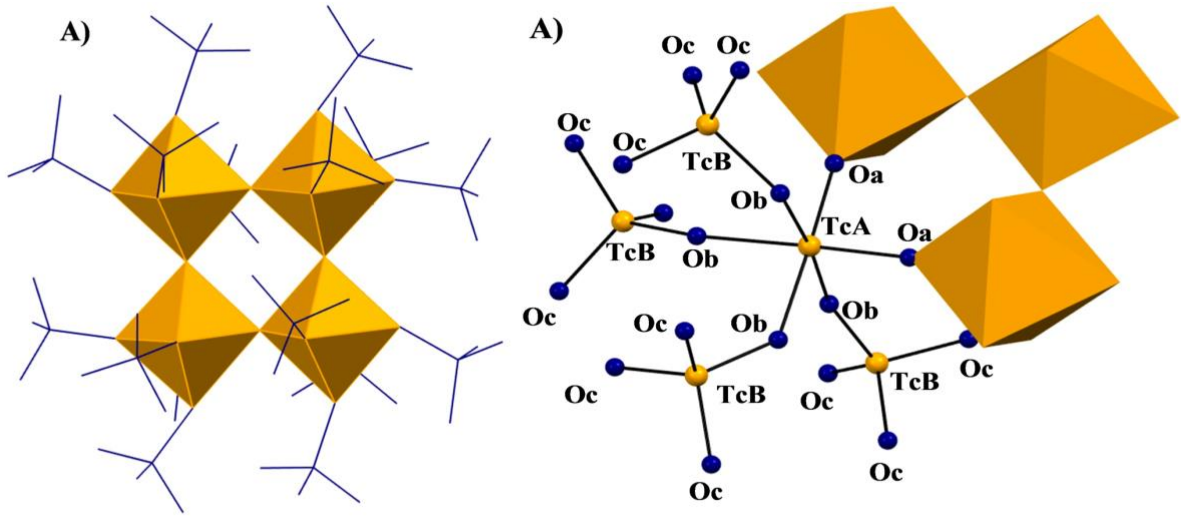

Figure 3: Structure of the polyoxometalate anion $[Tc_{20}O_{68}]^{4-}$: the $Tc(V)O_6$ units are shown as orange octahedra and the $Tc(VII)O_4$ units are shown as blue sticks.[20]

Zegke and co-workers confirmed the findings made by German and co-workers that high concentration of pertechnetic acid solutions may lead to the formation of polyoxometallates or spontaneous auto-reduction to lower oxidation states, producing oxotechnetate (V) ions. This is exemplified in Figure 3 and Figure 4, which show the relevant structures. Thus, care needs to be taken while working with concentrated pertechnetic acid.

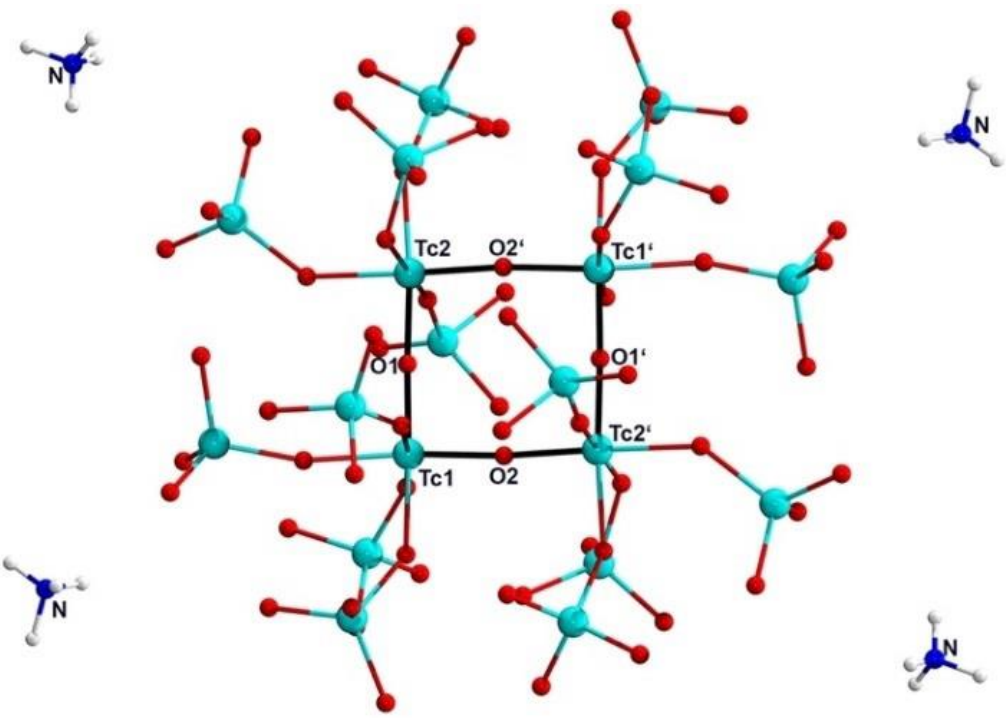

Figure 4: Structure of $(NH_4)_4[\{TcO(OTcO_3)_4\}_4]$.[21]

1.3 The Knowledge Gaps in Technetium Chemistry

^{99}Tc is, as already mentioned, a significant component of nuclear waste generated from fission processes with a fission yield of 6%.[8] As part of the nuclear waste stream and as a highly mobile, water-soluble anion, understanding pertechnetate is important when it comes to leaching processes or accidental release into the environment. For instance, Tc(I) carbonyl species were found to be present near the waste tanks at the Hanford site.[22] These obviously come most likely from pertechnetate and show that reduction occurs in nature all the way down from oxidation state +7 to +1. Thus, the pertechnetate anion is able to leach from nuclear waste storage facilities or contaminated sites into groundwater, surface water and biological systems, posing risks to human health and ecosystems.[23,24] Studying the fate and transport of pertechnetates in natural environments can help assess the extension of contamination. Despite researchers coming up with strategies to immobilise pertechnetate,[25,26] there is still a significant lack of understanding in the mobility of technetium in the environment.

Even though $[TcO_4]^-$ and $[ReO_4]^-$ have similar ionic radii, it was only recently established by Shohel and co-workers *via* Small-Angle X-ray Scattering (SAXS) that both of them behaved differently, i.e., pertechnetate forms more extensive bonds with Zr/Hf compared to perrhenate, which tend to remain as free perrhenate in solution.[27]

Despite being centrally located in the periodic table, there is an immense knowledge gap in the coordination chemistry of Tc. For instance, the elements surrounding Tc (Mn, Mo, Ru and Re) have 20132, 7470, 3948 and 2036 crystallographic entries in the Inorganic Crystal Structure Database (ICSD), respectively. In stark contrast, Tc has only 303 crystallographic entries a on Tc-related compounds (less than 1% the sum of its neighbouring elements). Research in the group of Strub has significantly enhanced the knowledge of the coordination chemistry of the pertechnetate salts of transition chemistry and main group chemistry,[28] yet systematic studies of technetium with the lanthanoids are still lacking.

1.4 The Lanthanoid Series

The lanthanoid elements are a series of 15 metallic elements with atomic numbers 57 to 71, with 57 being lanthanum and 71 being lutetium. The lanthanoids, alongside the chemically similar scandium and yttrium, are often collectively known as rare-earth elements (REE).

Lanthanoid chemistry first began in the year 1794 when Finnish mineralogist-chemist Johan Gadolin analysed a black heavy mineral that was found by geologist-chemist Carl Axel Arrhenius in the Swedish village of Ytterby. In his analysis, Gadolin concluded that 38% of the sample contained an unknown oxide, later named yttria.[29] Yttria, more commonly known as yttrium oxide, was the first known REE compound. The sample he analysed was later named gadolinite in honour of Gadolin. In the subsequent decades, seven more lanthanoids, were extracted from gadolinite: terbium, dysprosium, holmium, thulium, ytterbium, and lutetium.[29,30] On the other hand, the first element of the actual lanthanoid series that was discovered was cerium in 1803 by Swedish chemist Martin Heinrich Klaproth and Jöns Jakob Berzelius, and independently by German chemist Wilhelm Hisinger in the same year. It was in the late 1830s, though, that Swedish chemist Carl Gustaf Mosander managed to isolate pure ceria by separating ceriterde into cerium oxide, lanthanum oxide and ‘didymia’ oxide (a mixture of praseodymium, neodymium, samarium, europium, and gadolinium oxides).[30]

Historically, the lanthanoids were extremely difficult to separate, leading to claims of discovering as many as 70 ‘new’ elements in the 19th century. Even Dmitri Mendeleev’s revolutionary creation of the periodic table of elements was unable to resolve the number of lanthanoids due to unreliable information of atomic mass as well as some elements having not been isolated yet.[31] Similar to the discovery of technetium, British physicist Henry Moseley’s use of the X-ray spectrometer to measure the X-ray spectra of chemical elements, and established that there were exactly 15 elements from lanthanum to lutetium.[2,32] He also able accurately predict the existence of element 61, radioactive promethium, which was first identified in Oak Ridge National Laboratory in 1945 by the separation of nuclear fission products from uranium fuel.[33]

The lanthanoids exhibit unique characteristics in their chemistry, primarily existing in the +3 oxidation state, which is the reason for the inherent difficulty in separating ores like gadolinite and cerite into individual metals. In contrast to d-block metals – which can lose several valence d-electrons – the lanthanoids tend to only lose one 4f-electron. When ionised, the 6s-electrons are lost first because they are furthest from the nucleus and are shielded by inner electrons. As ionisation progresses, the increasing positive charge causes all the radial distribution functions (RDF) contract. Following the loss of one 4f-electron, the 4f orbitals become more stabilised such that the fourth ionisation requires too much energy and cannot be offset by chemical bond formation. As such, the +3 oxidation state dominates the lanthanoid chemistry.[34]

The second characteristic is the gradual decrease in the ionic radius for each Ln^{3+} from La to Lu. This is attributed to the lanthanoid contraction, due to the 4f-orbitals having a high degree of angular nodality – three angular nodes. As such, the 5s and 5p-orbitals are poorly shielded from increasing nuclear charge. Hence, this results in increasing effective nuclear charge and decreasing radius from La to Lu.[35] The 4f-orbitals are so contracted that they are effectively shielded from their chemical environment by the $5s^2$ and $5p^6$ (Figure 5).[36] The lanthanoid contraction is commonly used for lanthanoid separation *via* cationic ion-exchanger or reversed-phase chromatography (see below, Chapter 1.6). Consequently, Ln–X bonding is mostly ionic.

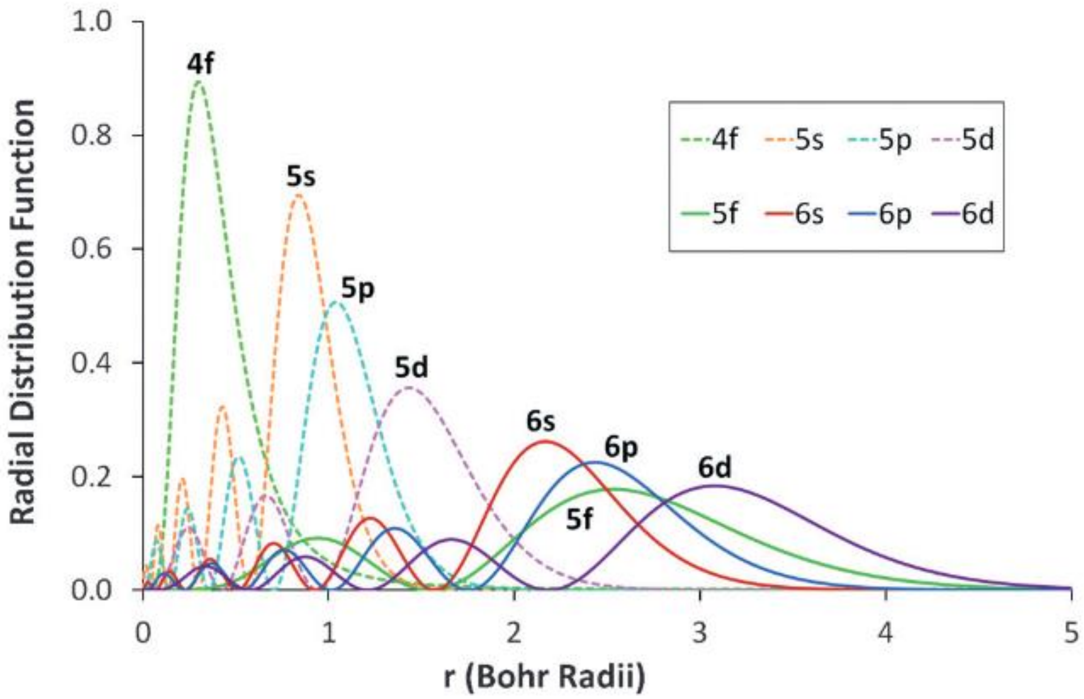

Figure 5: Radial distribution functions for the 4f, 5s, 5p, 5d, 5f, 6s, 6p, and 6d atomic orbitals.[36]

In the Ln^{3+} ions, the 4f-electrons are well shielded by the 'outer' 5s and 5p orbitals from the environment, leading to weak crystal field splitting. As a consequence of weak crystal field effect, the f–f absorption bands in the UV-visible spectrum are very narrow and have well-defined energies.[37] The intensity of the 4f–4f transition is weak, as according to the Laporte selection rule, the f–f transition is symmetry forbidden.[38] The selection rule also applies rigidly to the lanthanoids, unlike the transitional metal complexes, because the 4f-orbitals are core-like in character, hence vibronic coupling does not occur to a great extent to momentarily break symmetry.[37] The intra-configurational 4f–4f transition is the deciding transition in giving the colour of the lanthanoid ion,[37] as well as distinguishing the lanthanoids from one another (see below, Chapter 2.2.3 and 2.2.5). The allowed f–d transition does not affect the visible colour of the trivalent lanthanoid ions as they occur only at less than 200 nm.[39] The only exceptions are Ce^{3+} and Tb^{3+}, however their f–d transition bands are found in the UV spectral region.[37] The electronic spectra of lanthanoid compounds resemble those of the free ions and therefore are not helpful in distinguishing between coordination geometries.

The common coordination numbers for the early and late lanthanoids are nine and eight respectively, with the intermediate lanthanoids displaying a mixed variety of species.[40] The nine-coordinate species take on the tricapped trigonal prism structure and the eight-coordinate species take on the square antiprism or dodecahedral structure as shown in Figure 6.[41] As the f-orbitals are radially contracted, they are shielded from the environment and do not participate in directional bonding. The coordination number of the lanthanoid complex is ultimately determined by the steric effect of the ligand and the size of the lanthanoid cation.

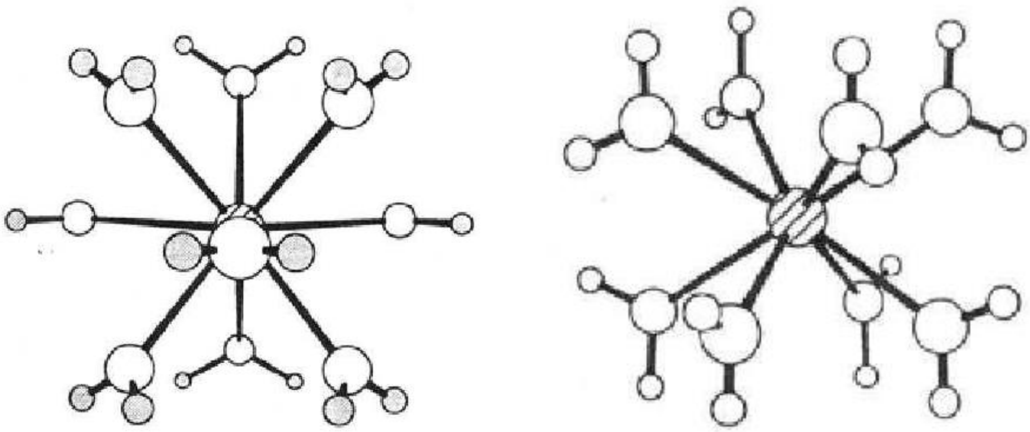

Figure 6: Tricapped trigonal prism structure of nine-coordinate $[Ln(H_2O)_9]^{3+}$ ion on the left and square antiprism structure of eight-coordinate $[Ln(H_2O)_8]^{3+}$ ion on the right.[41] The Ln atom is marked with dashes.

In addition, the lanthanoid series is also part of the nuclear waste stream.[42] Understanding the behaviour of lanthanoids in nuclear waste (specifically with highly mobile pertechnetates) is important for developing nuclear waste management and long-term storage of disposal. As the trivalent lanthanoids are homologues to actinium and the transplutonium elements, studying the lanthanoids can also provide valuable insights into the chemistry, spectroscopy, and behaviour of actinoids with pertechnetates due to their similarities in electronic structures, coordination chemistry and magnetic properties.[43]

Since most Tc remains in the raffinate after the PUREX (Plutonium Uranium Redox Extraction) process,[44] understanding the chemistry of the lanthanoid pertechnetates can offer insights into improving subsequent reprocessing steps, such as the TRUEX (TRansUranic Extraction) and the TALSPEAK (Trivalent Actinide-Lanthanide Separations by Phosphorous-reagent Extraction from Aqueous Komplexes) processes. TRUEX uses an organic phase (a mixture of octyl(phenyl)-N,N-diisobutylcarbamoylmethylphosphine oxide (CMPO) and tri-n-butyl phosphate (TBP)) to extract the transuranic elements from the lanthanoids, while TALSPEAK employs a complexing agent (diethylenetriaminepentaacetic acid (DTPA)) to extract the trivalent actinoids of Am and Cm from the lanthanoids.[45,46] Despite advancements, the main challenge is the co-extraction between the transuranic elements and the lanthanoids.[47–49]

1.5 Promethium

Promethium (Pm) is a lanthanoid element with the atomic number of 61 and is the second lightest element (after technetium) with no stable isotopes. In 1902, Czech chemist Bohuslav Brauner found that the differences in properties between neodymium (Nd) and samarium (Sm) were the largest between any consecutive lanthanoids. He concluded that there needs to be another element between them.[50] His prediction was supported in 1913 when Henry Moseley observed that characteristic X-rays for elements were based on proportionality to charge.[2] There was a gap for atomic number 61. There were several claims of discovery made by a pair of Italian chemists in Florence, and a group of American chemists from Urbana, Illinois.[51,52] Both of their reported discoveries of "florentium" and "illinium" were questioned as their spectral lines turned out to belong to impurities.[53]

In 1945, element 61 was first produced and characterised at the Oak Ridge National Laboratory (then Clinton Laboratories) by Jacob Marinsky, Lawrence Glendenin and Charles Coryell by separation and analysis of fission products of uranium fuel.[54] The name "prometheum" was suggested by Grace Coryell, Charles Coryell's wife. It is named after Prometheus, the Titan in Greek mythology who defied the gods by stealing fire from them from Mt Olympus and giving it to humanity. It symbolises "both the daring and the possible misuse of the mankind intellect". The spelling was then changed to "promethium", in accordance with other metal elements.[55] Promethium belongs to the cerium group of lanthanoids and is chemically similar to its neighbouring elements.[53] Because of its radioactivity, there is little chemical study and data of Pm. Like most of the other lanthanoids, it forms only one stable oxidation state of +3, with an electronic configuration of [Xe] $4f^4$. Treatment of Pm^{3+} with strong oxidising or reducing agents has so far not lead to the isolation or characterisation of Pm^{4+} or Pm^{2+}. The Pm^{3+} ion is pink in colour, and promethium compounds are pink or red in colour. The coordination number of Pm^{3+} in water is 9, in line with the early lanthanoids.[56] Known Pm(III) compounds include the simple inorganic solids such as the oxide, halides, nitrates, sulphates, hydroxide and oxalates.[57] The observation of a promethium complex in solution, $[Pm(PyDGA)_3]^{3+}$ (PyDGA = bispyrrolidine diglycolamide), was recently published, having synthesised it from $^{147}Pm(NO_3)_3{\cdot}nH_2O$ ($n < 9$) and PyDGA, which was analysed by X-ray absorption spectroscopy.[58] Its Pm–O bond length of 2.76(16) Å aligns with quantum chemical calculations and is consistent with Ln–O bond lengths across the lanthanoid series.[58]

Promethium isotopes are known from ^{126}Pm to ^{166}Pm, where the most stable isotopes are ^{145}Pm ($t_{1/2}$ = 17.7 years), ^{146}Pm ($t_{1/2}$ = 5.53 years), and ^{147}Pm ($t_{1/2}$ = 2.62 years). ^{145}Pm decays by electron capture to ^{145}Nd with negligible α-decay to ^{141}Pr. ^{146}Pm decays by electron capture 66% of the time to ^{146}Nd and by β^--decay 34% of the time to ^{146}Sm. ^{147}Pm decays by β^--decay 99.99% of the time to ^{147}Sm with a maximum energy of 224.5 keV, with an average energy of 62 keV. [59,60] ^{147}Pm also γ-decays 0.00285% of the time.[61]

Promethium is produced as ^{147}Pm as it is the only isotope with industrial applications. It is obtained as a fission product of the nuclear fission of ^{235}U, yielding ^{147}Pm at a relatively high fission yield of 2.6%.[53] Another way to obtain ^{147}Pm is *via* the β^--decay of ^{147}Nd, while the ^{147}Nd can be obtained from the neutron bombardment of ^{146}Nd.[62] ^{147}Pm is used in nuclear batteries by capturing the beta particles (electrons) and converting them into a steady usable electrical current. This is usually done by surrounding a small source of ^{147}Pm with semiconductors to catch the flying electrons.[60] Such batteries have a useful lifetime of at least five years. It can also be used as a luminous paint. The luminous paint usually contains phosphoric material that absorbs the beta radiation by ^{147}Pm and emits light. The advantage is that the phosphoric material does not age from the beta emitters, unlike alpha emitters.[63] It is also used as a thickness gauge by measuring the amount of radiation from a promethium source that passes through the sample.[64]

Similar to technetium, the reason for promethium's radioactivity is due to the fact that Pm isotopes are surrounded by relatively more stable neighbouring elements. As shown in Table 2, for A = 144 – 145, the stable nuclides are ^{144}Nd and ^{145}Nd. For A = 147 – 148, the stable nuclides are ^{147}Sm and ^{148}Sm. For A = 146, ^{146}Pm is unstable to both β^- decay to ^{146}Sm at 34.3% and β^+ decay or electron capture to ^{146}Nd at 65.7%.[65]

Table 2: Mass excess values or binding energies for neodymium, promethium, and samarium isotopes. The most stable nuclei, indicated by the lowest mass excess or largest binding energy, are highlighted in bold.[66]

Atomic Weight, A	$_{60}$Nd, MeV	$_{61}$Pm, MeV	$_{62}$Sm, MeV
144	**–83.75**	–81.42	–81.97
145	**–81.43**	–81.27	–80.65
146	**–80.93**	–79.45	**–81.00**
147	–78.15	–79.04	**–79.27**
148	–77.41	–76.87	**–79.34**

1.6 Separation of Lanthanoids by Column Separation

As ^{147}Pm β^--decays to ^{147}Sm with a relatively short half-life of 2.62 years, it is essential that ^{147}Pm is purified before use. However, due to the lanthanoid contraction, as well as sharing a common oxidation state, the separation of lanthanoids, especially adjacent lanthanoids, is extremely difficult and complex. By exploiting the slight difference in ionic sizes, liquid chromatography (LC) is a powerful tool for the separation of lanthanoids and can be used to purify ^{147}Pm. Examples of modern LC for REE separation are ion exchange chromatography (IEC), ion chromatography (IC), ion pair chromatography (IPC), normal and reverse-phase (RP) LC, extraction chromatography and centrifugal partition chromatography.[67]

A systematic study by Ward and co-workers using Eichrom Industries' LN resin was successful in separating lanthanoids rapidly in high resolution based on a range of acid concentrations and column lengths.[68] The LN resin, a reverse phase extraction resin, is made of a cationic di(2-ethylhexl)orthophosphoric acid (HDEHP) ligand bound to a stationary hydrophobic resin bead surface *via* weak hydrophobic interactions. The separation of lanthanoids is made possible by taking advantage of the increasing charge density across the lanthanoid series and the competition of the Ln^{3+} and H^+ ions for the active sites on the resin. Distribution coefficients by Horwitz and co-workers show that the light lanthanoids are eluted in low acid concentrations, and the heavy lanthanoids are eluted in high acid concentrations (e.g.>6 M).[69] The study by Ward and co-workers found the resolution value of the separation of Nd/Sm to be 1.2 for a 21.5 cm long column using 0.25 M HNO_3, with Nd eluting after 60 to 100 mL of HNO_3, and Sm eluting after another 50 mL of HNO_3 added as shown in Figure 7.[68]

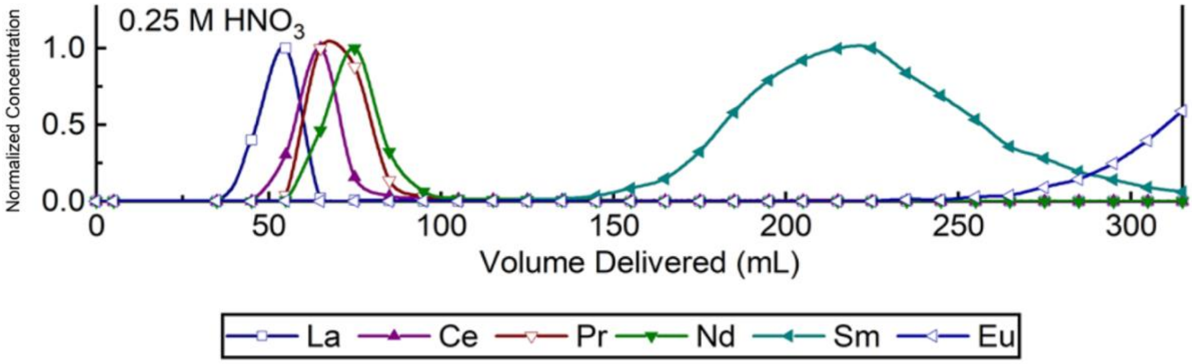

Figure 7: Separation of lanthanoids using a 21.5 cm long column and 0.25 M HNO_3 as the eluant.[68]

From the same study, they found the optimal separation setup by using a 31.5 cm column to elute Nd using 40 mL of 0.35 M HNO_3 and elute Sm by using 60 mL of 0.5 M HNO_3. This is shown in Figure 8.[68]

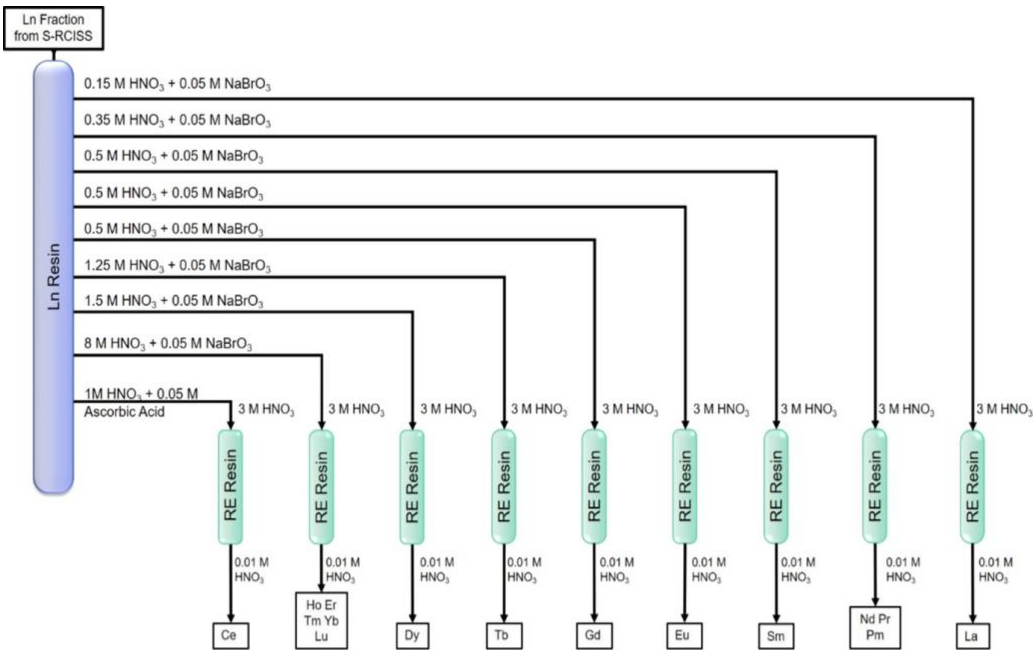

Figure 8: Flowchart of procedural steps using a 31.5 cm long column filled with 50–100 µm LN resin.[68]

In another study by Pin and co-workers, the sequential separation of light REE involved the use of a miniaturised extraction column chromatography.[70] In their work, LN resin (also by Eichrom Industries made from HDEHP) was used. A silica glass column (4 mm in diameter and 8 cm in length) was packed with 300 mg of resin in a slurry of 1 M HCl with a porous frit placed at the upper bed end. The column was stored in a diluted HCl bath between uses. The lanthanoids were then separated by using HCl with increasing concentration of up to 0.75 M. In this procedure, Nd elutes after approximately 3.5 mL of eluate were collected using 0.25 M

HCl as the eluent. Sm was eluted using 0.75 M HCl as the eluent. This is summarised in the elution profile in Figure 9.

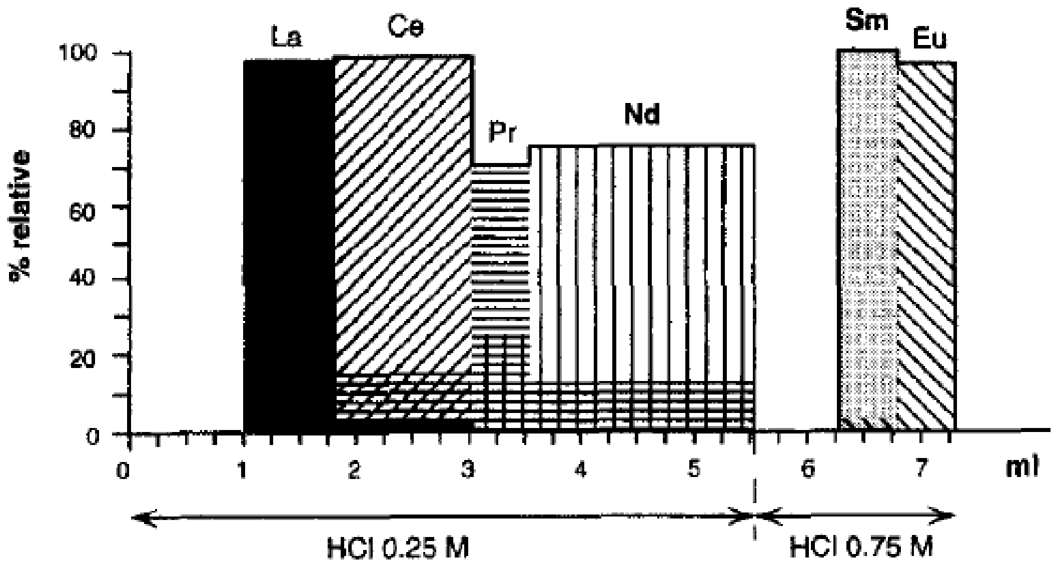

Figure 9: Elution profile of lanthanoid separation using an 8 cm column filled with 50–100 µm LN resin.[70]

In another study by Arrigo and co-workers, the use of 1.56 g and 2.34 g of LN resin with a particle size of 100–150 µm led the early lanthanoids from La to Nd to elute with 10 mL of 0.5 M HNO_3.[71] Sm was eluted with 0.75 M of HNO_3. With the use of 0.78 g of LN resin with a smaller particle size of 50–100 µm, La to Nd were eluted with 8 mL of 0.25 M HNO_3 and 8 mL of 0.3 M HNO_3, and then Sm with 0.4 M HNO_3 (Figure 10).

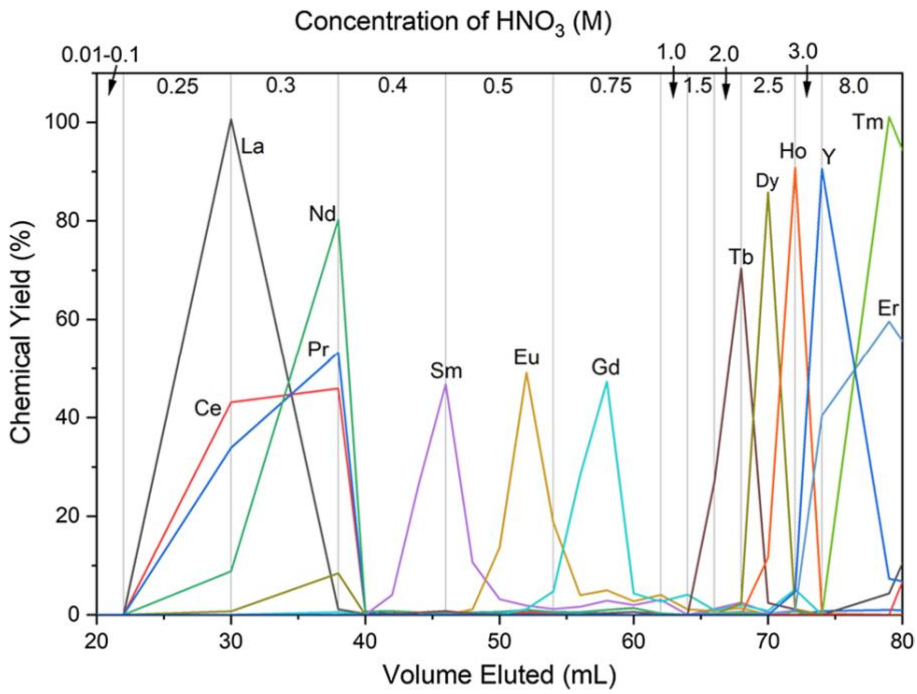

Figure 10: Elution profile of lanthanoid separation using a 20 cm column filled with 50–100 µm LN resin.[71]

2. Results and Discussion

2.1 Separation of ^{147}Pm from its Decay Product ^{147}Sm

In the classic separation of lanthanoids using cationic ion-exchange resin and α-hydroxyisobutyrate as the eluent, the smaller lanthanoid elutes first, i.e., Lu eluting before La.[72] However, this is not ideal in the purification of ^{147}Pm as the daughter nuclide, ^{147}Sm, will elute first, with the possibility of ^{147}Sm tailing coinciding with the peak of the desired ^{147}Pm product.

Thus, the separation of the lanthanoids was achieved using LN resin from Eichrom Industries. LN resin, made from HDEHP, was chosen because the larger lanthanoid will elute first, i.e., ^{147}Pm eluting before Sm. This is ideal for the purification as the ^{147}Pm obtained will be pure and free of Sm. The column is set up as shown in Figure 11 and the preparation of the lanthanoid separation column is as described in the experimental (Chapter 4.3.1.1). The volume of one drop that elutes from the column is approximately 40 µL.

Figure 11: Lanthanoid separation column charged with LN Resin 20-50, topped and bottomed with Dowex 1X8 100-200 (Cl).

2.1.1 Separation of Neodymium and Samarium

The aims of separating inactive Nd and Sm with different concentrations of eluent are to ascertain the drop counts of the Nd and Sm peaks and the resolution of the elution profiles by ICP-MS. By extension, the drop count of the Pm peak can be interpolated and should match the drop count of the Pm peak during the actual Pm purification.

100 µL of 0.353 mM (126.88 ppm) of $NdCl_3$ and 100 µL of 0.353 mM (126.88 ppm) of $SmCl_3$ were loaded onto three different pre-equilibrated columns of different concentrations (0.65 M, 0.70 M, and 0.75 M). The lanthanoids were then eluted with HCl at their respective concentrations. Eluants were collected, diluted, and analysed *via* ICP-MS as described in the experimental (Chapter 5.2.4 and 5.3.1.2).

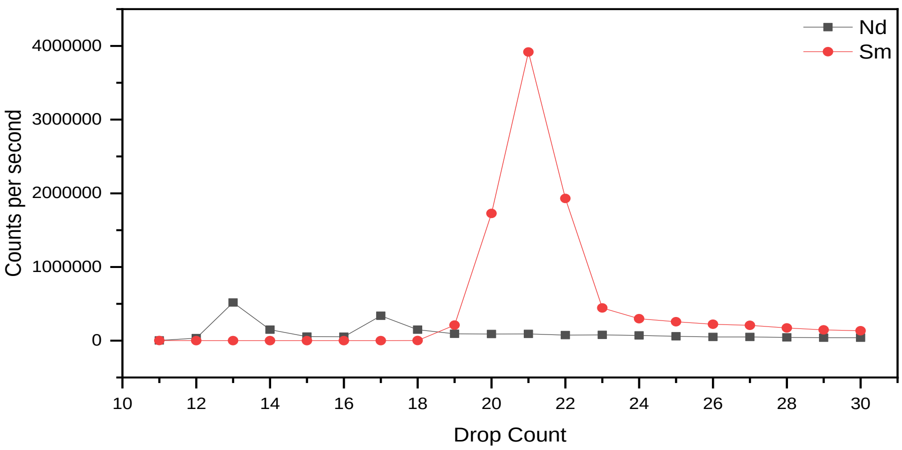

Figure 12: Elution profile of Nd and Sm with 0.75 M HCl. For full data, see Appendix Table S8.

Using 0.75 M HCl as the eluent on a pre-equilibrated column, Nd was eluted from drop 12 to drop 19 with two broad peaks with peak maxima at drop 13 (516825 cps) and 17 (337061 cps). Sm was eluted from drop 19 to 24 with a relatively sharper peak with a peak maximum at drop 21 (3918293 cps) (Figure 12). Crossover between Nd and Sm is observed at drop 19 with Nd and Sm having a count value of 92780 cps and 210666 cps respectively.

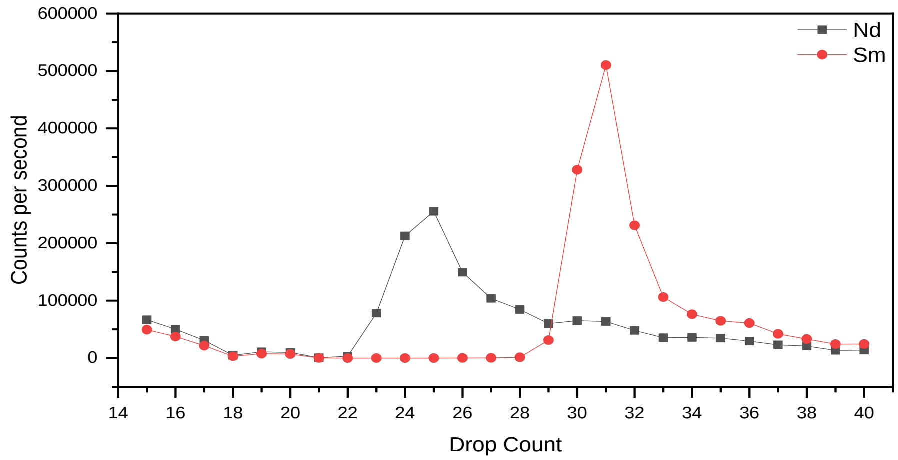

Figure 13: Elution profile of Nd and Sm with 0.70 M HCl. For full data, see Appendix Table S9.

Using 0.70 M HCl as the eluent on a pre-equilibrated column, Nd was eluted from drop 22 to drop 39 with one peak with significant tailing, with a peak maximum at drop 25 (255542 cps). Sm was eluted from drop 29 to 39 with a relatively sharper peak with significant tailing, with a peak maximum at drop 31 (510257 cps) (Figure 13). Despite the peaks being six drops apart, there is significant crossover between Nd and Sm as observed from drop 29 to drop 39 with Nd and Sm having a count value of 63707 cps and 510257 cps respectively at the Sm peak of drop 31.

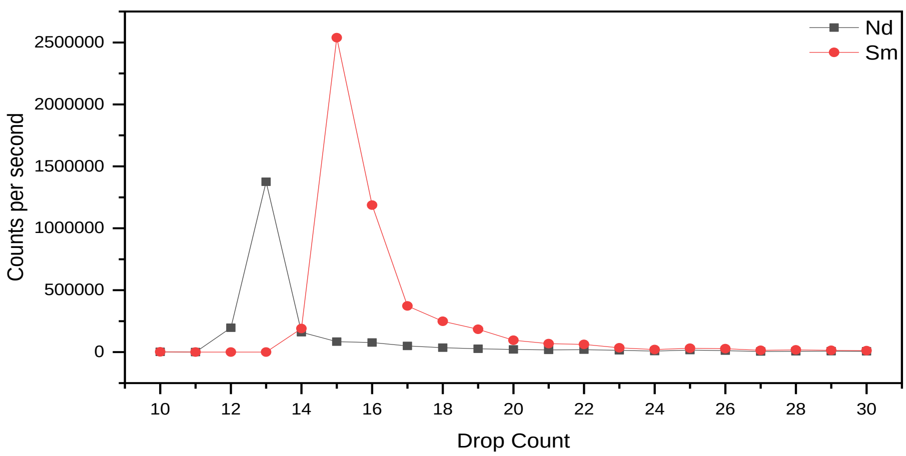

Figure 14: Elution profile of Nd and Sm with 0.70 M HCl. For full data, see Appendix Table S10.

Using the same 0.70 M pre-equilibrated column as before, the column was flushed with 1 M HCl to remove both Nd and Sm, and then pre-equilibrated with 0.70 M HCl. Using 0.70 M HCl as the eluent, Nd was eluted from drop 12 to drop 15 with one peak with some tailing, with a peak maximum at drop 13 (1374832 cps). Sm was eluted from drop 14 to 22 with a relatively sharper peak with significant tailing, with a peak maximum at drop 15 (2538196 cps) (Figure 14). Despite using the same column, the same pre-equilibration concentration and the same concentration of the eluent, the Nd- and Sm-peaks not only arrived earlier, but they were also only two drops apart. These deviations could be due to formation of channels during the flushing and/or pre-equilibrating process. It is also likely that the concentration of HCl in the column is higher than 0.70 M due to possible incomplete pre-equilibration after the 1 M HCl flushing.

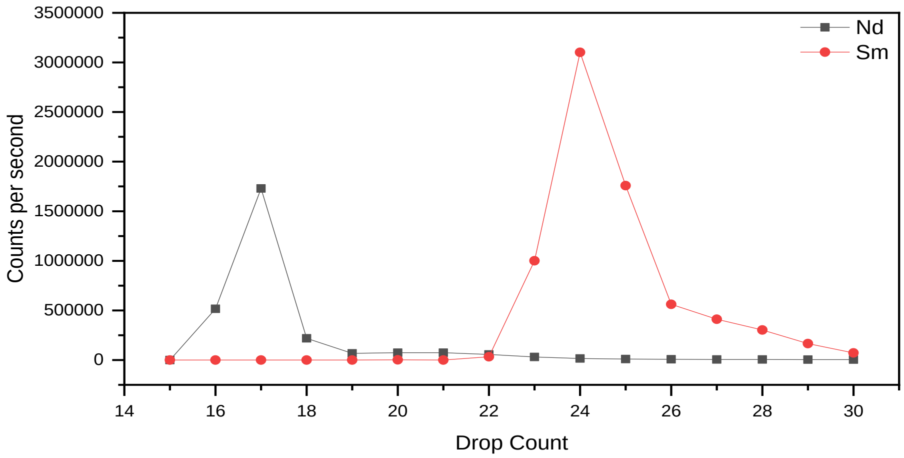

Figure 15: Elution profile of Nd and Sm with 0.65 M HCl. For full data, see Appendix Table S11.

Using 0.65 M HCl as the eluent on a pre-equilibrated column, Nd was eluted from drop 16 to drop 22 with one peak with some tailing, with a peak maximum at drop 17 (1729007 cps). Sm was eluted from drop 23 to 29 with one peak with significant tailing, with a peak maximum at drop 24 (3101756 cps) (Figure 15). The peaks are seven drops apart, and there is insignificant crossover between the Nd and Sm peaks (drop 23 has a count value of 30652 cps and 1000821 cps respectively).

2.1.2 Elution Profile of Samarium

0.65 M HCl was determined to be the ideal concentration of the eluent for this column and purpose for a few reasons. Firstly, from the elution profile in Figure 14, the concentration of the eluent is low enough that there is high resolution between Nd and Sm (drop count 17 vs 24). The Pm peak can therefore be interpolated to lie between drop 20 and 21. Secondly, the concentration of the eluent is still relatively high enough such that it is practical to elute and separate Nd and Sm in under 40 drops. Thirdly, by the end of the separation at drop 30, the Nd and Sm count values were low and falling rapidly at 3865 cps and 71786 cps respectively. Hence, the column can just be flushed at the same concentration of the eluent so as to not have the same situation in Figure 13, where the lanthanoids elute earlier than expected due to possible incomplete 0.65 M HCl pre-equilibration.

The aims of determining the elution profile of Sm are to establish the drop count of the Sm peak at 126.88 ppm of lanthanoid (similar to 100 µL of stock $^{147}PmCl_3$ solution) and to verify the consistency of the drop count of the Sm peak when using 0.65 M HCl as the eluent.

Ensuring that the starting volume is the same as the previous elution, 100 µL of 0.353 mM (126.88 ppm) of $SmCl_3$ and 100 µL of Milli-Q water were loaded onto the 0.65 M HCl pre-equilibrated column. Sm was then eluted with 0.65 M HCl as the eluent. Eluants were collected, diluted, and analysed *via* ICP-MS as described in the experimental.

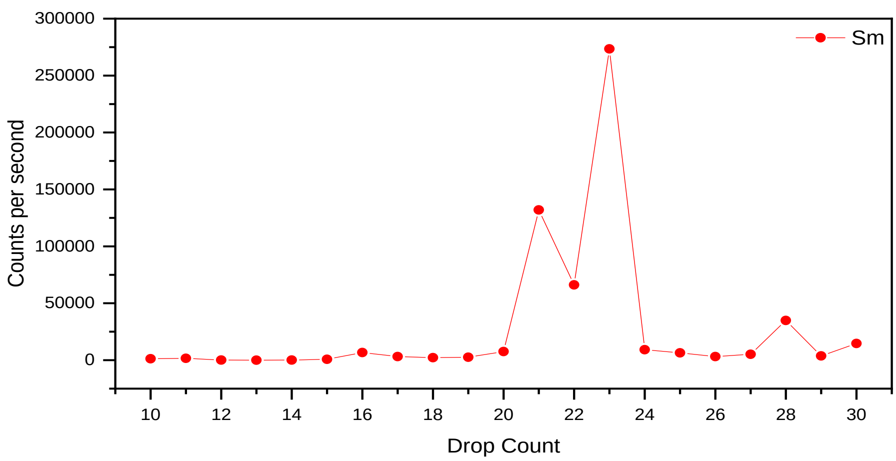

Figure 16: Elution profile of Sm with 0.65 M HCl. For full data, see Appendix Table S12.

Using 0.65 M HCl as the eluent on the previously-used pre-equilibrated column, Sm was eluted from drop 21 to 23 with two peaks, with peak maxima at drop 21 (154400 cps) and at drop 23 (327355 cps) (Figure 16). There is also a small peak at drop 28 (34898 cps).

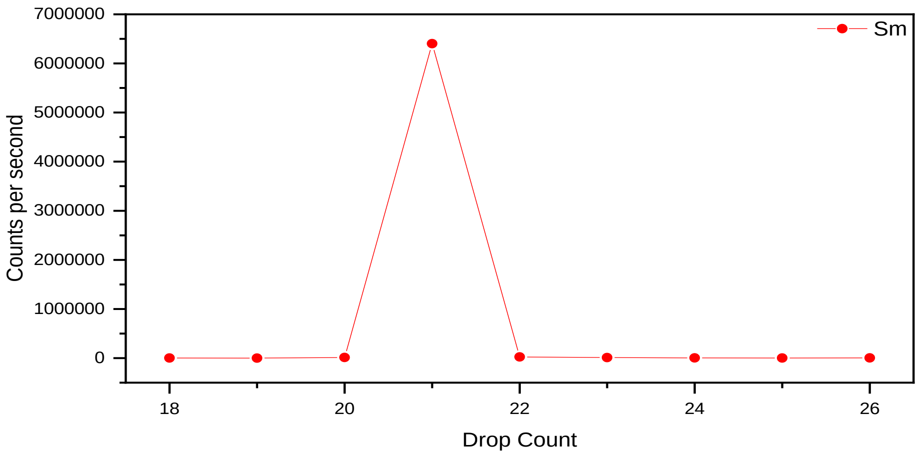

Figure 17: Elution profile of Sm with 0.65 M HCl. For full data, see Appendix Table S13.

Using 0.65 M HCl as the eluent on the pre-equilibrated column, Sm was eluted in a single large drop at drop 21 (6202653 cps) (Figure 17), with the preceding and following drops at 12501 cps and 25257 cps respectively.

2.1.3 Purification of Promethium

From the two Sm elution profiles in Figure 16 and Figure 17, it can be concluded that Sm elutes at drop 21. As such, when purifying ^{147}Pm with the same lanthanoid concentration through the same column with 0.65 M HCl as the eluent, its β^- decay product (^{147}Sm) should also elute at drop 21. From the elution profiles using 0.65 M HCl, it can be surmised that ^{147}Pm, at the same concentration as Nd and Sm, will also elute in one to three drops starting at around drop 17.

Measuring the Pm and Sm counts of the fractions for the actual ^{147}Pm purification by ICP-MS was not possible so as to avoid radioactive contamination. The activities of the fraction were measured by LSC instead so as to plot the elution profile of ^{147}Pm and also determine the total activity and, by that extension, the total mass of purified ^{147}Pm in the fractions before drop 21.

Following the previous setup in the elution of Sm, 100 µL of 0.353 mM of $^{147}PmCl_3$ (126.88 ppm, 200 MBq) and 100 µL of Milli-Q water were loaded onto the 0.65 M HCl pre-equilibrated column. ^{147}Pm was then eluted with 0.65 M HCl as the eluent.

However, the resultant eluants collected in the first attempt showed no activity. Upon further inspection, a ring of brown-tinted material where the meniscus of the solution was (Figure 18a) and a red solid unknown at the bottom was found inside the vial (Figure 18b); suggesting radiation damage or crystallisation of $^{147}PmCl_3$. Therefore, the $^{147}PmCl_3$ stock solution was transferred into a new vessel, and the activities of the stock solution and the empty stock-solution-vial were measured by gamma spectroscopy. The $^{147}PmCl_3$ stock solution and empty stock-solution-vial had activities of 530 cps (~150 MBq) and 3383 cps (~1.1 GBq) respectively, proving that most of the material had solidified in the vial.

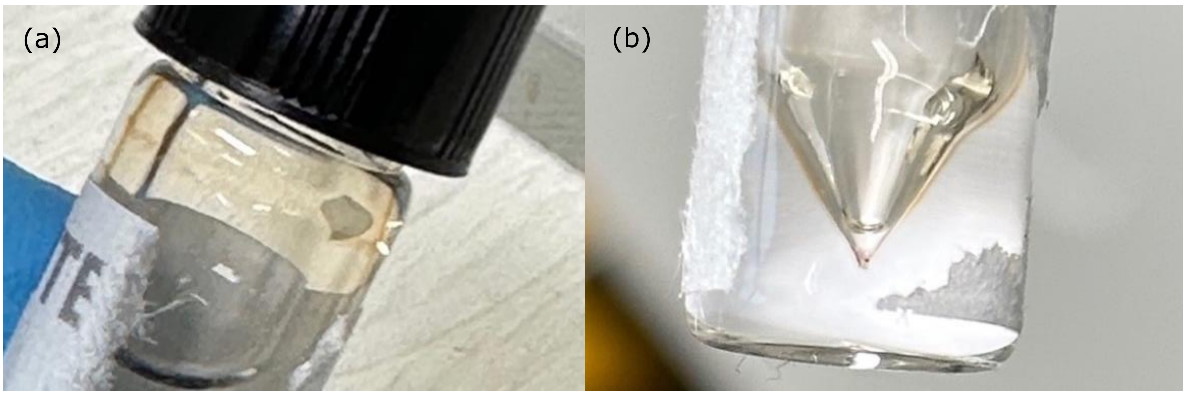

Figure 18: Brown ring of unidentified material in stock vial around the miniscule (a) and at the bottom (b).

500 μL of 0.65 M HCl was added into the empty stock-solution-vial and placed in an oven at 50 ºC overnight to dissolve the unidentified material. The resultant solution was transferred into another vessel, and the activities of the new solution and the empty stock-solution vial were measured by gamma spectroscopy. The 0.65 M HCl solution had an activity of 2840 cps (~850 MBq) while the empty stock-solution-bottle had an activity of 870 cps (~250 MBq), proving that most of the unidentified material containing ^{147}Pm could be recovered.

125 μL of 0.365 mM (131.19 ppm, 200 MBq) of $^{147}PmCl_3$ were loaded onto the 0.65 M HCl pre-equilibrated column. ^{147}Pm was then eluted with 0.65 M HCl as the eluent. Even though the starting volume and concentration differ from the column setup that gave the elution profiles of Nd and Sm, it can be extrapolated that ^{147}Pm will now elute five to six drops earlier than the expected drop 17 because the 125 uL of $^{147}PmCl_3$ was dissolved in the eluant, and there is an absence of 100 uL of Milli-Q water that was originally used to ensure the same starting volume as the previous elution. Eluants were collected, diluted, and analysed *via* LSC as described in the experimental.

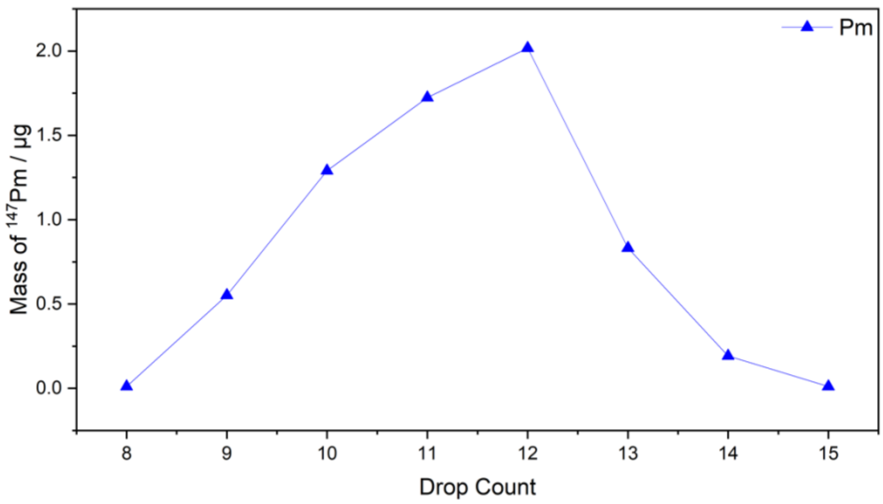

Figure 19: Elution profile of $^{147}PmCl_3$ with 0.65 M HCl. For full data, see Appendix Table S14.

Using 0.65 M HCl as the eluent on the pre-equilibrated column, ^{147}Pm was eluted from drop 9 to 14 with one peak with some tailing, with a peak maximum at drop 12 (494253 cpm, 69.5 MBq) (Figure 19). This coincides with the extrapolation that the peak of the ^{147}Pm elution profile will be at drop 12. Drop 9 to 13 are combined (~144 MBq) to be used for the reaction with pertechnetic acid. Drop 14 is excluded as there is the possibility that there is a crossover between ^{147}Pm and ^{147}Sm.

Repeating the same procedure as prior, 125 µL of 0.365 mM (131.19 ppm) of $^{147}PmCl_3$ were loaded onto the pre-equilibrated column. ^{147}Pm was then eluted with 0.65 M HCl as the eluent. Eluants were collected, diluted, and analysed *via* LSC as described in the experimental.

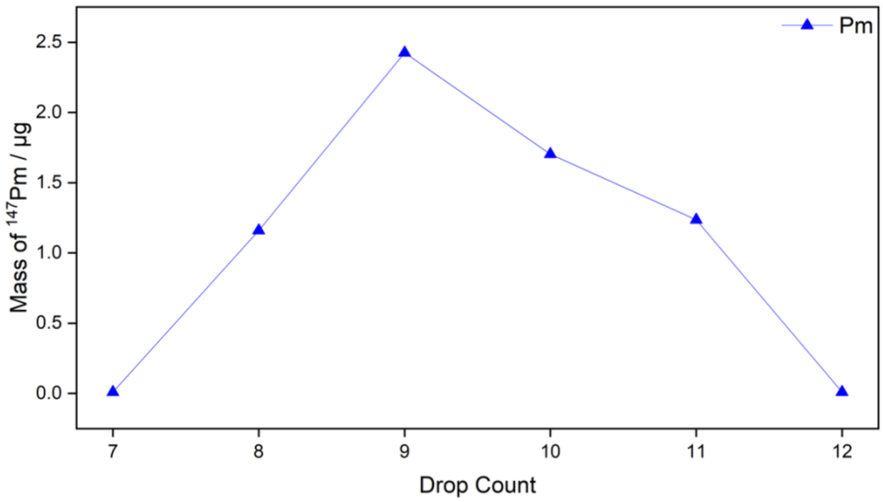

Figure 20: Elution profile of $^{147}PmCl_3$ with 0.65 M HCl. For full data, see Appendix Table S15.

Using 0.65 M HCl as the eluent on the pre-equilibrated column, ^{147}Pm was eluted from drop 8 to 11 with one peak with some tailing, with a peak maximum at drop 9 (594421 cpm, 131 MBq) (Figure 20). This peak maximum differs from the first purification procedure by two drops. Nonetheless, the activity falls sharply at drop 12 and gives confidence that combining drop 8 to 11 will have almost no ^{147}Sm present. Drop 8 to 11 are combined (~160 MBq) to be used for the reaction with perrhenic acid.

The purified $^{147}PmCl_3$ was used in an attempt to synthesise promethium pertechnetate and promethium perrhenate (see below, Chapter 2.2.10).

2.2 Synthesis and Characterisation of Lanthanoid Pertechnetates

2.2.1 Synthesis of Pertechnetic Acid

41 mM solutions of aqueous pertechnetic acid were obtained by passing aqueous NH_4TcO_4 (3.7 mg in 500 µL H_2O) through an acidic cation exchange resin. These solutions react with lanthanoid oxides, carbonates or chlorides to give hydrated lanthanoid pertechnetate salts. The procedures are as described in the experimental (Chapter 5.3.2) based on the same procedure by D. Zaratti and L. Dünnebier.[73,74]

2.2.2 Type I (Ln = La)

$$\frac{1}{2}\, La_2O_3 + 3\, HTcO_{4(aq)} \rightarrow [La(TcO_4)_3(H_2O)_3]$$

Scheme 1: Synthesis of $[La(TcO_4)_3(H_2O)_3]$ (**1-LaTc**)

The stoichiometric treatment of lanthanum(III) oxide with pertechnetic acid in aqueous solution (Scheme 1) and subsequent evaporation of the solution in air using a heat lamp led to the formation of colourless crystals of $[La(TcO_4)_3(H_2O)_3]$ (**1-LaTc**) covered in red-brown by-products (Figure 21). The crystals do not show any hygroscopic characteristics. The solid-state structure is shown in Figure 22.

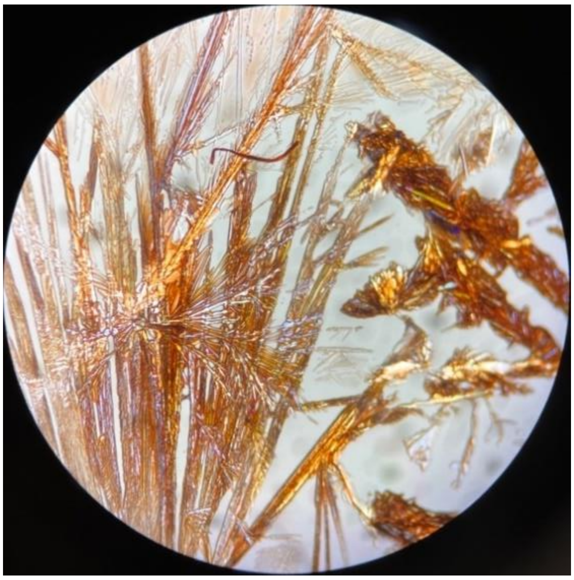

Figure 21: Colour crystals of $[La(TcO_4)_3(H_2O)_3]$ (**1-LaTc**) covered in red-brown by-products.

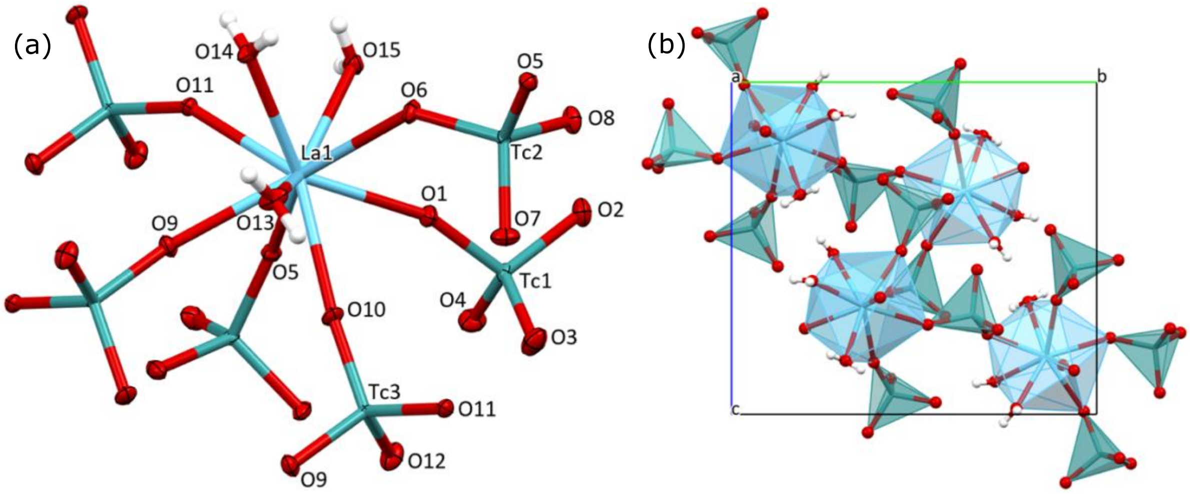

Figure 22: Solid-state structure (a) and unit cell with coordination polyhedra of the metal centres (b) of **1-LaTc**. Selected bond lengths (Å): La1–O1 2.488(3), La1–O5 2.523(2), La1–O6 2.537(3), La1–O9 2.517(2), La1–O10 2.544(2), La1–O11 2.558(2), La1–O13 2.518(2), La1–O14 2.516(3), La1–O15 2.586(2), Tc1–O1 1.736(2), Tc1–O2 1.697(2), Tc2–O5 1.732(2), Tc2–O7 1.697(2), Tc3–O9 1.719(2), Tc3–O12 1.688(2). Selected bond angles (°): La1–O1–Tc1 162.41(13), La1–O5–Tc2 147.47(12), La1–O9–Tc3 159.29(13).

The $[La(TcO_4)_3(H_2O)_3]$ (**1-LaTc**) crystallises in the monoclinic space group $P2_1/c$ and is isostructural to $[La(ReO_4)_3(H_2O)_3]$.[75] The La^{3+} centre forms a distorted tricapped trigonal prism, with three oxygen atoms (O13 – O15) of the aqua ligands and six oxygen atoms (O1, O5, O6, O9 – O11) of the pertechnetato units (Figure 22a). The La–OH_2 bond lengths (O13, O14 and O15, respectively) between La and the coordinated H_2O molecules are 2.518(2) Å, 2.516(3) Å and 2.586(2) Å. The La–OTc bond lengths between La and the pertechnetate units (O1, O5, O6, O9 – O11) range from 2.488(3) – 2.558(2) Å. The Tc–O_{coord} bond lengths (with respect to the oxygen atoms O1, O5, O6, O9 – O11 that coordinate to La) have an average value of 1.726 Å, and are slightly longer than the lengths of Tc to the other uncoordinated O atoms (O2 – O4, O7, O8, O12), with an average Tc–O bond length of 1.700 Å. The $[Tc(1)O_4]$ tetrahedron is bound to only one La^{3+} centre. The $[Tc(2)O_4]$ tetrahedron is bound to two La^{3+} centres bridging them along *b*-axis. The $[Tc(3)O_4]$ tetrahedron is bound to three La^{3+} centres bridging them in all three directions, forming a 3D network which can be described by the *Niggli* formula $^{3}_{\infty}[La(Tc(3)O_4)_{3/3}(Tc(2)O_4)_{2/2}(Tc(1)O_4)_{1/1}(H_2O)_3]$ (Figure 22b). All La–OTc bond lengths agree with reported La–ORe bond lengths.[75]

2.2.3 Type II (Ln = Ce)

$$CeCl_3 + 3\ HTcO_{4(aq)} \rightarrow [Ce(TcO_4)_3(H_2O)]$$

Scheme 2: Synthesis of $[Ce(TcO_4)_3(H_2O)]$ (**2-CeTc**)

The stoichiometric treatment of cerium(III) chloride with pertechnetic acid in aqueous solution (Scheme 2) and subsequent evaporation of the solution in air using a heat lamp led to the formation of yellow crystals of $[Ce(TcO_4)_3(H_2O)]$ (**2-CeTc**) (Figure 23). The crystals do not show any hygroscopic characteristics. The solid-state structure is shown in Figure 24.

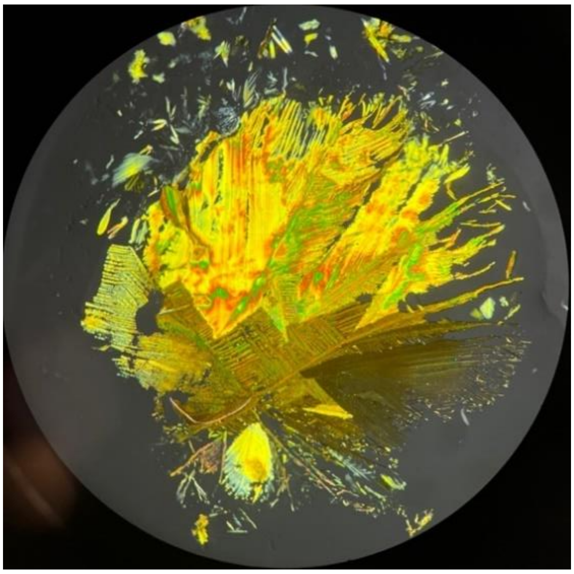

Figure 23: Yellow crystals of $[Ce(TcO_4)_3(H_2O)]$ (**2-CeTc**).

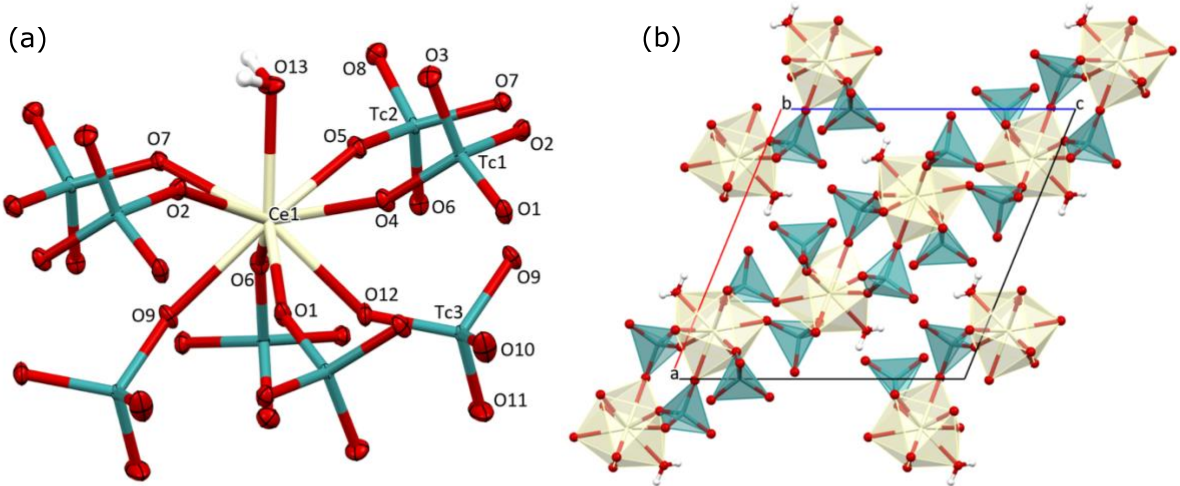

Figure 24: Solid-state structure (a) and unit cell with coordination polyhedra of the metal centres (b) of **2-CeTc**. Selected bond lengths (Å): Ce1–O1 2.518(4), Ce1–O2 2.504(4), Ce1–O4 2.537(4), Ce1–O5 2.455(4), Ce1–O6 2.541(4), Ce1–O7 2.509(4), Ce1–O9 2.483(4), Ce1–O12 2.491(4), Ce1–O13 2.490(4), Tc1–O1 1.712(4), Tc1–O3 1.692(4), Tc2–O5 1.722(4), Tc2–O8 1.687(4), Tc3–O9 1.735(4), Tc3–O10 1.699(4). Selected bond angles (°): Ce1–O1–Tc1 158.75(19), Ce1–O5–Tc2 158.0(2), Ce1–O9–Tc3 152.4(2).

[$Ce(TcO_4)_3(H_2O)_3$] (**2-CeTc**) crystallises in the monoclinic space group $P2_1/n$. The Ce^{3+} centre forms a distorted tricapped trigonal prism, with one oxygen atom (O13) of the water molecules and eight oxygen atoms (O1, O2, O4 – O7, O9 – O12) of the pertechnetate units (Figure 24a). The Ce–OH_2 bond length (O13) between cerium and the coordinated water is 2.490(4) Å. The Ce–OTc bond lengths between the Ce and pertechnetate units (O1, O2, O4 – O7, O9 – O12) range from 2.455(4) – 2.541(4) Å. The Tc–O_{coord} bond lengths (with respect to the oxygen atoms O1, O5, O6, O9–O11 that coordinate to Ce) average to a value of 1.726 Å. They are slightly longer than the lengths of Tc to the other uncoordinated O atoms, with an average Tc–O bond length (O2–O4, O7, O8, O12) of 1.700 Å. Each of the [$Tc(1)O_4$] and [$Tc(2)O_4$] tetrahedra is bound to three Ce^{3+} centres bridging them along *ac*-plane diagonal. The [$Tc(3)O_4$] tetrahedron is bound to two Ce^{3+} centres bridging them along *b*-axis, whereby the contacts can be described by the *Niggli* formula ${}^{2}_{\infty}[Ce(TcO_4)_{2/2}(TcO_4)_{2/2}(TcO_4)_{2/2}(H_2O)]$. The main building unit is a sheet, where the planes are perpendicular to the *ac*-face diagonal (Figure 24b). All Ce–OTc bond lengths here agree with reported Ce–ORe bond lengths as well as reported Ce-OTc bond lengths.[76,77]

2.2.4 Type III (Ln = Pr, Nd, Sm, Eu, Gd, Tb)

$$Pr_6O_{11} + 18\ HTcO_{4(aq)} \rightarrow 6\ [Pr(TcO_4)_3(H_2O)]$$

$$½\ Nd_2O_3 + 3\ HTcO_{4(aq)} \rightarrow [Nd(TcO_4)_3(H_2O)_3]$$

$$½\ Sm_2O_3 + 3\ HTcO_{4(aq)} \rightarrow [Sm(TcO_4)_3(H_2O)_3]$$

$$½\ Eu_2O_3 + 3\ HTcO_{4(aq)} \rightarrow [Eu(TcO_4)_3(H_2O)_3]$$

$$GdCl_3 + 3\ HTcO_{4(aq)} \rightarrow [Gd(TcO_4)_3(H_2O)_3]$$

$$TbCl_3 + 3\ HTcO_{4(aq)} \rightarrow [Tb(TcO_4)_3(H_2O)_3]$$

Scheme 3: Synthesis of $[Ln(TcO_4)_3(H_2O)_3]$ (Ln = Pr (**3-PrTc**), Nd (**4-NdTc**), Sm (**5-SmTc**), Eu (**6-EuTc**), Gd (**7a-GdTc**), Tb (**8-TbTc**) (**LnTc·3(H$_2$O)**))

The stoichiometric treatment of lanthanoid(III) oxide or lanthanoid(III) chloride with pertechnetic acid in aqueous solution (Scheme 3) and subsequent evaporation of the solution in air using a heat lamp led to the formation of yellow-green crystals of $[Pr(TcO_4)_3(H_2O)_3]$ (**3-PrTc**), lilac crystals of $[Nd(TcO_4)_3(H_2O)_3]$ (**4-NdTc**), colourless crystals of $[Sm(TcO_4)_3(H_2O)_3]$ (**5-SmTc**), colourless crystals of $[Eu(TcO_4)_3(H_2O)_3]$ (**6-EuTc**), colourless crystals of $[Gd(TcO_4)_3(H_2O)_3]$ (**7a-GdTc**), colourless crystals of $[Tb(TcO_4)_3(H_2O)_3]$ (**8-TbTc**), (Figure 25). The crystals do not show any hygroscopic characteristics. The datasets for **3-PrTc** and **5-SmTc** show twinning which cannot be modelled satisfactorily. However, they show connectivity, attesting the successful synthesis of these products. The solid-state structure is shown in Figure 26.

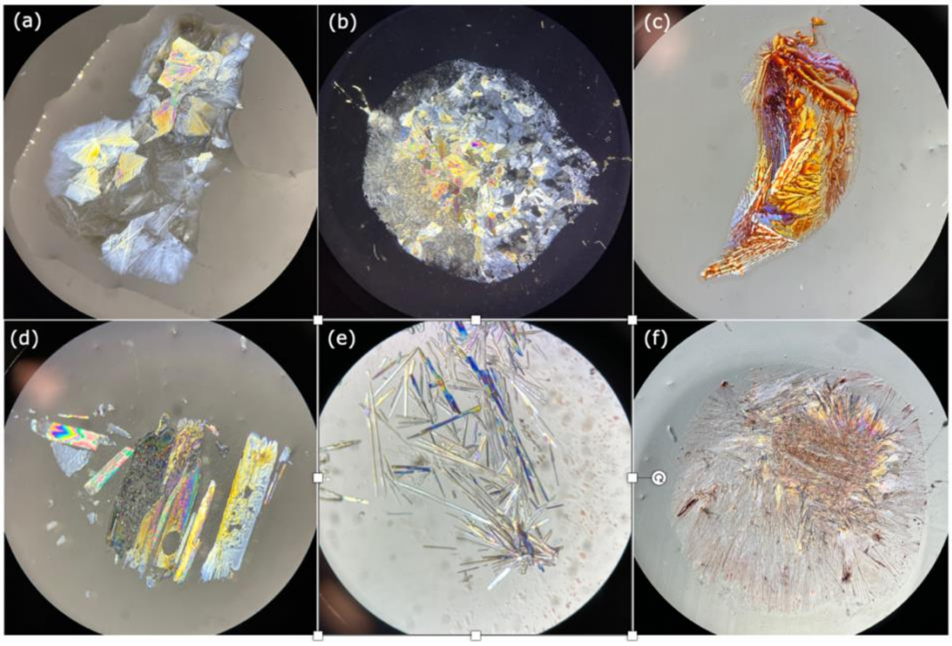

Figure 25: Crystals of $[Ln(TcO_4)_3(H_2O)_3]$ (Ln = (a) Pr (**3-PrTc**), (b) Nd (**4-NdTc**), (c) Sm (**5-SmTc**), (d) Eu (**6-EuTc**), (e) Gd (**7a-GdTc**), (f) Tb (**8-TbTc**) with some covered in red-brown by-products.

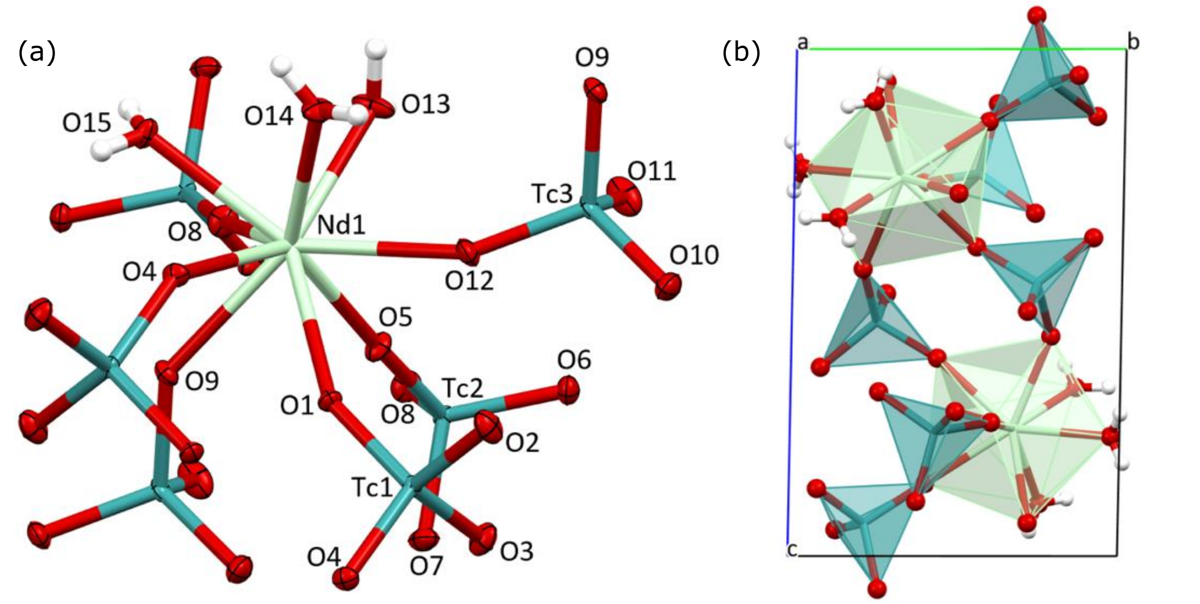

Figure 26: Solid-state structure (a) and unit cell with coordination polyhedra of the metal centres (b) of **LnTc·3(H$_2$O)**, by example of **4-NdTc**. Selected bond lengths (Å) and bond angles (°) are shown in Table 3.

Table 3: Selected bond bond lengths (Å) and bond angles (°) of [Ln(TcO$_4$)$_3$(H$_2$O)$_3$].

Bond Lengths of Ln─OH$_2$ [Å]	Bond Lengths of Ln─OTc [Å]	Bond Lengths of Tc─O [Å]	Bond Angles of Ln─O─Tc [°]
Nd1─O13 2.444(2) Nd1─O14 2.4609(19) Nd1─O15 2.4349(19)	Nd1─O1 2.4418(17) Nd1─O4 2.5188(17) Nd1─O5 2.4453(17) Nd1─O8 2.5639(18) Nd1─O9 2.4544(17) Nd1─O12 2.4815(18)	Tc1─O1 1.7253(17) Tc1─O2 1.6954(19) Tc1─O3 1.7052(18) Tc1─O4 1.7224(17) Tc2─O5 1.7254(17) Tc2─O6 1.7056(18) Tc2─O7 1.6991(18) Tc2─O8 1.7140(18) Tc3─O9 1.7290(17) Tc3─O10 1.6982(19) Tc3─O11 1.7040(19) Tc3─O12 1.7280(18)	Nd1─O1─Tc1 153.27(10) Nd1─O5─Tc2 178.15(11) Nd1─O9─Tc3 140.41(10)
Eu1─O13 2.398(2) Eu1─O14 2.424(2) Eu1─O15 2.393(2)	Eu1─O1 2.408(2) Eu1─O4 2.493(2) Eu1─O5 2.396(2) Eu1─O8 2.565(2) Eu1─O9 2.411(2) Eu1─O12 2.454(2)	Tc1─O1 1.723(2) Tc1─O2 1.701(2) Tc1─O3 1.704(2) Tc1─O4 1.723(2) Tc2─O5 1.729(2) Tc2─O6 1.715(2) Tc2─O7 1.698(2) Tc2─O8 1.713(2) Tc3─O9 1.732(2) Tc3─O10 1.695(3) Tc3─O11 1.702(2) Tc3─O12 1.727(2)	Eu1─O1─Tc1 153.73(12) Eu1─O5─Tc2 179.28(15) Eu1─O9─Tc3 140.55(13)
Gd1─O13 2.381(3) Gd1─O14 2.412(3) Gd1─O15 2.378(3)	Gd1─O1 2.392(3) Gd1─O4 2.481(2) Gd1─O5 2.385(2) Gd1─O8 2.560(3) Gd1─O9 2.401(2) Gd1─O12 2.444(3)	Tc1─O1 1.726(3) Tc1─O2 1.690(3) Tc1─O3 1.708(3) Tc1─O4 1.723(3) Tc2─O5 1.726(3) Tc2─O6 1.711(2) Tc2─O7 1.698(3) Tc2─O8 1.710(3) Tc3─O9 1.727(3) Tc3─O10 1.699(3) Tc3─O11 1.705(3) Tc3─O12 1.724(3)	Gd1─O1─Tc1 153.61(14) Gd1─O5─Tc2 179.54(17) Gd1─O9─Tc3 140.83(14)
Tb1─O13 2.356(3) Tb1─O14 2.391(3) Tb1─O15 2.351(3)	Tb1─O1 2.366(3) Tb1─O4 2.486(3) Tb1─O5 2.360(3) Tb1─O8 2.590(3) Tb1─O9 2.378(3) Tb1─O12 2.433(3)	Tc1─O1 1.728(3) Tc1─O2 1.697(3) Tc1─O3 1.711(3) Tc1─O4 1.717(3) Tc2─O5 1.730(3) Tc2─O6 1.708(3) Tc2─O7 1.697(3) Tc2─O8 1.706(3) Tc3─O9 1.726(3) Tc3─O10 1.695(3) Tc3─O11 1.707(3) Tc3─O12 1.726(3)	Tb1─O1─Tc1 153.78(15) Tb1─O5─Tc2 179.00(17) Tb1─O9─Tc3 141.03(15)

The trihydrates $[Ln(TcO_4)_3(H_2O)_3]$ (Ln = Pr (**3-PrTc**), Nd (**4-NdTc**), Sm (**5-SmTc**), Eu (**6-EuTc**), Gd (**7a-GdTc**), Tb (**8-TbTc**) (**LnTc·3(H$_2$O)**)) crystallise in the triclinic space group *P*-1. The Ln^{3+} centre forms a distorted tricapped trigonal prism, with three oxygen atoms (O13–O15) of the coordinating water molecules and six oxygen atoms of the pertechnetate ligands (Figure 26a, example shown for **4-NdTc**). The Ln–OH_2 bond lengths (O13, O14 and O15, respectively) between the lanthanoids and the coordinated aqua ligands are 2.444(2) Å, 2.4609(19) Å and 2.4349(19) Å (**4-NdTc**), 2.398(2) Å, 2.393(2) Å and 2.424(2) Å (**6-EuTc**), 2.381(3) Å, 2.412(3) Å and 2.378(3) Å (**7a-GdTc**), and 2.381(3) Å, 2.391(3) Å and 2.351(3) Å (**8-TbTc**). The Ln–OTc bond lengths between the lanthanoid atoms and pertechnetato ligands (O1, O4, O5, O8, O9, O12) range from 2.4418(17) – 2.5639(18) Å, 2.396(2) – 2.565(2) Å, 2.385(3) – 2.560(3) Å, 2.360(3) – 2.590(3) Å for Nd, Eu, Gd and Tb, respectively. The Tc–O_{coord} bond lengths (with respect to the oxygen atoms O1, O4, O5, O8, O9, O12 that coordinate to the lanthanoid) average to values of 1.725 Å, 1.723 Å, 1.722 Å for Tc–ONd, Tc–OEu, Tc–OGd and Tc–OTb, respectively. They are slightly longer than the Tc–O bond lengths of Tc to its uncoordinated O atoms (O2, O3, O6, O7, O10, O11), which average to 1.701 Å, 1.703 Å, 1.702 Å, 1.701 Å for **4-NdTc**, **6-EuTc**, **7a-GdTc** and **8-TbTc**, respectively. Each of the $[Tc(1)O_4]$ and $[Tc(2)O_4]$ tetrahedra in **LnTc·3(H$_2$O)** is bound to two Ln^{3+} centres, bridging them along the *c*-axis. The $[Tc(3)O_4]$ tetrahedron is bound to two Ln^{3+} centres bridging them along the *a*-axis, whereby the contacts can be described by the *Niggli* formula ${}^{2}_{\infty}[Ln(TcO_4)_{2/2}(TcO_4)_{2/2}(TcO_4)_{2/2}(H_2O)_3]$. The main building unit is a sheet in the *ac*-plane, held together by hydrogen bonding (Figure 26b). All Ln–OTc (Ln = Pr, Nd, Sm – Tb) bond lengths here agree with reported Ln–ORe (Ln = Pr, Nd, Sm – Tb) bond lengths.[78–83]

The room temperature solid-state UV-Vis absorption spectra for **3-PrTc** and **4-NdTc** are shown in Figure 27 and Figure 28 respectively. These spectra confirm the presence of the Laporte forbidden f–f transition from the $^3H_4$ ground state of Pr^{3+} and from the $^4I_{9/2}$ ground state of Nd^{3+}, which have been carefully assigned by Carnall and co-workers.[84] The transitions found are comparable to those found for $[Ln(ReO_4)(H_2O)_4Cl]Cl\cdot(H_2O)$ (Ln = Pr–Nd) reported by Polinski and co-workers.[83]

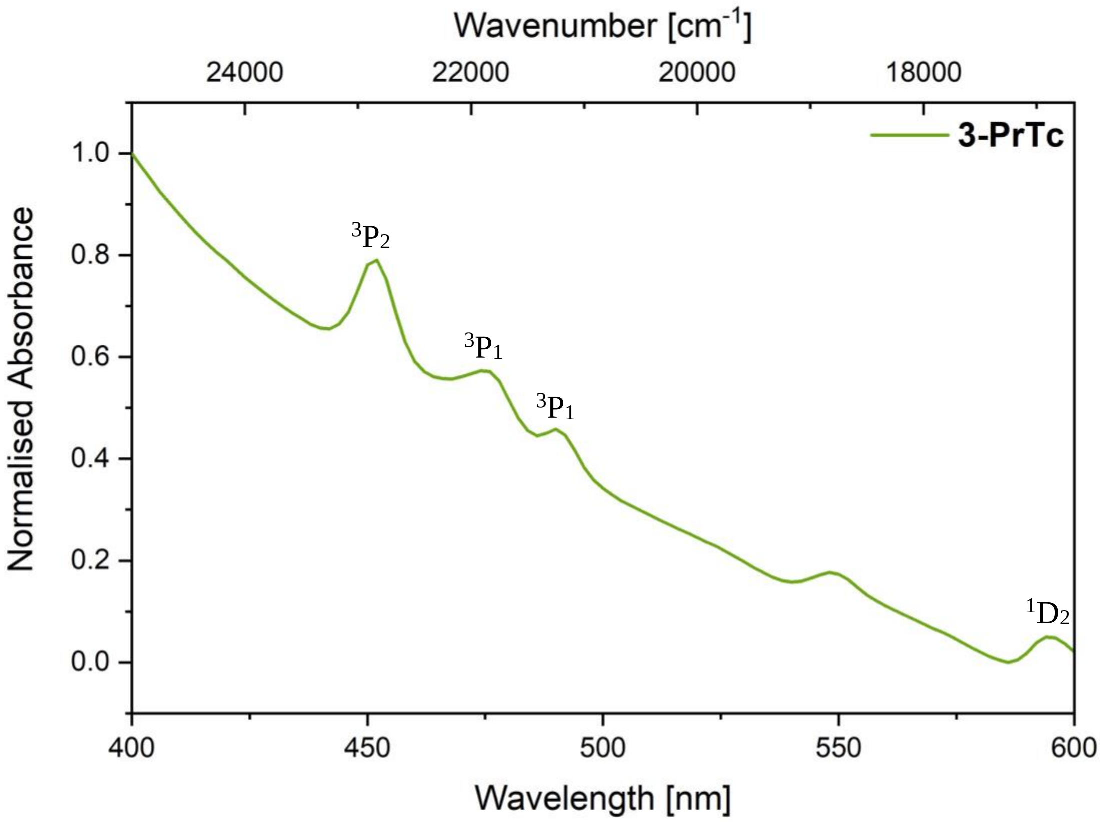

Figure 27: Solid-state UV-vis absorption spectrum for **3-PrTc**.

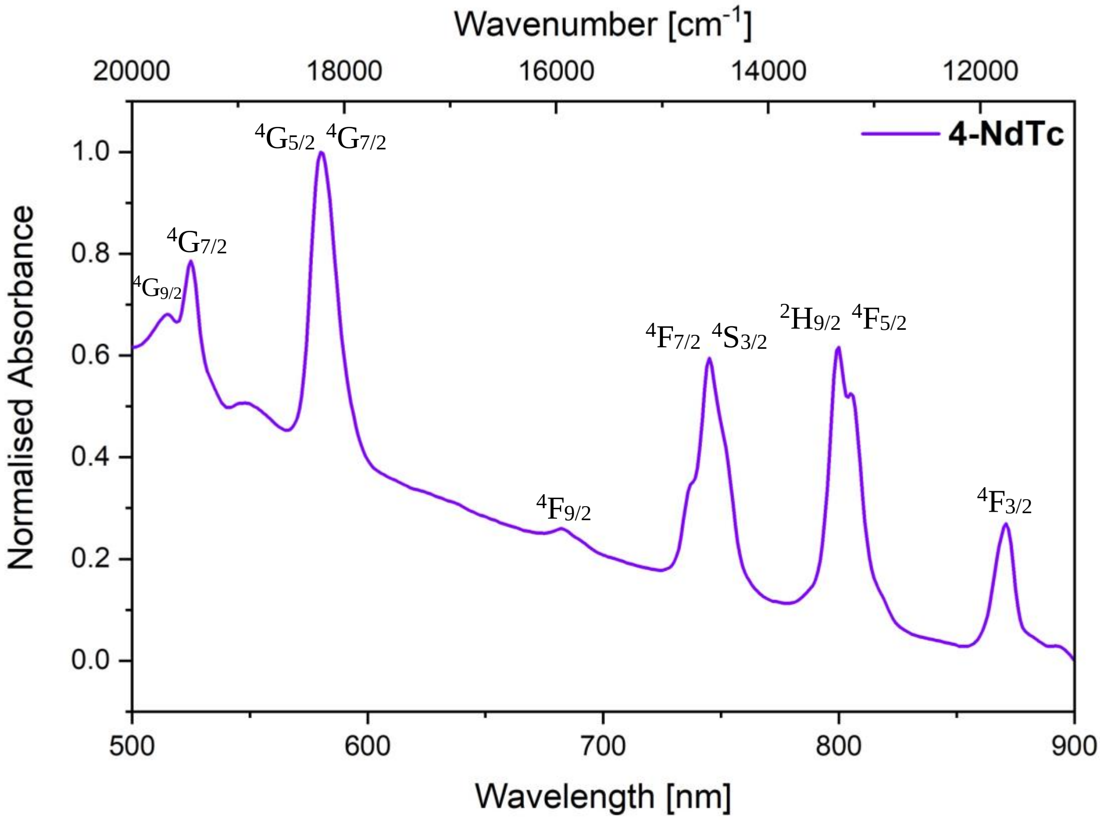

Figure 28: Solid-state UV-vis absorption spectrum for **4-NdTc**.

2.2.5 Type IV (Ln = Gd)

At the centre of the lanthanoid series, the stoichiometric treatment of gadolinium(III) chloride with pertechnetic acid in aqueous solution (Scheme 3) and subsequent evaporation of the solution in air using a heat lamp led to gadolinium crystallising both as a trihydrate and a tetrahydrate. The former has been described in the section above, the latter is described below. The colourless crystals $[Gd(TcO_4)_3(H_2O)_3](H_2O)$ (**7b-GdTc**) are shown in Figure 29. The crystals do not show any hygroscopic characteristics. The solid-state structure is shown in Figure 30.

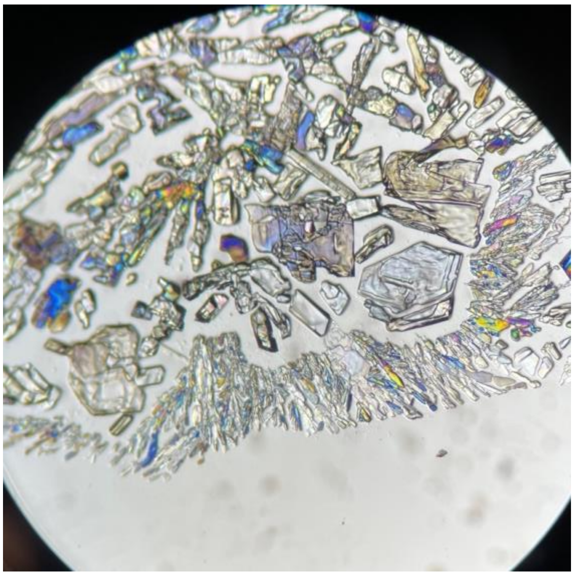

Figure 29: Colourless crystals of $[Gd(TcO_4)_3(H_2O)_3](H_2O)$ (**7b-GdTc**).

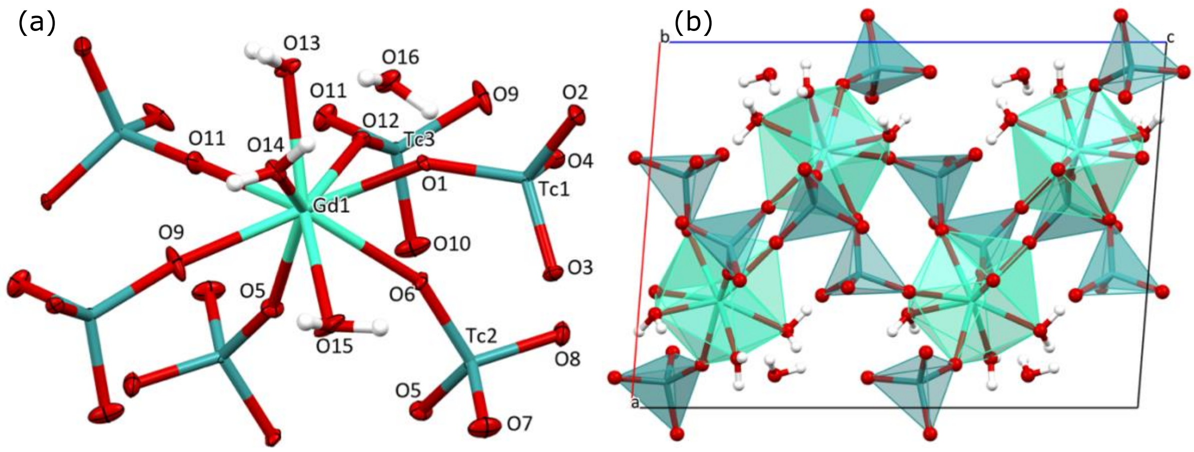

Figure 30: Solid-state structure (a) and unit cell with coordination polyhedra of the metal centres (b) of **8b-GdTc**. Selected bond lengths (Å): Gd1–O1 2.388(4), Gd1–O5 2.377(5), Gd1–O6 2.469(4), Gd1–O9 2.430(5), Gd1–O11 2.541(5), Gd1–O12 2.464(4), Gd1–O13 2.408(5), Gd1–O14 2.402(5), Gd1–O15 2.388(5), Tc1–O1 1.739(5), Tc1–O4 1.699(5), Tc2–O5 1.726(5), Tc2–O8 1.696(5), Tc3–O9 1.715(5), Tc3–O10 1.689(5). Selected bond angles (°): Gd1–O1–Tc1 138.4(2), Gd1–O5–Tc2 159.0(3), Gd1–O9–Tc3 168.5(3).

The tetrahydrate $[Gd(TcO_4)_3(H_2O)_3](H_2O)$ (**7b-GdTc**) crystallises in the triclinic space group $P2_1/c$ (Figure 30a). The Gd^{3+} centre forms a distorted tricapped trigonal prism, with three oxygen atoms (O13 – O15) of the coordinating water molecules and six oxygen atoms of the pertechnetate ligands. An unbound water molecule is present in the crystal structure. The Ln–OH_2 bond lengths (O13, O14 and O15, respectively) between the Gd and the coordinated waters are 2.408(5) Å, 2.402(5) Å and 2.388(5) Å. The Gd–OTc (O1, O5, O6, O9, O11, O12) bond lengths range from 2.377(5) – 2.469(4) Å. The Tc–O_{coord} bond lengths of the technetium to the respective O atom bound to Gd average to 1.724 Å. They are slightly longer than the Tc–O bond lengths of Tc to its uncoordinated O atoms (O2, O3, O4, O7, O8, O10), which average to 1.697 Å. The $[Tc(1)O_4]$ tetrahedron is bound to only one Gd^{3+} centre. The $[Tc(2)O_4]$ tetrahedron is bound to two Gd^{3+} centres bridging them along the *c*-axis. The $[Tc(3)O_4]$ tetrahedron is bound to three Gd^{3+} centres bridging them in all three directions, whereby the contacts can be described by the *Niggli* formula ${}^{2}_{\infty}[Gd(TcO_4)_{3/3}(TcO_4)_{2/2}(TcO_4)_{1/1}(H_2O)_3]$. The main building unit is a sheet held together by hydrogen bonds. Residing in the interlayer space is an unbound water molecule (Figure 30b). All Gd–OTc bond lengths here agree with reported Gd–ORe bond lengths.[80]

2.2.6 Type V (Ln = Dy, Ho, Er, Tm, Yb, Lu)

$$\tfrac{1}{2}\ Dy_2O_3 + 3\ HTcO_{4(aq)} \rightarrow [Dy(TcO_4)_3(H_2O)_3](H_2O)$$

$$\tfrac{1}{2}\ Ho_2O_3 + 3\ HTcO_{4(aq)} \rightarrow [Ho(TcO_4)_3(H_2O)_3](H_2O)$$

$$\tfrac{1}{2}\ Er_2O_3 + 3\ HTcO_{4(aq)} \rightarrow [Er(TcO_4)_3(H_2O)_3](H_2O)$$

$$\tfrac{1}{2}\ Tm_2O_3 + 3\ HTcO_{4(aq)} \rightarrow [Tm(TcO_4)_3(H_2O)_3](H_2O)$$

$$\tfrac{1}{2}\ Yb_2O_3 + 3\ HTcO_{4(aq)} \rightarrow [Yb(TcO_4)_3(H_2O)_3](H_2O)$$

$$\tfrac{1}{2}\ Lu_2CO_3 + 3\ HTcO_{4(aq)} \rightarrow [Lu(TcO_4)_3(H_2O)_3](H_2O)$$

Scheme 4: Synthesis of $[Ln(TcO_4)_3(H_2O)_3](H_2O)$ (Ln = Dy (**9-DyTc**), Ho (**10-HoTc**), Er (**11-ErTc**), Tm (**12-TmTc**), Yb (**13-YbTc**), Lu (**14-LuTc**)) (**LnTc·4(H_2O)**).

The stoichiometric treatment of lanthanoid(III) oxide or lanthanoid(III) carbonate with pertechnetic acid in aqueous solution (Scheme 4) and subsequent evaporation of the solution in air using a heat lamp led to the formation of colourless crystals of $[Dy(TcO_4)_3(H_2O)_3](H_2O)$ (**9-DyTc**), pale pink crystals of $[Ho(TcO_4)_3(H_2O)_3](H_2O)$ (**10-HoTc**), pale pink crystals of $[Er(TcO_4)_3(H_2O)_3](H_2O)$ (**11-ErTc**), colourless crystals of $[Tm(TcO_4)_3(H_2O)_3](H_2O)$ (**12-TmTc**), colourless crystals of $[Yb(TcO_4)_3(H_2O)_3](H_2O)$ (**13-YbTc**), colourless crystals of $[Lu(TcO_4)_3(H_2O)_3](H_2O)$ (**14-LuTc**), (Figure 31). The crystals do not show any hygroscopic characteristics. The solid-state structure is shown in Figure 32.

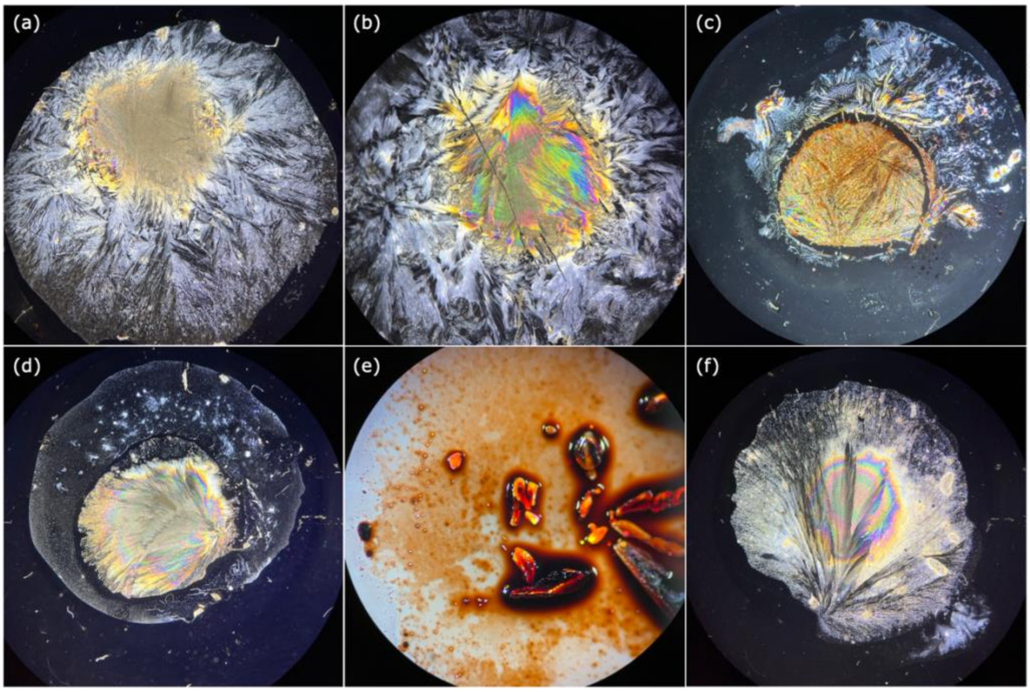

Figure 31: Crystals of $[Ln(TcO_4)_3(H_2O)_3](H_2O)$ (Ln = (a) Dy (**10-DyTc**), (b) Ho (**11-HoTc**), (c) Er (**12-ErTc**), (d) Tm (**13-TmTc**), (e) Yb (**14-YbTc**), (f) Lu (**15-LuTc**)) with some covered in red-brown by-products.

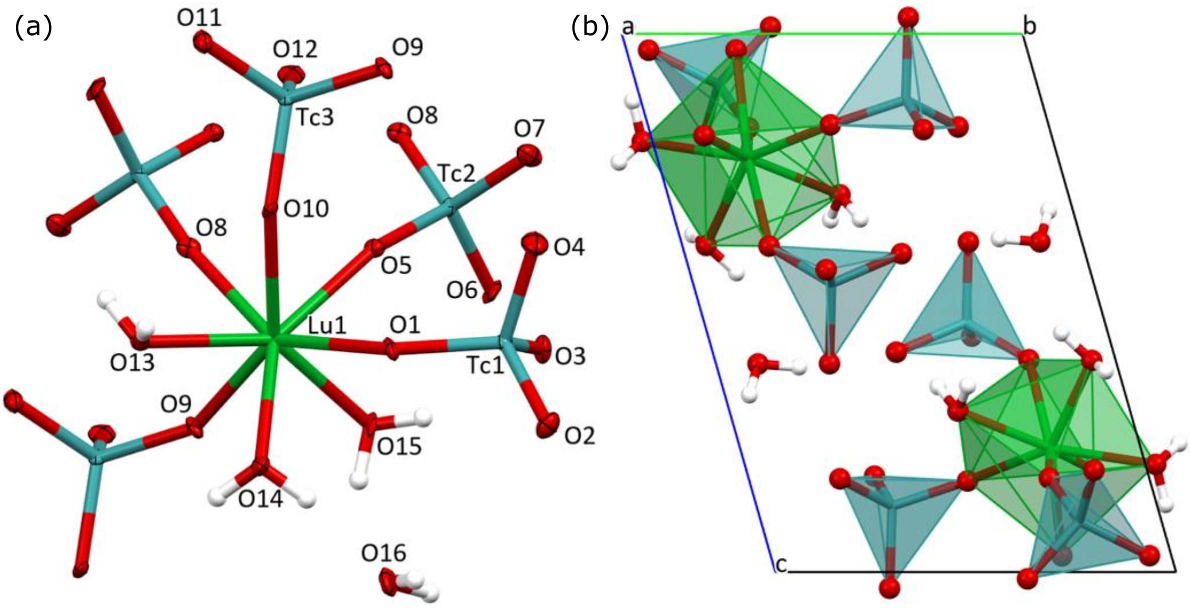

Figure 32: Solid-state structure (a) and unit cell with coordination polyhedra of the metal centres (b) of **LnTc·4(H₂O)**, shown for **15-LuTc**. Selected bond lengths (Å) and bond angles (°) are shown in Table 4.

Table 4: Selected bond bond lengths (Å) and bond angles (°) of $[Ln(TcO_4)_3(H_2O)_3](H_2O)$.

Bond Lengths of Ln─OH₂ [Å]	Bond Lengths of Ln─OTc [Å]	Bond Lengths of Tc─O [Å]	Bond Angles of Ln─O─Tc [°]
Dy1─O13 2.335(3) Dy1─O14 2.350(3) Dy1─O15 2.349(4)	Dy1─O1 2.362(4) Dy1─O5 2.324(3) Dy1─O8 2.331(4) Dy1─O9 2.356(3) Dy1─O10 2.402(3)	Tc1─O1 1.736(4) Tc1─O2 1.712(4) Tc2─O5 1.734(3) Tc2─O6 1.692(4) Tc3─O9 1.729(4) Tc3─O12 1.693(4)	Dy1─O1─Tc1 139.77(19) Dy1─O5─Tc2 158.9(2) Dy1─O9─Tc3 148.9(2)
Ho1─O13 2.320(9) Ho1─O14 2.334(10) Ho1─O15 2.338(9)	Ho1─O1 2.341(9) Ho1─O5 2.318(9) Ho1─O8 2.311(9) Ho1─O9 2.337(9) Ho1─O10 2.388(9)	Tc1─O1 1.737(9) Tc1─O2 1.701(9) Tc2─O5 1.727(9) Tc2─O6 1.705(9) Tc3─O9 1.731(9) Tc3─O12 1.681(10)	Ho1─O1─Tc1 140.5(5) Ho1─O5─Tc2 159.9(5) Ho1─O9─Tc3 150.1(5)
Er1─O13 2.313(2) Er1─O14 2.321(2) Er1─O15 2.328(2)	Er1─O1 2.339(2) Er1─O5 2.303(2) Er1─O8 2.306(2) Er1─O9 2.334(2) Er1─O10 2.370(2)	Tc1─O1 1.735(2) Tc1─O2 1.710(2) Tc2─O5 1.737(2) Tc2─O6 1.695(2) Tc3─O9 1.727(2) Tc3─O12 1.690(2)	Er1─O1─Tc1 139.92(11) Er1─O5─Tc2 159.21(13) Er1─O9─Tc3 149.70(12)
Tm1─O13 2.3030(17) Tm1─O14 2.3169(16) Tm1─O15 2.3201(17)	Tm1─O1 2.3282(16) Tm1─O5 2.2953(17) Tm1─O8 2.2956(17) Tm1─O9 2.3221(17) Tm1─O10 2.3614(16)	Tc1─O1 1.7370(17) Tc1─O2 1.7071(18) Tc2─O5 1.7343(17) Tc2─O6 1.6978(18) Tc3─O9 1.7270(17) Tc3─O12 1.6920(17)	Tm1─O1─Tc1 140.18(9) Tm1─O5─Tc2 159.34(10) Tm1─O9─Tc3 150.79(10)
Yb1─O13 2.305(3) Yb1─O14 2.302(3) Yb1─O15 2.287(3)	Yb1─O1 2.328(3) Yb1─O5 2.279(3) Yb1─O8 2.292(3) Yb1─O9 2.323(3) Yb1─O10 2.354(3)	Tc1─O1 1.738(3) Tc1─O2 1.709(3) Tc2─O5 1.736(3) Tc2─O6 1.694(3) Tc3─O9 1.725(3) Tc3─O12 1.689(3)	Yb1─O1─Tc1 139.74(15) Yb1─O5─Tc2 159.83(16) Yb1─O9─Tc3 150.97(15)
Lu1─O13 2.351(8) Lu1─O14 2.194(8) Lu1─O15 2.308(7)	Lu1─O1 2.305(7) Lu1─O5 2.278(7) Lu1─O8 2.282(7) Lu1─O9 2.300(7) Lu1─O10 2.351(8)	Tc1─O1 1.733(7) Tc1─O2 1.712(8) Tc2─O5 1.731(8) Tc2─O6 1.691(8) Tc3─O9 1.738(7) Tc3─O12 1.690(8)	Lu1─O1─Tc1 140.7(4) Lu1─O5─Tc2 159.9(4) Lu1─O9─Tc3 151.6(4)

The tetrahydrates [$Ln(TcO_4)_3(H_2O)_3$](H_2O) (Ln = Dy (**9-DyTc**), Ho (**10-HoTc**), Er (**11-ErTc**), Tm (**12-TmTc**), Yb (**13-YbTc**), Lu (**14-LuTc**)) (**LnTc·4(H2O)**) crystallise in the triclinic space group *P*-1 (Figure 32a, example shown for **14-LuTc**). The Ln^{3+} centre forms a square antiprism, with three oxygen atoms (O13 – O15) of the coordinating water molecules and five oxygen atoms of the pertechnetate units. An unbound water molecule is present in the crystal structure. The Ln–OH_2 bond lengths (O13, O14 and O15, respectively) between the lanthanoids and the coordinated waters are 2.335(3) Å, 2.349(4) Å and 2.350(3) Å (**9-DyTc**), 2.320(9) Å, 2.334(1) Å and 2.338(9) Å (**10-HoTc**), 2.328(2) Å, 2.313(2) Å and 2.321(2) Å (**11-ErTc**), 2.3030(17) Å, 2.3201(17) Å, 2.3169(16) Å (**12-TmTc**), 2.305(3) Å, 2.302(3) Å, 2.287(3) Å (**13-YbTc**), and 2.283(7) Å, 2.294(8) Å, 2.308(7) Å (**14-LuTc**). The Ln–OTc bond lengths between the lanthanoids and pertechnetate ligands (O1, O5, O8, O9, O10) range from 2.324(3) – 2.402(3) Å, 2.311(9) – 2.388(9) Å, 2.303(2) – 2.370(2) Å, 2.2953(17) – 2.3614(16) Å, 2.279(3) – 2.354(3) Å and 2.278(7) Å – 2.351(8) Å for **9-DyTc**, **10-HoTc**, **11-ErTc**, **12-TmTc**, **13-YbTc** and **14-LuTc**, respectively. The Tc–O_{coord} bond lengths of the Tc to the respective O atom (O1, O5, O8, O9, O10) average to 1.735 Å (Tc–ODy), 1.736 Å (Tc–OHo), 1.727 Å (Tc–OEr), 1.735 Å (Tc–OTm), 1.735 Å (Tc–OYb), and 1.735 Å (Tc–OLu). They are slightly longer than the Tc–O bond lengths of Tc to its uncoordinated O atoms (O2, O3, O4, O6, O7, O11, O12), which average to 1.700 Å, 1.693 Å, 1.699 Å, 1.701 Å, 1.700 Å, 1.699 Å for all **LnTc·4(H2O)** complexes. In each case, the [$Tc(1)O_4$] tetrahedron is bound to only one Ln^{3+} centre, while the [$Tc(2)O_4$] tetrahedron is bound to two Ln^{3+} centres bridging them along the *c*-axis. The [$Tc(3)O_4$] tetrahedron is bound to two Ln^{3+} centres bridging them along the *a*-axis, whereby the contacts can be described by the *Niggli* formula $^{1}_{\infty}$ [$Ln(TcO_4)_{2/2}(TcO_4)_{2/2}(TcO_4)_{1/1}(H_2O)_3$] The main building unit is a chain, running along the *a*-axis. Residing between the chains in the *ac*-plane is an unbound water molecule (Figure 32b). All Ln–OTc (Ln = Dy – Lu) bond lengths in **LnTc·4(H2O)** agree with reported Ln–ORe (Ln = Dy – Lu) bond lengths.[83,85,86]

The room temperature solid-state UV-Vis absorption spectra for **9-DyTc**, **10-HoTc**, **11-ErTc** and **12-TmTc** are shown in Figure 33, Figure 34, Figure 35, and Figure 36 respectively. These spectra confirm the presence of the Laporte forbidden f–f transition from the $^6H_{15/2}$ ground state of Dy^{3+}, the $^5I_8$ ground state of Ho^{3+}, the $^4I_{15/2}$ ground state of Er^{3+} and the $^3H_6$ ground state of Tm^{3+}, which have been assigned by Carnall and co-workers.[84] The transitions found are comparable to those found for [$Ln(ReO_4)(H_2O)_2$] (Ln = Ho–Er) reported by Polinski and co-workers.[83]

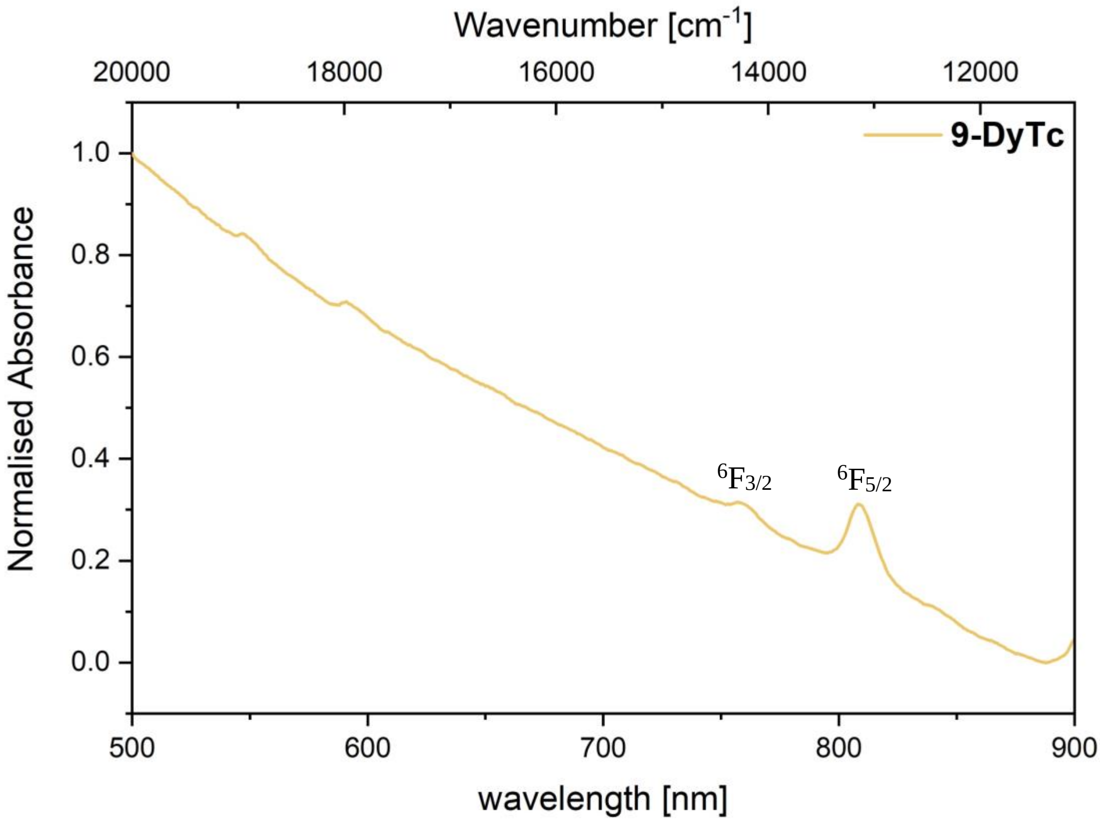

Figure 33: Solid-state UV-vis absorption spectrum for **9-DyTc**.

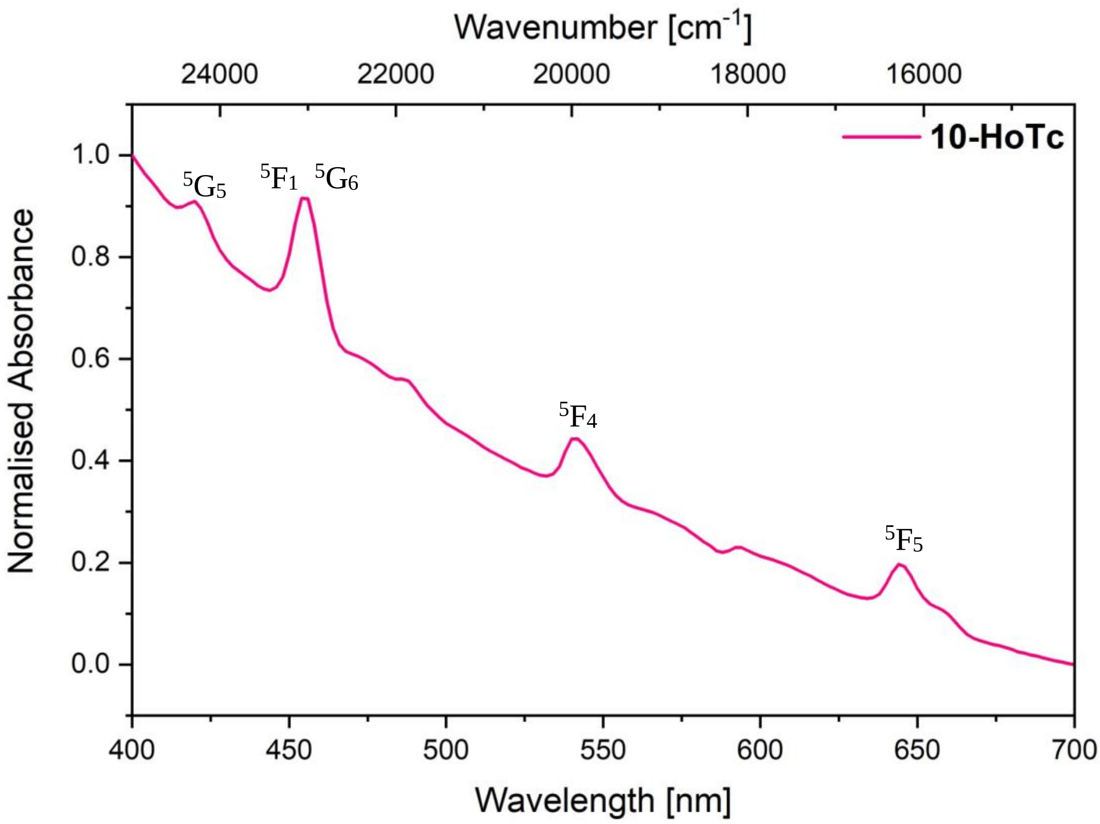

Figure 34: Solid-state UV-vis absorption spectrum for **10-HoTc**.

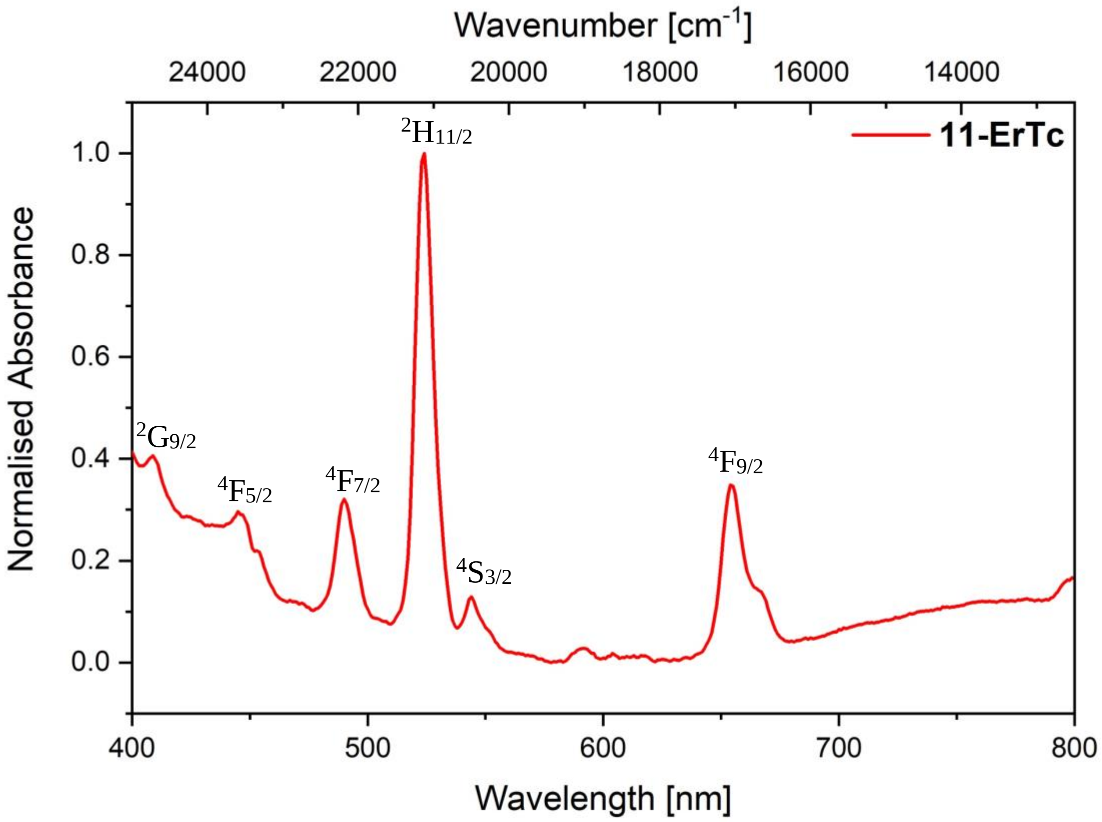

Figure 35: Solid-state UV-vis absorption spectrum for **11-ErTc**.

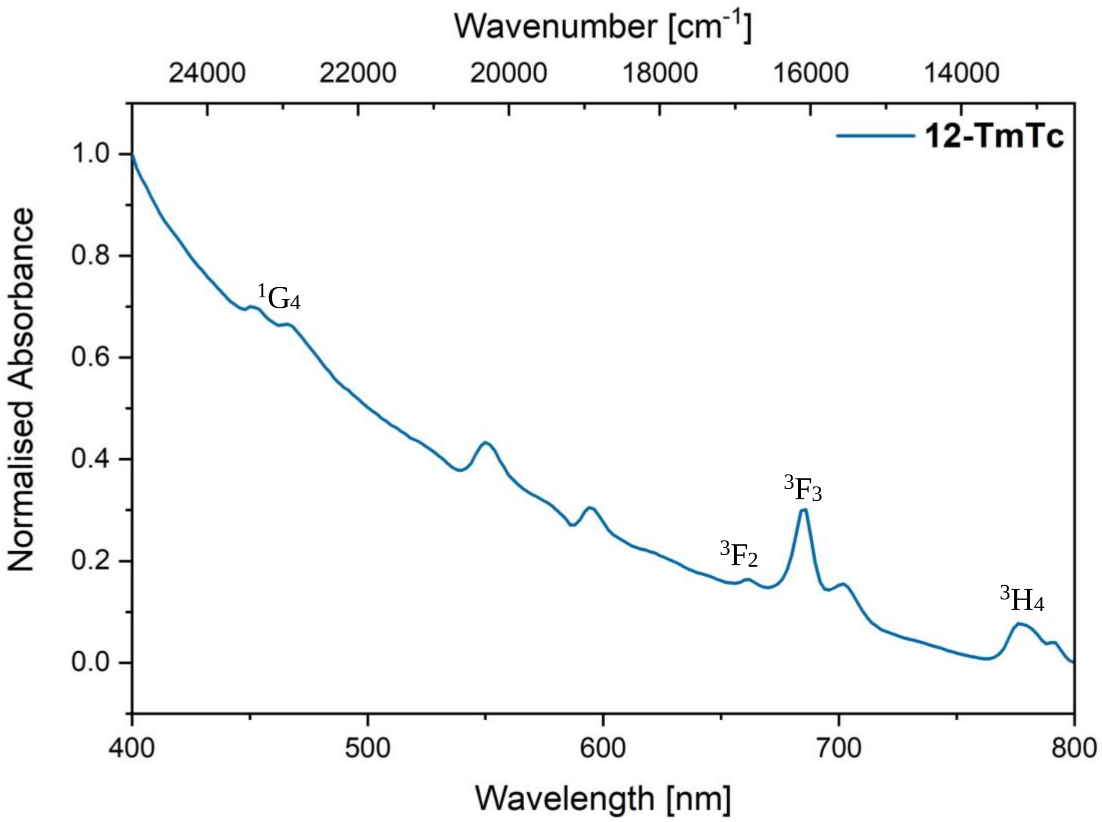

Figure 36: Solid-state UV-vis absorption spectrum for **12-TmTc**.

2.2.7 Type VI (Heteroleptic Cl, Ln = Ce)

$$CeCl_3 + HTcO_{4(aq)} \rightarrow [Ce(TcO_4)(H_2O)_4Cl]Cl\cdot(H_2O)$$

Scheme 5: Synthesis of $[Ce(ReO_4)(H_2O)_4Cl]Cl\cdot(H_2O)$ (**15-CeTcCl**)).

The 1:1 treatment of cerium(III) chloride with pertechnetic acid in aqueous solution (Scheme 5) and subsequent evaporation of the solution in air using a heat lamp led to the formation of yellow crystals of $[Ce(TcO_4)(H_2O)_4Cl]Cl\cdot(H_2O)$ (**15-CeTcCl**) (Figure 37). The crystals do not show any hygroscopic characteristics. The solid-state structure is shown in Figure 38.

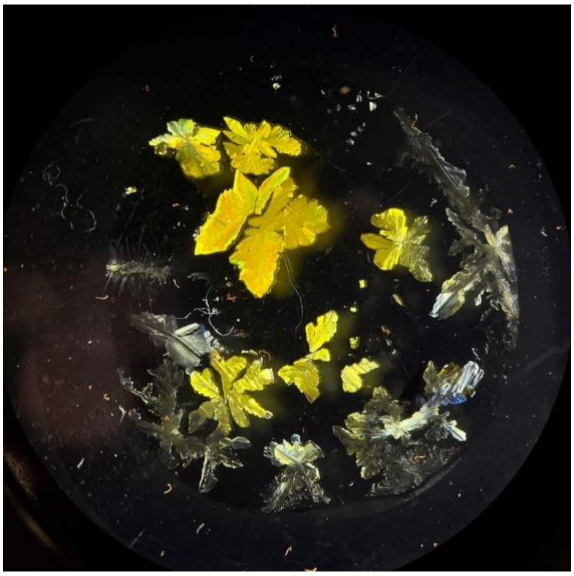

Figure 37: Yellow crystals of [Ce (**15-CeTcCl**).

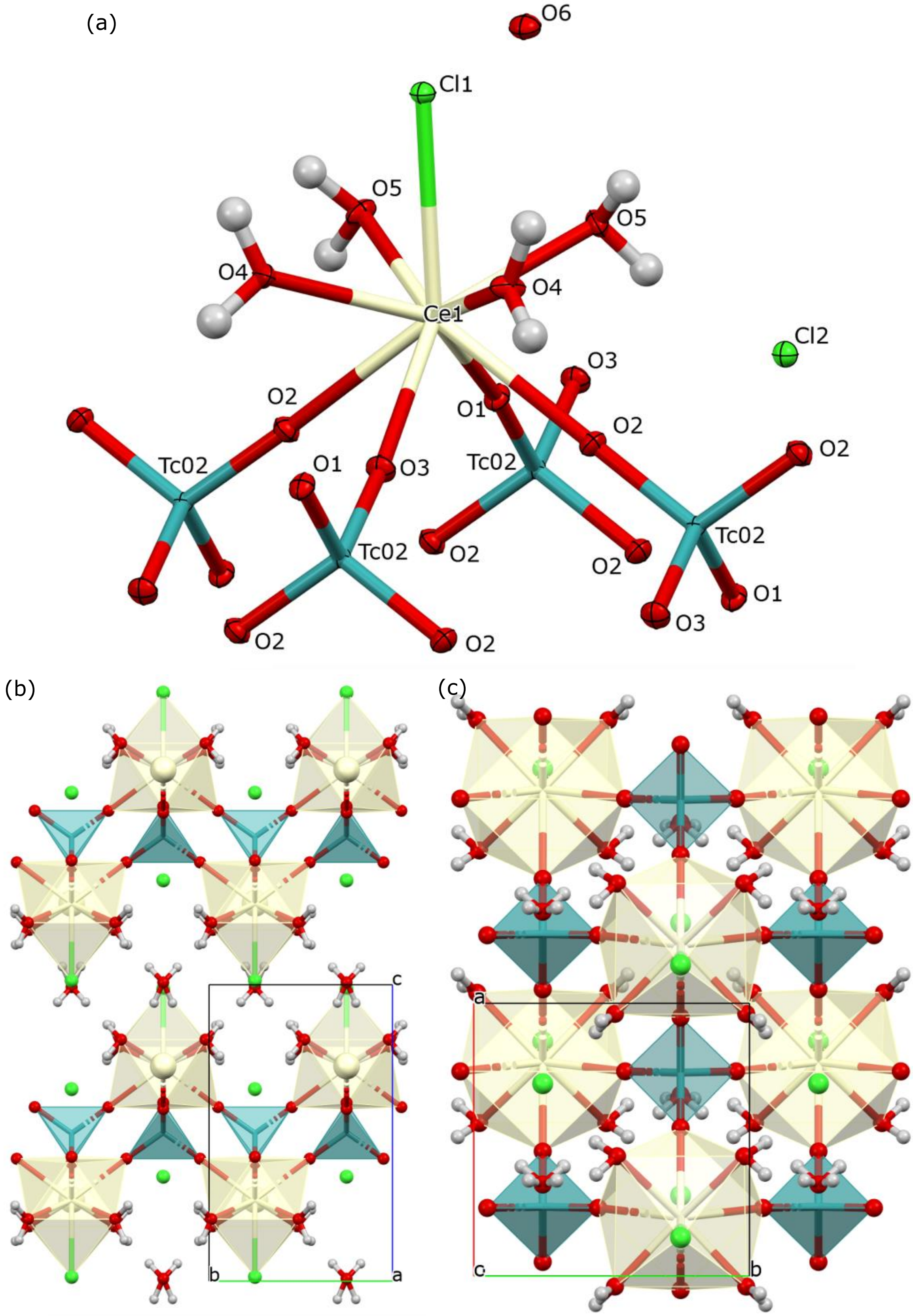

Figure 38: Solid-state structure (a) and unit cell with coordination polyhedra of the metal centres (b) as sheets (c) of **15-CeTcCl**. Selected bond lengths (Å): Ce1─O4 2.460(2), Ce1─O5 2.487(2), Ce1─O1 2.546(3), Ce1─O2 2.584(2), Ce1─O3 2.548(3), Tc02─O1 1.715(3), Tc02─O2 1.708(2), Tc02─O3 1.715(3), Ce1─Cl1 2.9201(11).

$[Ce(TcO_4)(H_2O)_4Cl]Cl\cdot(H_2O)$ (**15-CeTcCl**) crystallises in the monoclinic space group $P2_1/m$ and is isostructural to $[Ln(ReO_4)(H_2O)_4Cl]Cl\cdot(H_2O)$ (Ln = La – Nd).[83] The Ce^{3+} centre forms a mono-capped square antiprism, with four oxygen atoms (symmetrical O4 – O5) of the coordinating water molecules attaching to the top of the mono-capped square antiprism, four oxygen atoms of the pertechnetate units (symmetrical O2, and O1 and O3) coordinating to the bottom and one capping chlorine (Cl1) in the apical position and orientated to the interlayer space (Figure 38a). An unbound water molecule (O6) and chloride (Cl2) are present in the crystal structure. The Ln–OH_2 bond lengths (O4 and O5, respectively) between the lanthanoids and the coordinated waters are 2.460(2) Å and 2.487(2) Å. The Ln–OTc bond lengths between the lanthanoids and pertechnetate ligands (O1 – O3) range from 2.546(3) – 2.584(2) Å. The Tc–O_{coord} bond lengths of the Tc to the respective O atom (O1 – O3) average 1.712 Å (Tc–OCe). The Ln–Cl bond lengths between the lanthanoids and the coordinated chloride is 2.9201(11) Å. In each case, the $[Tc(02)O_4]$ tetrahedron is bound to four Ln^{3+} centre bridging them along the *ab*-plane, whereby the contacts can be described by the *Niggli* formula $^{2}_{\infty}[Ce(TcO_4)_{4/4}(H_2O)_4Cl]$ (Figure 38b). The main building unit is a sheet held together by hydrogen bonds (Figure 38c). Residing in the interlayer space is an unbound water molecule and chloride anion. (Figure 38b) All Ce–OTc bond lengths in **15-CeTcCl** agree with reported Ce–ORe bond lengths.[83]

2.2.8 Type VII (Heteroleptic Br, Ln = La)

$$LaBr_3 + HTcO_{4(aq)} \rightarrow [La(TcO_4)_2(H_2O)_5]Br\cdot(H_2O)_2$$

Scheme 6: Synthesis of $[La(TcO_4)2(H_2O)_5]Br\cdot(H_2O)_2$ (**16-LaTcBr**)).

The 1:1 treatment of lanthanum(III) bromide with pertechnetic acid in aqueous solution (Scheme 6) and subsequent evaporation of the solution in air led to the formation of yellow crystals of $[La(TcO_4)_2(H_2O)_5]Br\cdot(H_2O)_2$ (**16-LaTcBr**) (Figure 39). The crystals do not show any hygroscopic characteristics. The solid-state structure is shown in Figure 40.

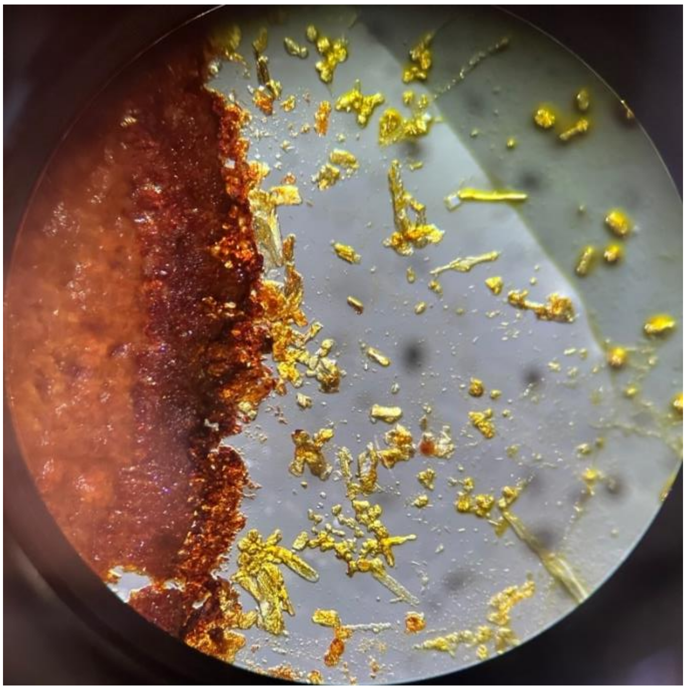

Figure 39: Yellow crystals of $[La(TcO_4)_2(H_2O)_5]Br\cdot(H_2O)_2$ (**16-LaTcBr**).

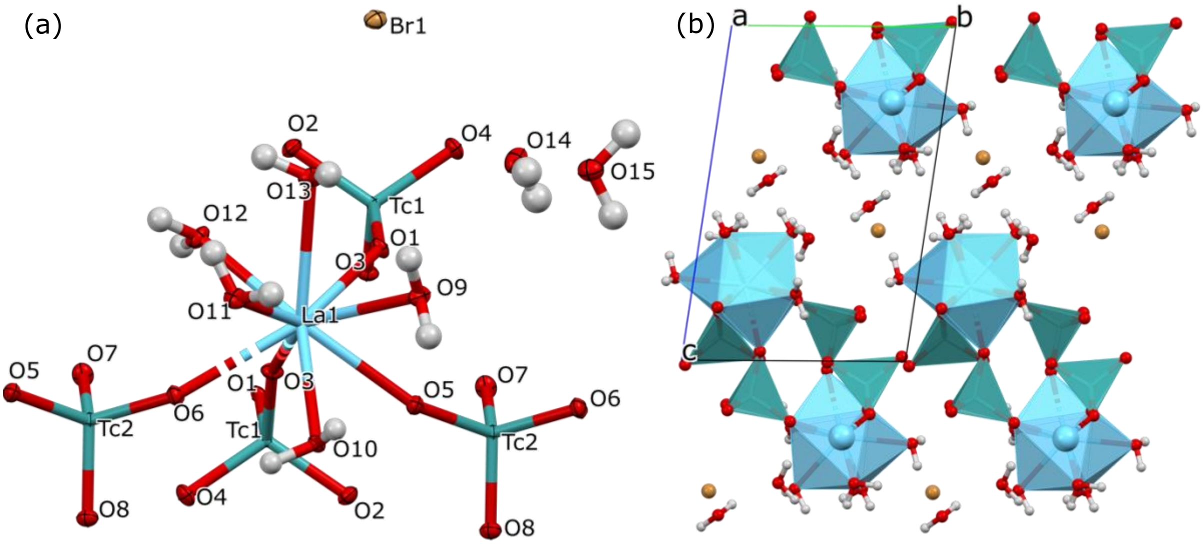

Figure 40: Solid-state structure (a) and unit cell with coordination polyhedra of the metal centres (b) of **16-LaTcBr**. Selected bond lengths (Å): La1—O1 2.535(3), La1—O3 2.554(3), La1—O5 2.508(3), La1—O6 2.507(3), La1—O9 2.543(3), La1—O10 2.623(2), La1—O11 2.529(3), La1—O12 2.516(2), La1—O13 2.607(3), Tc1—O1 1.740(3), Tc1—O2 1.699(3), Tc1—O3 1.730(3), Tc1—O4 1.706(3), Tc2—O5 1.730(3), Tc2—O6 1.732(3), Tc2—O7 1.398(3), Tc2—O8 1.697(3).

$[La(TcO_4)_2(H_2O)_5]Br\cdot(H_2O)_2$ (**16-LaTcBr**) crystallises in the triclinic space group *P*-1. The La^{3+} centre forms a mono-capped square antiprism, with three oxygen atoms (O9, O11 – O12) of the coordinating water molecules and one oxygen atom (O3) of the pertechnetate unit attaching to the top of the mono-capped square antiprism, one oxygen atom (O10) of the coordinating water molecule and three oxygen (O3, O5 – O6) of the pertechnetate units attaching to the bottom and one capping oxygen (O13) of the coordinating water molecule in the apical position and orientated to the interlayer space (Figure 40a). Two unbound water molecules (O14 – O15) and bromide (Br1) are present in the crystal structure. The Ln–OH_2 bond lengths (O9, O10, O11, O12 and O13, respectively) between the La^{3+} and the coordinated waters are 2.543(3) Å, 2.623(2) Å, 2.529(3) Å, 2.516(2) Å, and 2.607(3) Å. The Ln–OTc bond lengths between the lanthanoids and pertechnetate ligands (O1, O3, O5 and O6) range from 2.507(3) – 2.554(3) Å. The Tc–O_{coord} bond lengths of the Tc to the respective O atom (O1, O3, O5 and O6) average 1.733 Å (Tc–OLa). In each case, the $[Tc(1)O_4]$ tetrahedron is bound to two Ln^{3+} centre bridging them along the *c*-axis. The $[Tc(2)O_4]$ tetrahedron is bound to two Ln^{3+} centres bridging them along the *b*-axis, whereby the contacts can be described by the *Niggli* formula $^{1}_{\infty}[Ln(TcO_4)_{2/2}(TcO_4)_{2/2}(TcO_4)(H_2O)_5]$ The main building unit is a chain, running along the *b*-axis. Residing between the chains in the *ab*-plane are the two unbound water molecules and bromide anion (Figure 40b). All La–OTc bond lengths agree with reported La–ORe bond lengths.[75]

2.2.9 The Non-Lanthanoid REE (Sc and Y)

The transition metals of scandium (Sc) and yttrium (Y) are with the lanthanoids, grouped together as rare-earth elements. Both are predominately in their +3 oxidation state and have ionic radii that are similar to the lanthanoids. In this work, yttrium pertechnetate was synthesised and characterised, while scandium pertechnetate, that was synthesised and characterised by Strub and co-workers,[28] will be discussed alongside the other lanthanoids.

$$ScCl_3 + 3\ HTcO_{4(aq)} \rightarrow [Sc(TcO_4)_3(H_2O)_2]$$
$$YCl_3 + 3\ HTcO_{4(aq)} \rightarrow [Y(TcO_4)_3(H_2O)_3](H_2O)$$

Scheme 7: Synthesis of $[Sc(TcO_4)_3(H_2O)_2]$ (**17-ScTc**) and $[Y(TcO_4)_3(H_2O)_3](H_2O)$ (**18-YTc**).[28]

The stoichiometric treatment of scandium chloride with pertechnetic acid in aqueous solution (Scheme 7) and subsequent evaporation of the solution in air using a heat lamp led to the formation of colourless crystals of $[Sc(TcO_4)_3(H_2O)_2]$ (**17-ScTc**) that show hygroscopic characteristics (Figure 41a).[28] The stoichiometric treatment of yttrium chloride with pertechnetic acid in aqueous solution (Scheme 7) and subsequent evaporation of the solution in air using a heat lamp led to the formation of colourless crystals of $[Y(TcO_4)_3(H_2O)_3](H_2O)$ (**18-YTc**) that does not show any hygroscopic characteristics (Figure 41b). The solid-state structures for **17-ScTc** and **18-YTc** are shown in Figure 42 and Figure 43 respectively.

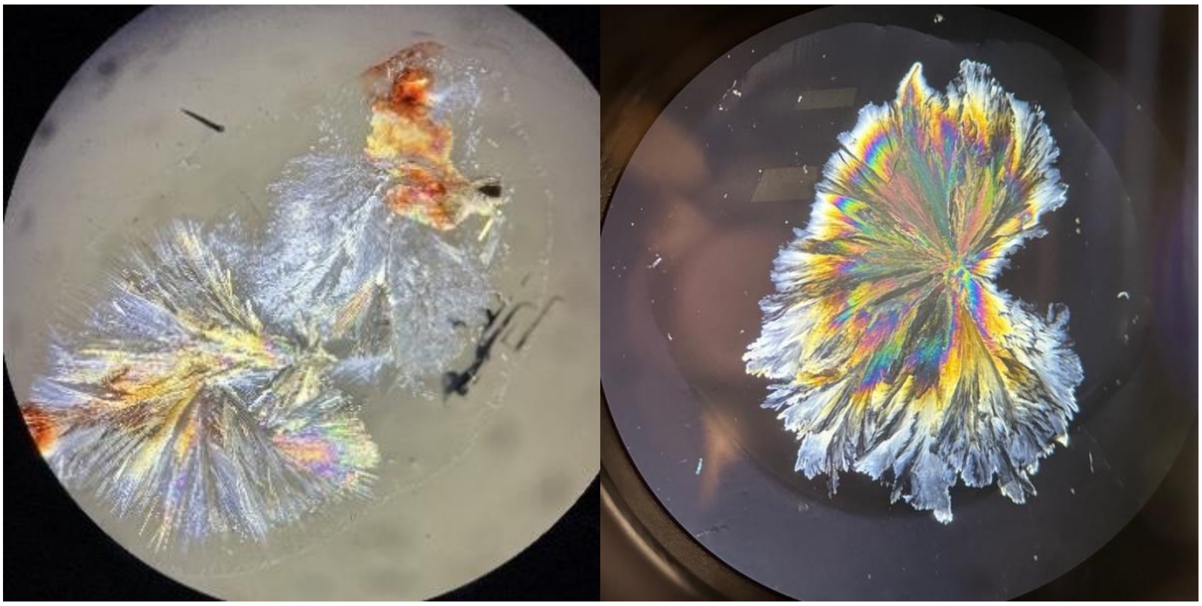

Figure 41: Crystals of $Sc(TcO_4)_3(H_2O)_2]$ (**17-ScTc**) (a) and $[Y(TcO_4)_3(H_2O)_3](H_2O)$ (**18-YTc**) (b).[28]

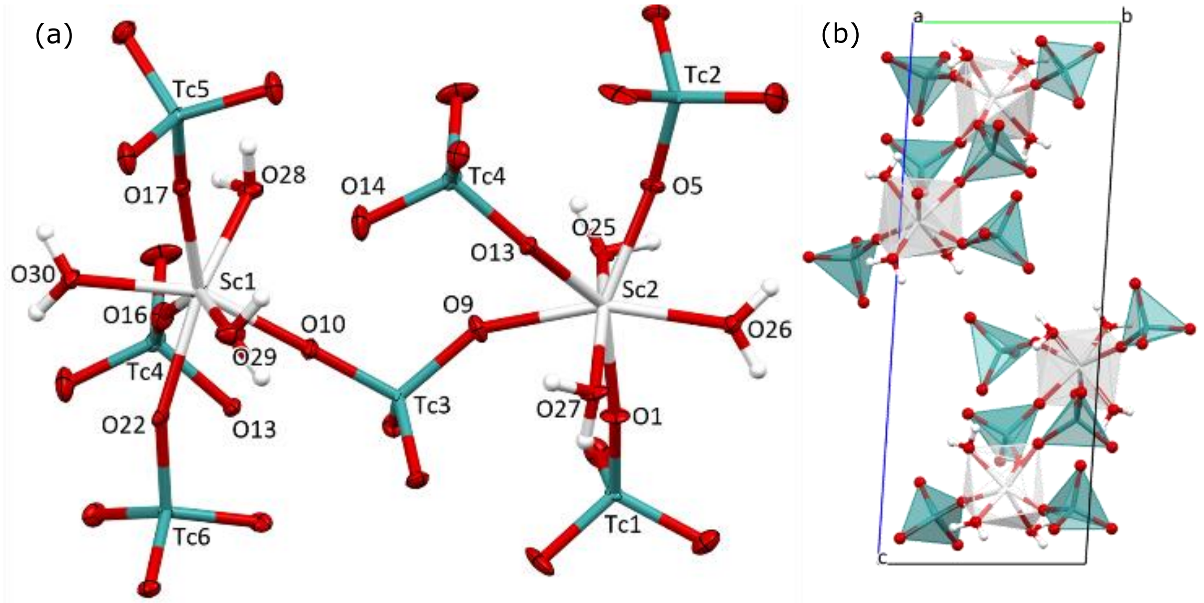

Figure 42: Solid-state structure (a) and unit cell with coordination polyhedra of the metal centres (b) of **17-ScTc**. All ellipsoids are drawn at 50% probability level. Hydrogen atoms are drawn with ball-stick model. Selected bond lengths (Å): Sc1–O1 2.193(7), Sc1–O5 2.123(7), Sc1–O9 2.130(7), Sc1–O13 2.177(8), Sc1–O25 2.153(8), Sc1–O26 2.2.14(7), Sc–O27 2.136 (8), Sc2–O4 2.250 (8), Sc2–O16 2.149 (7), Sc2–O17 2.144 (8), Sc2–O28 2.162 (8), Sc2–O29 2.147 (8), Sc2–O30 2.125 (5), Tc1–O1 1.734 (7), Tc1–O2 1.686 (8), Tc2–O5 1.746 (7), Tc2–O6 1.699 (8), Tc4–O13 1.732(7), Tc4–O14 1.700 (8), Tc5–O17 1.746 (8), Tc5–O18 1.437 (16). Selected bond angles (°) Sc1–O1–Tc1 150.6(4), Sc1–O5–Tc2 167.2(5), Sc1–O9–Tc3 154.0(4), Sc1–O13–Tc4 148.7(5), Sc2–O4–Tc1 168.3(4), Sc2–O16–Tc4 178.9(5), Sc2–O17–Tc5 165.9(5), Sc2–O24–Tc6 146.5(5).[28]

[Sc(TcO_4)$_3$(H_2O)$_2$] (**17-ScTc**) crystallises in the triclinic space group *P*-1, showing about 5% of disorder.[28] In the main unit, the Sc^{3+} cation forms a distorted capped trigonal prism with three oxygen atoms (O25 – O27) of the water molecules and four oxygen atoms (O1, O5, O9, O13) of the pertechnetate units (Figure 42a). The Sc–OH_2 bond lengths average to 2.14 Å. The Sc–OTc bond lengths range between 2.123(7) Å – 2.193(7) Å. **17-ScTc** crystallises with pertechnetato ligands coordinated at the corner of two scandium atoms in a zig-zag fashion (Figure 42b). The main framework can be described by the *Niggli* formula $^{1}_{\infty}$[Sc(TcO_4)$_{2/1}$(TcO_4)$_{2/2}$(H_2O)$_3$].[28]

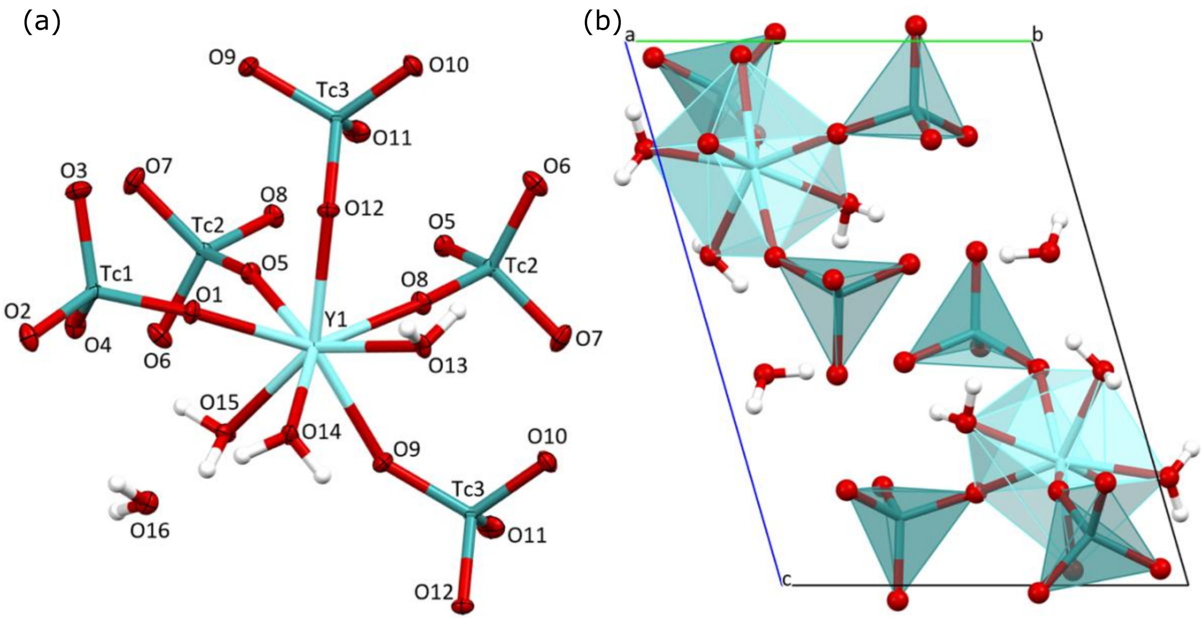

Figure 43: Solid-state structure (a) and unit cell with coordination polyhedra of the metal centres (b) of **18-YTc**. All ellipsoids are drawn at 50% probability level. Hydrogen atoms are drawn with ball-stick model. Selected bond lengths (Å): Y1–O1 2.3465(19), Y1–O5 2.315(2), Y1–O8 2.3183(19), Y1–O9 2.342(2), Y1–O12 2.382(2), Y1–O13 2.323(2), Y1–O14 2.337(2), Y1–O15 2.339(2), Tc1–O1 1.738(2), Tc1–O2 1.711(2), Tc2–O5 1.736(2), Tc2–O6 1.693(2), Tc3–O9 1.727(2), Tc3–O10 1.700(2). Selected bond angles (°) Y1–O1–Tc1 139.89(11), Y1–O5–Tc2 159.21(12), Y1–O9–Tc3 150.25(12).

$[Y(TcO_4)_3(H_2O)_3](H_2O)$ (**18-YTc**) crystallises in the triclinic space group *P*-1. The Y^{3+} centre forms a square antiprism with three oxygen atoms (O13 – O15) of the coordinating water molecules, and five oxygen atoms (O1, O5, O8, O9, O12) of the pertechnetate units (Figure 43a). An unbound water of hydration is present in the crystal structure (O16). The Y–OH_2 bond lengths (O13, O14 and O15, respectively) between the Y atom and the coordinated waters are 2.323(2) Å, 2.337(2) Å and 2.339(2) Å. The Y–OTc bond lengths between the Y atom and the pertechnetate units (O1, O5, O8, O9, O12) range from 2.315(2) Å – 2.3822(19)Å. The Tc–O_{coord} bond lengths (with respect to the oxygen atoms O1, O5, O8, O9, O12 that coordinate to Y) have an average value of 1.736 Å, and are slightly longer than the lengths of Tc to the other uncoordinated O atoms (O2 – O4, O6 – O7, O10 – O11), with an average value of 1.698 Å. The $[Tc(1)O_4]$ tetrahedron is bound to only one Y^{3+} centre. The $[Tc(2)O_4]$ tetrahedron is bound to two Y^{3+} centres bridging them along the *c*-axis. The $[Tc(3)O_4]$ tetrahedron is bound to two Y^{3+} centres bridging them along the *a*-axis, whereby the contacts can be described with the *Niggli* formula ${}^{1}_{\infty}[Y(TcO_4)_{2/2}(TcO_4)_{2/2}(TcO_4)_{1/1}(H_2O)_3]$. The main building unit is a 1D chain running along the *a*-axis. Residing between the chains in the *ac*-plane is the unbound water of hydration (Figure 43b). All Y–OTc bond lengths here agree with reported Y–ORe bond lengths.[83]

2.2.10 Attempted Syntheses with Promethium

The syntheses and characterisations of promethium pertechnetate and promethium perrhenate were attempted using the promethium that was purified (see above, Chapter 2.1.3).

$$PmCl_3 + 3\ HTcO_{4(aq)} \rightarrow [Pm(TcO_4)_3(H_2O)_3]$$
$$PmCl_3 + 3\ \text{“}HReO_4\text{”}_{(aq)} \rightarrow [Pm(ReO_4)_3(H_2O)_3]$$

Scheme 8: Planned synthesis of $[Pm(TcO_4)_3(H_2O)_3]$ and $[Pm(ReO_4)_3(H_2O)_3]$.

The stoichiometric treatment of promethium(III) chloride with pertechnetic acid in aqueous solution or perrhenic acid in aqueous solution (Scheme 8) and subsequent evaporation of the solution in air led to the formation of $(NH_4)_2[TcCl_6]$ on the glass slide that contained $^{147}PmCl_3$ and pertechnetic acid (Figure 44a), and NH_4ReO_4 on the glass slide that contained $^{147}PmCl_3$ and perrhenic acid (Figure 44b). The solid state structure of $(NH_4)_2[TcCl_6]$ shown in Figure 45 is already known.[87]

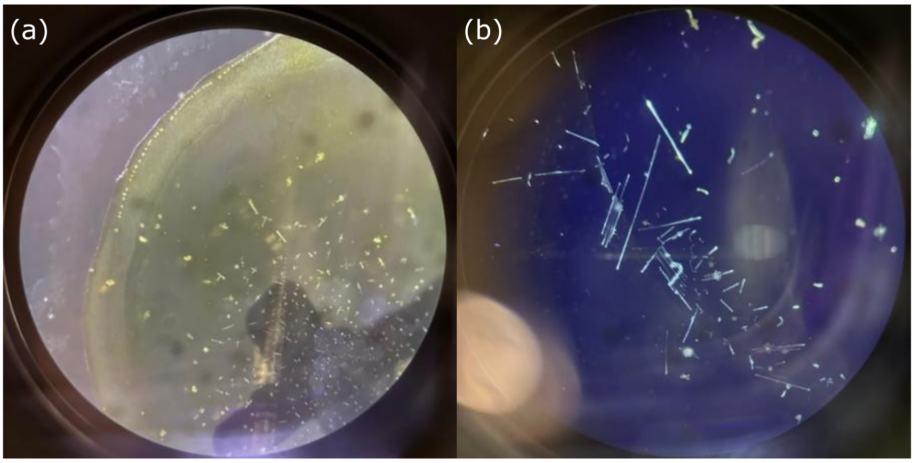

Figure 44: Crystals of (a) $(NH_4)_2[TcCl_6]$ and (b) NH_4ReO_4.

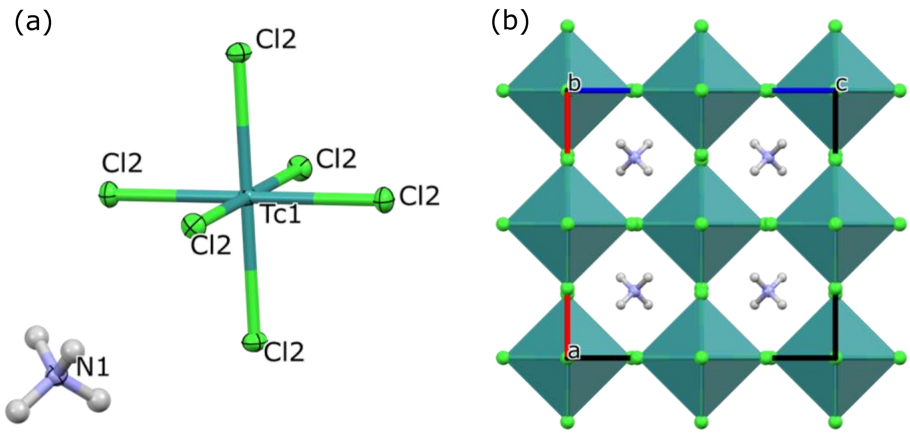

Figure 45: Solid-state structure (a) and unit cell with coordination polyhedra of the metal centres (b) of $(NH_4)_2[TcCl_6]$.

2.3 Trends Across the Lanthanoid Series

2.3.1 Coordination Geometry and Coordination Number

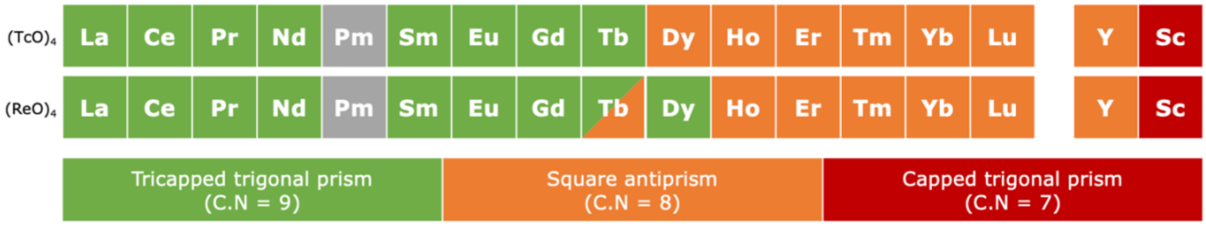

Figure 46:1 Ln coordination motifs in their aqueous pertechnetate and perrhenate complexes.

The Ln^{3+} cations in **1-LaTc**, **2-CeTc**, [$Ce(TcO_4)_3(H_2O)_3$] synthesised and reported by Shohel and co-workers,[77] **$LnTc(H_2O)_3$** and **7b-GdTc** are coordinated as distorted tricapped trigonal prisms (CN = 9), while the Ln^{3+} cations in **$LnTc{\cdot}4(H_2O)$** and **18-YTc** are coordinated as distorted square antiprisms (CN = 8). In addition, Sc^{3+} in **17-ScTc** is coordinated as a distorted capped trigonal prism (CN = 7). The Ln^{3+} cations in **1-LaTc**, [$Ce(TcO_4)_3(H_2O)_3$],[77] **$LnTc(H_2O)_3$** and **7b-GdTc** are coordinated to six TcO_4^- units and three H_2O units, and the Ln^{3+} cations in **$LnTc{\cdot}4(H_2O)$** and Y^{3+} in **18-YTc** are coordinated to five TcO_4^- units and three H_2O units. The Sc^{3+} cation in **17-ScTc** is coordinated to four TcO_4^- units and three H_2O units. **2-CeTc** that was synthesised in this work is an exception in this series, as it is a monohydrate with eight coordinated TcO_4^- and one H_2O. The decrease in coordination number and in number of coordinated pertechnetato ligands corresponds to the lanthanoid contraction, i.e., the decrease in ionic radius upon traversing the lanthanoid series (Figure 46).

2.3.2 Degree of Hydration

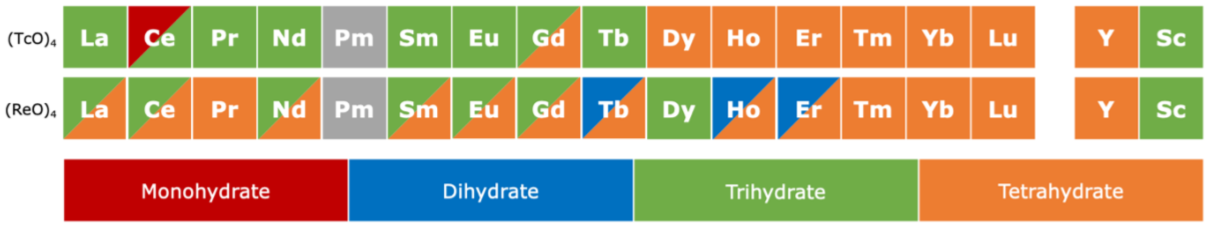

Figure 47: Level of hydration in aqueous Ln pertechnetates and perrhenates.

With respect to their level of hydration, it may be concluded that the earlier lanthanoid elements (La – Eu) favour to crystallise as trihydrates, while the later lanthanoids (Dy – Lu) favour to crystallise as the tetrahydrates. In this work, gadolinium crystallises readily as either the trihydrate or the tetrahydrate. However, the tetrahydrate of terbium has so far not been isolated, which, has only been isolated as a trihydrate (Figure 47).

As $[TcO_4]^-$ and $[ReO_4]^-$ have similar ionic radii, steric influences do not appear to be a factor in the difference of the level of hydration. The same applies to the number of coordinated pertechnetates *versus* perrhenates (Figure 48).

<u>2.3.3 Comparative Study Between Coordinated Pertechnetates and Perrhenates</u>

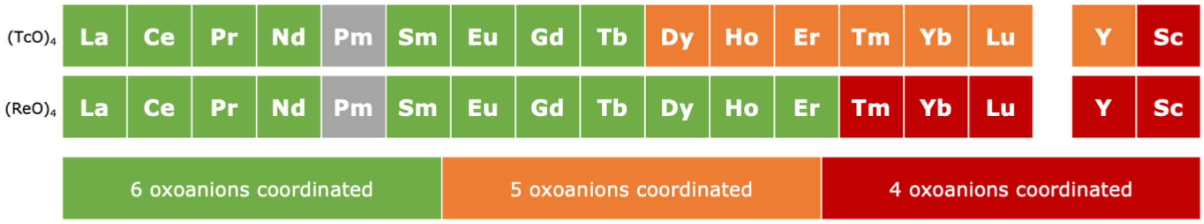

Figure 48:2 Coordination of TcO_4^- *vs*. ReO_4^- in Ln complexes.

In previously reported $Ln(ReO_4)_3$ (Ln = La – Nd, Sm – Lu), the early to middle lanthanoids (La – Nd, Sm – Er) are coordinated to six perrhenate units and three water molecules. Similarly, the early to middle lanthanoids (La – Nd, Sm – Tb) in this study are also coordinated to six pertechnetate units and three water molecules. The late lanthanoids (Tm – Lu) and Y in previous reports are coordinated to four perrhenate units and four water molecules. In comparison, the late lanthanoids (Dy – Lu) and Y in this study are coordinated to five pertechnetate units and three water molecules (Figure 48).

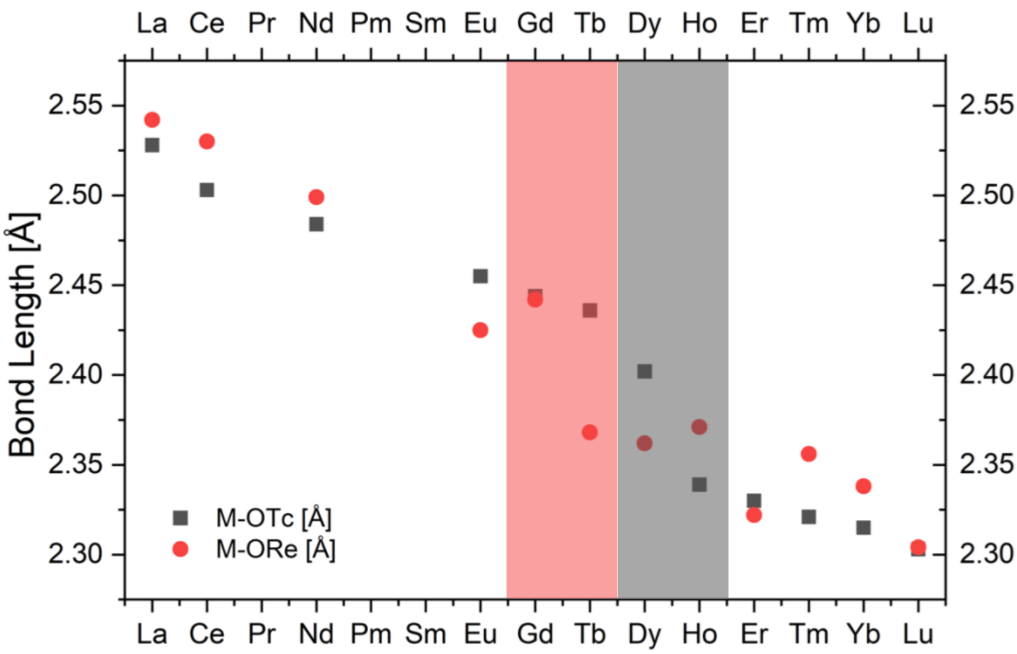

Figure 49: Bond lengths of Ln–OTc (black square, this work) *vs*. Ln–ORe (red circle, literature data) in Ln complexes.

The M(III)–OTc bond lengths of the lanthanoid pertechnetates in this work as well as the M(III)–ORe bond lengths of the lanthanoid perrhenates in literature are shown in Figure 49. The plot shows a clear decreasing trend in the bond lengths across the lanthanoid series, corresponding to the lanthanoid contraction, which further exemplifies the trends shown in Figure 46, Figure 47, and Figure 48.

The plot also reflects the greatest change in the M(III)–OTc and M(III)–ORe bond lengths as a grey transition zone and a red transition zone respectively. This is also reflected in the change in hydration between Tb and Dy for the pertechnetates in this work and between Gd and Tb for the perrhenates in literature shown in Figure 47.

3. Conclusion

In summary, the effective separation of ^{147}Pm from its decay product of ^{147}Sm using LN resin is achieved in this work. Through the careful selection of acid concentrations (0.65 M HCl), the lanthanoids could be separated at a high resolution on a microgram-scale using a miniaturised gravimetric column. The same acid concentration also allowed for the flushing of the column at the end of the separation without changing the pH in the column, thus eliminating the need to pre-equilibrate the column before separation. Also, the use of new LN resin for low blank levels is therefore not necessary. In addition, the repeated use of the column yielded similar elution profiles, allowing for the column's multiple use. Consequently, the elution volume of the lanthanoids can be estimated to a high certainty. For 200 MBq of $^{147}PmCl_3$ sample loaded on to a column, 72% to 80% of $^{147}PmCl_3$ were purified and collected. Further refinements in the separation process might be increasing the column length to give better resolution. One challenge to that will be the longer separation timeline (currently at five minutes for one drop or ~40 µL). As such, a hand-pump or peristaltic pump could be installed such that the elution timeline could be shortened despite a longer column length.

Through the synthesis and structural (and, when possible, spectroscopic) characterisation of lanthanoid pertechnetates in their solid-state, this work has increased the number of known inorganic pertechnetate salts derived from aqueous solutions by 16. Sc and Y demonstrated their ability to serve as lighter homologues for the lanthanoid elements, primarily the heavier lanthanoids. Trends across the lanthanoid series such as the degree of hydration and coordination could be established. An interesting observation is that the earlier lanthanoids tend to form trihydrates, while the later lanthanoids tend to form tetrahydrates. The lanthanoid series also shows distinct contrasts in their degree of hydration, their number of coordinated pertechnetates/perrhenates and their coordination geometry, with observable changes at Tb/Dy for pertechnetates and at Er/Tm for perrhenates. By understanding the lanthanoid pertechnetates, inferences could be drawn about the structures of the actinium and transplutonic-actinoid pertechnetates.

4. Outlook

The established separation method of ^{147}Pm from ^{147}Sm may now be used to prepare pure ^{147}Pm solutions prior to further experiments, in particular the synthesis of $Pm(TcO_4)_3$. In future works, the synthesis of **3-PrTc** and **5-SmTc** should be repeated and their crystallisation perfected so as to measure non-twinned SC-XRD. Similarly, the crystallisation condition will also be the focus for the synthesis of Type VI crystal structure for Ln = La, Pr and Nd. The synthesis of divalent Eu^{2+} and Sm^{2+} and tetravalent Ce^{4+} and Yb^{4+} pertechnetates should be the focus on understanding the lanthanoids beyond their +3 oxidation state. This can be achieved by using the isolated materials as starting materials for redox chemistry, i.e., the controlled reduction of $Eu(TcO_4)_3$ to $Eu(TcO_4)_2$, or the oxidation of $Ce(TcO_4)_3$ to $Ce(TcO_4)_4$. As this work has showed that pertechnetate is able to form a variety of complexes in aqueous solution, further experiments may show how pertechnetate changes upon decreasing pH, whether oxotechnetates will be formed as exemplified by Zegke and co-workers,[88] or whether low-valent (e.g. Sm(II)) starting materials may form pertechnetates or technetates(VI). A deeper study into their degree of hydration might also help us understand the difference in the coordination chemistry between pertechnetates and perrhenates to the late lanthanoids even though pertechnetate and perrhenate have similar ionic radii. Outside of the lanthanoids, the focal point should be on the synthesis of the 5p and 6p pertechnetates due to their similar crystal radii to the lanthanoids. A non-aqueous synthetic route should also be explored in order to synthesise the moisture and oxygen sensitive 5f pertechnetates as well as the hygroscopic early 3d pertechnetates.

5. Experimental

5.1 General Procedure

Caution! Technetium-99 ($t_{1/2}$ = $2.14 \cdot 10^5$ y; *a* = $6.25 \cdot 10^5$ Bq/mg)[89] and Promethium-147 ($t_{1/2}$= 2.62 y; *a* = $3.43 \cdot 10^{16}$ Bq/mg)[90] are radioactive with medium-energy β^--emissions (maximum energy: 293.8 keV and 224.5 keV respectively, average energy: 84.6 keV and 61.78 keV respectively).[90,91] All experiments were carried out in licensed radiochemical laboratories of the University of Cologne and Helmholtz-Zentrum Dresden-Rossendorf, and all handling of radioactive material was choreographed with non-radioactive material (rhenium for technetium, neodymium and samarium for promethium), and operational procedures were approved by radiation safety prior to any experiments involving radioactive material. To avoid contamination, all work was monitored with appropriate detectors. All surfaces were wiped clean before and after use. Standard PPE was worn at all times. All synthetic steps were executed in a licensed radiochemical fume hood. Special precautions were also taken towards the disposal of radioactive materials.

^{99}Tc was provided as an aqueous solution of 1.87 mg NH_4TcO_4 in ca. 20 μL of water. The sample is a stock solution dated 1965 and produced at the Oak Ridge National Laboratory, USA. The Tc concentration has been checked by liquid scintillation counting (LSC) of an aliquot. ^{147}Pm was provided as a 1 mL aqueous solution of 2 GBq $^{147}PmCl_3$. The sample is a stock solution last assayed on 17 November 2022 at the Oak Ridge National Laboratories, USA.

All reactions were performed under ambient temperature and pressure. Chemicals were obtained from Thermo Scientific, Sigma-Aldrich and Johnson Matthey, and they were used as received.

5.2 Equipment and Analytical Methods

5.2.1 Single-Crystal X-ray Diffraction (SC-XRD)

Single crystal data were collected at 100 K with a Bruker D8 Venture diffractometer (Mo-K_α radiation λ = 0.71073 Å) equipped with a Bruker APEX-II CCD detector. A suitable single crystal was selected and immersed in an inert oil. The crystal was then mounted on a MiTiGen MicroLoop. The crystal was cooled to 100 K with liquid nitrogen with the Oxford Cryosystems Cryostream 1000.[92] The full data set was recorded and the images processed using APEX4.[93] Structure solution by direct methods or intrinsic phasing[94] was achieved through the use of SHELXS programs,[95] and the structural model refined by full matrix least squares on F^2 using SHELXL-2014.[96] Semi-empirical absorption correction was executed using SADABS-2016/2.[97] Molecular graphics were plotted using Mercury.[98] Editing of CIFs and construction of tables and bond lengths and angles was achieved using Olex2-1.5 Software Suite.[99] All non-hydrogen atoms were refined anisotropically. Where possible, hydrogen atoms were placed according to residual electron density peaks, otherwise placed using idealised geometric positions and allowed to move in a "riding model" along with the atoms to which they are attached and refined isotropically. CSD numbers can be found at the end of this document in the section "Crystallographic details". These data are provided free of charge by the Crystal Structure Database. The datasets for **3-PrTc** and **5-SmTc** are available free of charge at zenodo.org/records/10488703.

5.2.2 UV-Vis Spectroscopy (UV-Vis)

The UV-vis absorption spectra were obtained in 10mm quartz cells using VWR UV-1600PC UV/Visible spectrophotometer. The solid-state UV-vis absorption spectra for **3-PrTc**, **4-NdTc**, **9-DyTc**, **10-HoTc**, **11-ErTc** and **12-TmTc** were obtained from crystals placed on a quartz slide using the same instrument. All data were recorded at ambient pressure and temperature.

5.2.3 Liquid Scintillation Count (LSC)

LSC measurements were performed using a HIDEX SL-300 TDCR counter. For yield control, typically 5 µL aliquots of supernatant were taken and diluted with 20 mL H_2O to obtain a suitable pH value for LSC: Of these dilutions, again 10 µL aliquots were pipetted into 20 mL LSC PP vial containing 5 mL H_2O and 10 mL scintillation cocktail (Perkin Elmer Ultima Gold). This procedure resulted in samples with typical count rates of several hundred to several thousand cpm (counts per minute). Samples were measured for 5-10 minutes.

5.2.4 Inductively Coupled Plasma Mass Spectroscopy (ICP-MS)

ICP-MS measurements were performed using a Thermo Scientific iCAP-Q Quadrupole ICP-MS. For yield control, aliquots of each fraction were diluted with 900 µL H_2O. Of these dilutions, 100 µL aliquots were pipetted into a vial containing 3900 µL of 0.28 M HNO_3. This procedure resulted in samples with typical count rates of several hundred to several million cps (counts per second). Samples were measured for one minute.

5.2.5 Gamma Spectroscopy

Gamma spectroscopy was performed using a GeLi gamma spectrometer. The samples were placed in the chamber and measured for one minute, with typical count rates of zero to a thousand cps (counts per second). The spectra were analysed using GammaVision.

5.3 Experimental Procedure

5.3.1 Lanthanoid Separation

5.3.1.1 Preparation of Lanthanoid Separation Column

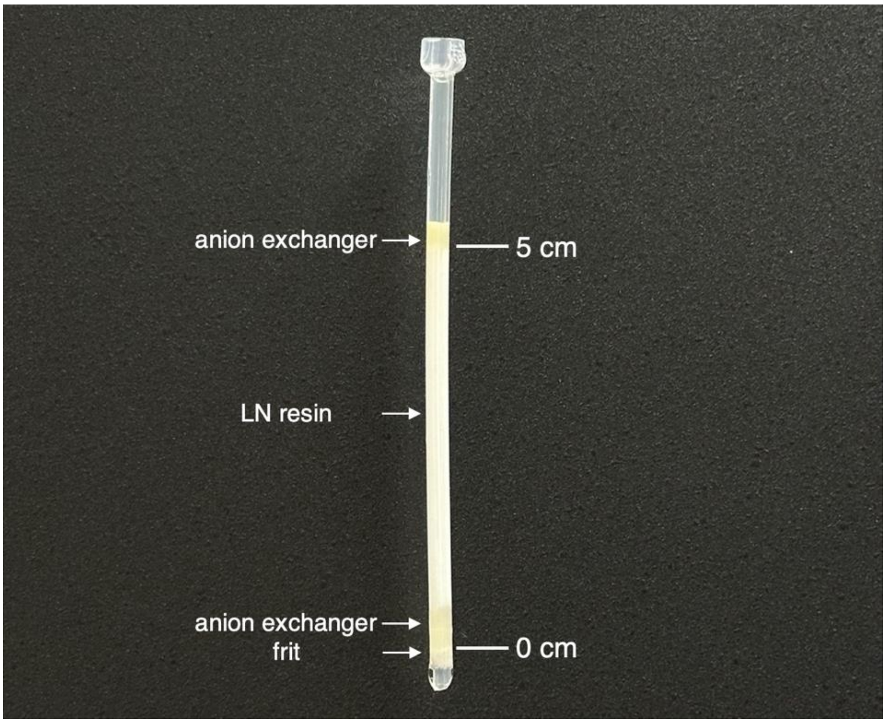

Figure 50: Lanthanoid separation column charged with LN Resin 20-50, topped and bottomed with Dowex 1X8 100-200 (Cl).

Separation of the lanthanoid elements was achieved by the use of LN resin. As the separation is on a microgram scale, a small separation column was set up (Figure 50). The suction bulb of a 0.8 mL plastic Pasteur pipette was cut open. A 2 mm x 2 mm x 2 mm block of sintered glass was inserted *via* the top of the column as the bottom frit. 40 µL of Dowex 1X8 100-200 (Cl), used as the lower bed, was loaded into the column. The column was then packed with 0.107 g of LN resin, with a bead size of 25 – 50 µm, in a slurry of HCl at the same concentration as the intended eluent. 80 µL of Dowex 1X8 100-200 (Cl), used as the upper bed to keep the LN resin in place, was loaded into the column. The column was pre-equilibrated with HCl at the same concentration as the intended eluent before use, and the column was stored in a HCl bath at the same concentration as the intended eluent between use.

The column has an inner diameter of 3 mm and an overall length of 52 mm, of which 2 mm consist of the lower bed, 47 mm consist of the LN resin, and 3 mm consist of the upper bed.

5.3.1.2 Separation of Neodymium and Samarium

To a pre-equilibrated column, 100 µL of 0.353 mM (126.88 ppm) of $NdCl_3$ and 100 µL of 0.353 mM (126.88 ppm) of $SmCl_3$ were loaded on to the resin. The column was eluted with HCl at their intended concentrations. Eluants were collected by individual drops, diluted, and analysed *via* ICP-MS.

5.3.1.3 Elution of Samarium

To a 0.65 M HCl pre-equilibrated column, 100 µL of 0.353 mM (126.88 ppm) of $SmCl_3$ and 100 µL of Milli-Q water were loaded on to the resin. The column was eluted with 0.65 M HCl. Eluants were collected by individual drops, diluted, and analysed *via* ICP-MS.

In a typical elution of Sm, the Sm was found in the eluent fraction between 21 and 23.

5.3.1.4 Promethium Purification Process

The promethium used for this work was assayed on 17 November 2022 at 2 GBq. After approximately 15 months of decay, 72% of the original ^{147}Pm remained with the remaining portion of the material being the daughter, ^{147}Sm. 1 mL of this material were split into ten equal batches, and each fraction was purified separately.

Due to the unforeseeable radiation damage or possible crystallisation of the $^{147}PmCl_3$ solution and therefore, requiring extraction by dissolving the solute with 500 µL of 0.65 M HCl, the concentration of the $^{147}PmCl_3$ was changed. 500 µL of this solution was split into four equal batches, and each fraction was purified separately.

To a 0.65 M HCl pre-equilibrated column, 125 µL of 0.365 mM (131.19 ppm) of $^{147}PmCl_3$ was loaded on to the resin. The column was eluted with 0.65 M HCl. Eluants were collected by individual drops, diluted, and analysed *via* LSC.

5.3.2 Preparation of Pertechnetic Acid

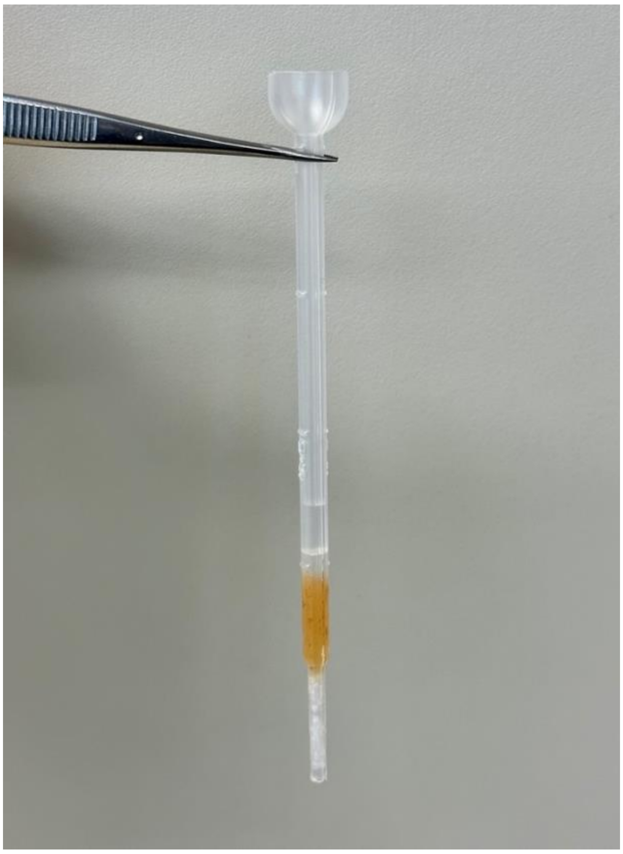

Figure 51: Cation exchange column charged with Amberchrom 50W X8 100-200 (H).

Pertechnetic acid was prepared by conversion from ammonium pertechnetate (NH_4TcO_4) with the aid of a cation exchanger. As the acid required is on a milligram scale, a small cation exchange column was set up (Figure 51). The suction bulb of a 1 mL plastic Pasteur pipette was cut open. A 3 cm strip of Teflon was rolled and inserted into the tip of the pipette. 200 mL of Amberchrom 50W X8 100-200 (H), used as the resin, was loaded into the column, washed twice with water (200 mL each) until the eluate was neutral. A stock solution of NH_4TcO_4 (40 mL, 3.74 mg, 20.6 µmol) dissolved in water (60 mL) was added to the column. Further elution with water (2 × 200 mL) was carried out until elution is complete where the final drop of eluate is no longer acidic. The cation-exchange column was used for up to four successive elutions.

5.3.3 Preparation of Perrhenic Acid

Following the same procedure in setting up a small cation exchange column (see above, Chapter 5.3.2), NH_4ReO_4 (5.70 mg, 21.2 µmol) dissolved in water (100 mL) was added to the column. Further elution with water (2 × 200 mL) is carried out until elution is complete where the final drop of eluate is no longer acidic. The cation-exchange column was used for up to four successive elutions.

5.3.4 Synthesis of Lanthanoid Pertechnetates

5.3.4.1 Synthesis of $[La(TcO_4)_3(H_2O)_3]$ (**1-LaTc**)

500 µL of pertechnetic acid (0.04 M, 3.4 mg, $2.1\cdot10^{-2}$ mmol, 6 eq.) was added to La_2O_3 (1.12 mg, $3.4\cdot10^{-3}$ mmol, 1 eq.) and heated in a water bath (6 h, 100 °C). The reaction mixture was centrifuged, and the product was obtained by evaporation of the solution in air using a heat lamp as colourless crystals covered in red-brown by-products.

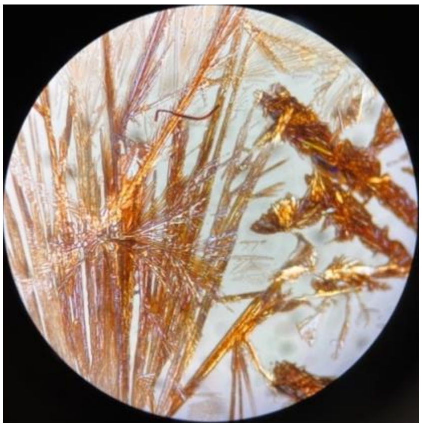

Figure S1: Colourless crystals of **1-LaTc**.

5.3.4.2 Synthesis of [$Ce(TcO_4)_3(H_2O)$] (**2-CeTc**)

500 µL of pertechnetic acid (0.04 M, 3.4 mg, $2.1\cdot10^{-2}$ mmol, 3 eq.) was added to $CeCl_3\cdot7H_2O$ (0.61 mg, $7.2\cdot10^{-3}$ mmol, 1 eq.). The product was obtained by evaporation in air using a heat lamp as yellow crystals.

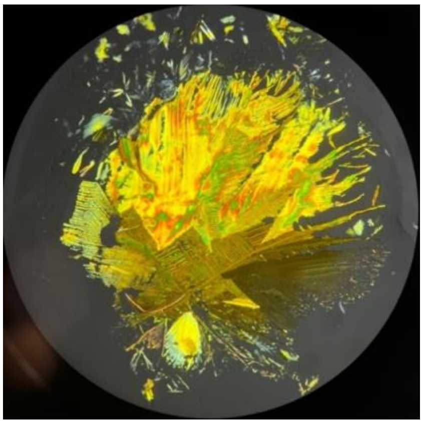

Figure S2: Yellow crystals of **2-CeTc**.

5.3.4.3 Synthesis of [$Pr(TcO_4)_3(H_2O)_3$] (**3-PrTc**)

500 µL of pertechnetic acid (0.04 M, 3.4 mg, $2.1\cdot10^{-2}$ mmol, 6 eq.) was added to Pr_4O_{11} (3.81 mg, $3.7\cdot10^{-3}$ mmol, 1 eq.) and heated in a water bath (6 h, 100 °C). The reaction mixture was centrifuged, and the product was obtained by evaporation of the solution in air using a heat lamp as yellow-green crystals.

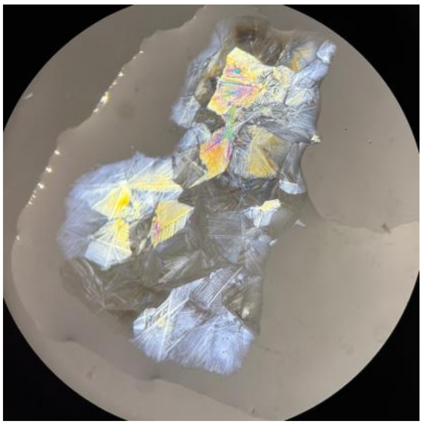

Figure S3: Crystals of **3-PrTc**.

5.3.4.4 Synthesis of $[Nd(TcO_4)_3(H_2O)_3]$ (**4-NdTc**)

500 µL of pertechnetic acid (0.04 M, 3.4 mg, $2.1 \cdot 10^{-2}$ mmol, 6 eq.) was added to Nd_2O_3 (1.19 mg, $3.5 \cdot 10^{-3}$ mmol, 1 eq.) and heated in a water bath (6 h, 100 °C). The reaction mixture was centrifuged, and the product was obtained by evaporation of the solution in air using a heat lamp as lilac crystals.

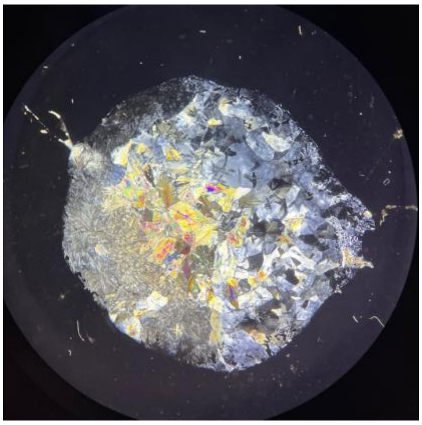

Figure S4: Crystals of **4-NdTc**.

5.3.4.5 Attempted synthesis of $[Pm(TcO_4)_3(H_2O)_3]$

$$PmCl_3 + 3\ HTcO_{4(aq)} \rightarrow [Pm(TcO_4)_3(H_2O)_3]$$

4.5 µL of pertechnetic acid (0.024 M, 18.4 µg, 0.112 µmol, 3 eq.) was added to $^{147}PmCl_3$ (~5.49 µg, $3.73 \cdot 10^{-2}$ µmol, 1 eq.). The resultant solution was added and evaporated 1 µL at a time on to a glass slide. An attempt to obtain single crystalline material by slow evaporation yield colourless crystalline impurities of $(NH_4)_2[TcCl_6]$.

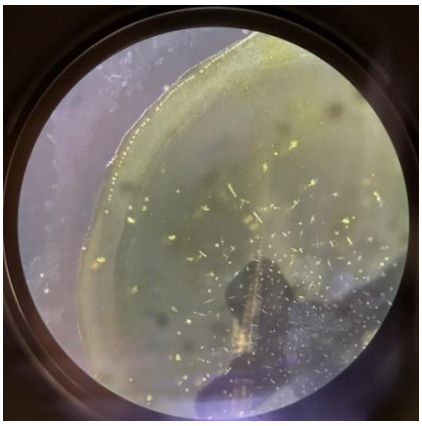

Figure S5: Colourless crystals of $(NH_4)_2[TcCl_6]$

5.3.4.6 Synthesis of [Sm(TcO_4)$_3$(H_2O)$_3$] (**5-SmTc**)

500 µL of pertechnetic acid (0.04 M, 3.4 mg, $2.1 \cdot 10^{-2}$ mmol, 6 eq.) was added to Sm_2O_3 (1.20 mg, $3.4 \cdot 10^{-3}$ mmol, 1 eq.) and heated in a water bath (12 h, 100 °C). The reaction mixture was centrifuged, and the product was obtained by evaporation of the solution in air using a heat lamp as colourless crystals covered in red-brown by-products.

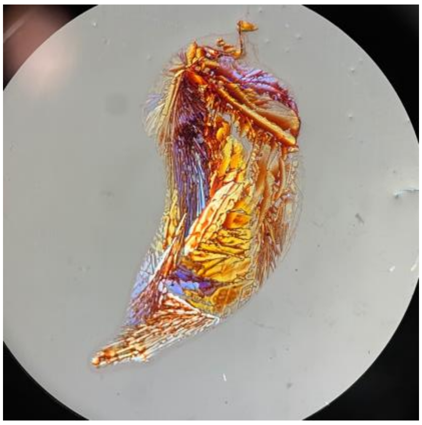

Figure S6: Crystals of **5-SmTc**.

5.3.4.7 Synthesis of [Eu(TcO_4)$_3$(H_2O)$_3$] (**6-EuTc**)

500 µL of pertechnetic acid (0.04 M, 3.4 mg, $2.1 \cdot 10^{-2}$ mmol, 6 eq.) was added to Eu_2O_3 (1.21 mg, $3.4 \cdot 10^{-3}$ mmol, 1 eq.) and heated in a water bath (12 h, 100 °C). The reaction mixture was centrifuged, and the product was obtained by evaporation of the solution in air using a heat lamp as colourless crystals.

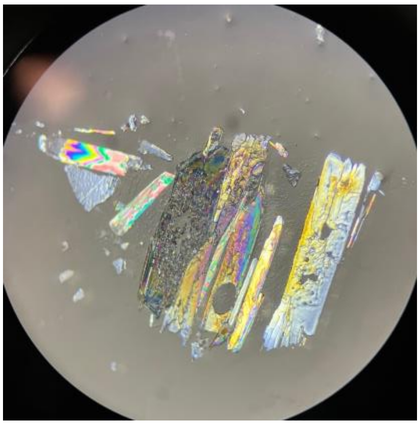

Figure S7: Crystals of **6-EuTc**.

5.3.4.8 Synthesis of [$Gd(TcO_4)_3(H_2O)_3$] (**7a-GdTc**) and [$Gd(TcO_4)_3(H_2O)_3$](H_2O) (**7b-GdTc**)

500 µL of pertechnetic acid (0.04 M, 3.4 mg, $2.1\cdot10^{-2}$ mmol, 3 eq.) was added to $GdCl_3$ (2.20 mg, $8.3\cdot10^{-3}$ mmol, 1 eq.). Two products of different morphologies were obtained by evaporation in air using a heat lamp as colourless crystals.

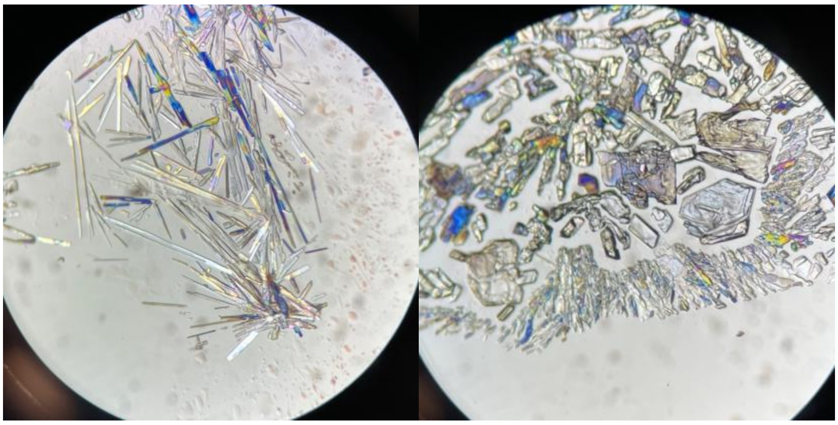

Figure S8: Crystals of **7a-GdTc** and **7b-GdTc**.

5.3.4.9 Synthesis of [$Tb(TcO_4)_3(H_2O)_3$] (**8-TbTc**)

500 µL of pertechnetic acid (0.04 M, 3.4 mg, $2.1\cdot10^{-2}$ mmol, 3 eq.) was added to $TbCl_3$ (1.84 mg, $6.9\cdot10^{-3}$ mmol, 1 eq.). The product was obtained by evaporation in air using a heat lamp as colourless crystals covered in red-brown by-products.

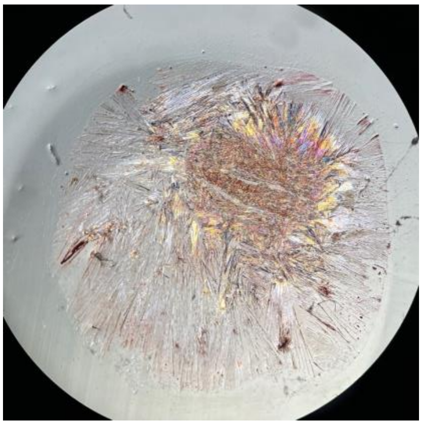

Figure S9: Crystals of **8-TbTc**.

5.3.4.10 Attempted synthesis of $[Tb(TcO_4)_3(H_2O)_3](H_2O)$

$$TbCl_3 + 3\ HTcO_4 \rightarrow [Tb(TcO_4)_4(H_2O)_3](H_2O)$$

500 µL of pertechnetic acid (0.04 M, 3.4 mg, $2.1\cdot10^{-2}$ mmol, 3 eq.) was added to $TbCl_3$ (1.84 mg, $6.9\cdot10^{-3}$ mmol, 1 eq.). The solution was left to evaporate slowly in the fridge but yield crystals of NH_4TcO_4 instead.

5.3.4.11 Synthesis of $[Dy(TcO_4)_3(H_2O)_3](H_2O)$ (**9-DyTc**)

500 µL of pertechnetic acid (0.04 M, 3.4 mg, $2.1\cdot10^{-2}$ mmol, 6 eq.) was added to Dy_2O_3 (1.27 mg, $3.4\cdot10^{-3}$ mmol, 1 eq.) and heated in a water bath (12 h, 100 °C). The reaction mixture was centrifuged, and the product was obtained by evaporation of the solution in air using a heat lamp as colourless crystals.

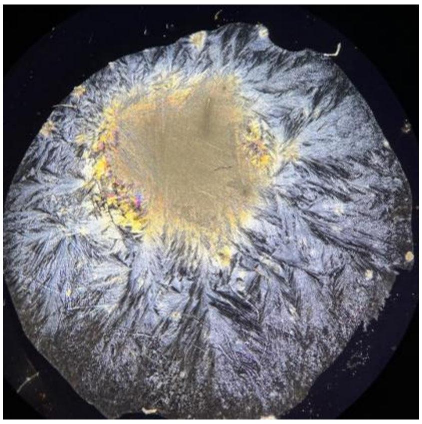

Figure S10: Crystals of **9-DyTc**.

5.3.4.12 Synthesis of $[Ho(TcO_4)_3(H_2O)_3](H_2O)$ (**10-HoTc**)

500 µL of pertechnetic acid (0.04 M, 3.4 mg, $2.1\cdot10^{-2}$ mmol, 6 eq.) was added to Ho_2O_3 (1.39 mg, $3.7\cdot10^{-3}$ mmol, 1 eq.) and heated in a water bath (12 h, 100 °C). The reaction mixture was centrifuged, and the product was obtained by evaporation of the solution in air using a heat lamp as pale pink crystals.

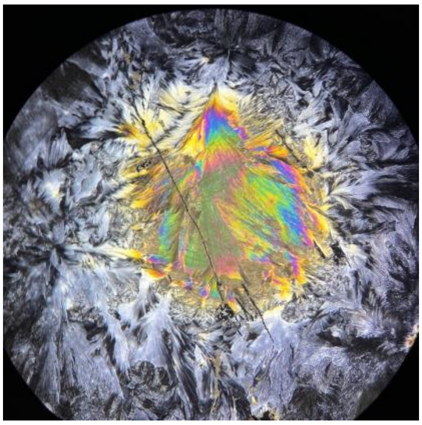

Figure S11: Crystals of **10-HoTc**.

5.3.4.13 Synthesis of $[Er(TcO_4)_3(H_2O)_3](H_2O)$ (**11-ErTc**)

500 µL of pertechnetic acid (0.04 M, 3.4 mg, $2.1\cdot10^{-2}$ mmol, 6 eq.) was added to Er_2O_3 (1.37 mg, $3.5\cdot10^{-3}$ mmol, 1 eq.) and heated in a water bath (12 h, 100 °C). The reaction mixture was centrifuged, and the product was obtained by evaporation of the solution in air using a heat lamp as pale pink crystals covered in red-brown by-products.

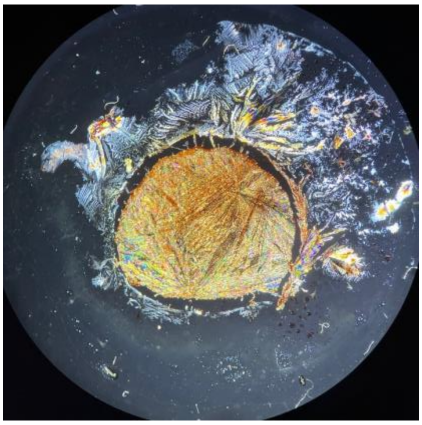

Figure S12: Crystals of **11-ErTc**.

5.3.4.14 Synthesis of $[Tm(TcO_4)_3(H_2O)_3](H_2O)$ (**12-TmTc**)

500 µL of pertechnetic acid (0.04 M, 3.4 mg, $2.1\cdot10^{-2}$ mmol, 6 eq.) was added to Tm_2O_3 (1.33 mg, $3.4\cdot10^{-3}$ mmol, 1 eq.) and heated in a water bath (12 h, 100 °C). The reaction mixture was centrifuged, and the product was obtained by evaporation of the solution in air using a heat lamp as colourless crystals.

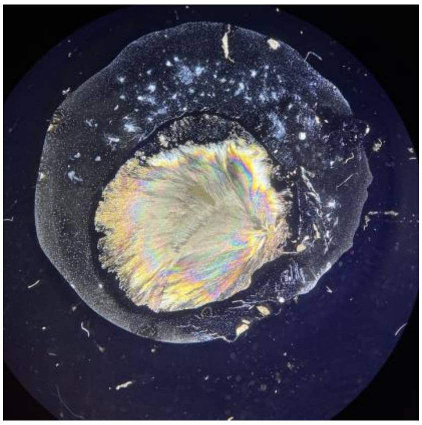

Figure S13: Crystals of **12-TmTc**.

5.3.4.15 Synthesis of $[Yb(TcO_4)_3(H_2O)_3](H_2O)$ (**13-YbTc**)

500 µL of pertechnetic acid (0.04 M, 3.4 mg, $2.1\cdot10^{-2}$ mmol, 6 eq.) was added to Yb_2O_3 (1.42 mg, $3.6\cdot10^{-3}$ mmol, 1 eq.) and heated in a water bath (12 h, 100 °C). The reaction mixture was centrifuged, and the product was obtained by evaporation of the solution in air using a heat lamp as colourless crystals covered in red-brown by-products.

Figure S14: Crystals of **13-YbTc**.

5.3.4.16 Synthesis of $[Lu(TcO_4)_3(H_2O)_3](H_2O)$ (**14-LuTc**)

500 µL of pertechnetic acid (0.04 M, 3.4 mg, $2.1\cdot10^{-2}$ mmol, 6 eq.) was added to $Lu_2(CO_3)_3$ (2.14 mg, $4.0\cdot10^{-3}$ mmol, 1 eq.) and heated in a water bath (3 h, 100 °C) until there was no more effervescence. The reaction mixture was centrifuged, and the product was obtained by evaporation of the solution in air using a heat lamp as colourless crystals.

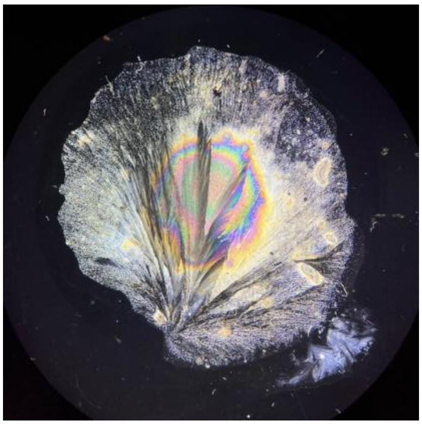

Figure S15: Crystals of **14-LuTc**.

5.3.4.17 Attempted synthesis of $[La(TcO_4)(H_2O)_4Cl]Cl\cdot(H_2O)$

$$LaCl_3 + HTcO_{4(aq)} \rightarrow [La(TcO_4)(H_2O)_4Cl]Cl\cdot(H_2O)$$

500 µL of pertechnetic acid (0.04 M, 3.4 mg, $2.1\cdot10^{-2}$ mmol, 1 eq.) was added to $LaCl_3\cdot7H_2O$ (7.8 mg, $2.1\cdot10^{-2}$ mmol, 1 eq.). The product was obtained by drying in a desiccator as colourless crystals that were too small for SC-XRD.

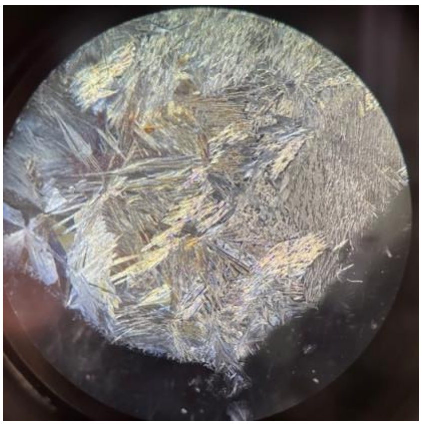

Figure S16: Crystals formed after adding $LaCl_3$ and $HTcO_4$ in equimolar ratio.

5.3.4.18 Synthesis of $[Ce(TcO_4)(H_2O)_4Cl]Cl\cdot(H_2O)$ (**15-CeTcCl**)

500 µL of pertechnetic acid (0.04 M, 3.4 mg, $2.1\cdot10^{-2}$ mmol, 1 eq.) was added to $CeCl_3\cdot7H_2O$ (7.66 mg, $2.1\cdot10^{-2}$ mmol, 1 eq.) and heated in a water bath (3 h, 100 °C). The product was obtained by evaporation in air using a heat lamp as yellow crystals.

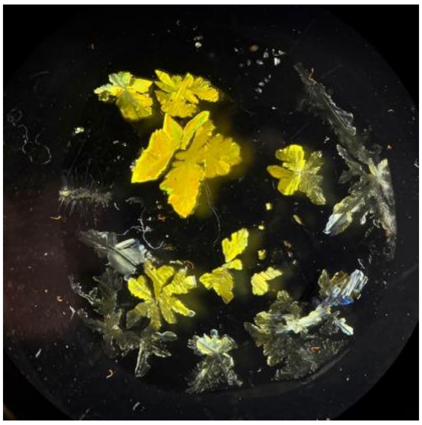

Figure S17: Crystals of **15-CeTcCl**.

5.3.4.19 Attempted synthesis of $[Pr(TcO_4)(H_2O)_4Cl]Cl\cdot(H_2O)$

$$PrCl_3 + HTcO_{4(aq)} \rightarrow [Pr(TcO_4)(H_2O)_4Cl]Cl\cdot(H_2O)$$

500 µL of pertechnetic acid (0.04 M, 3.4 mg, $2.1\cdot10^{-2}$ mmol, 1 eq.) was added to $PrCl_3\cdot6H_2O$ (7.50 mg, $2.1\cdot10^{-2}$ mmol, 1 eq.). The product was obtained by evaporation in a desiccator as yellow-green crystals that were too small and heavily twinned for SC-XRD.

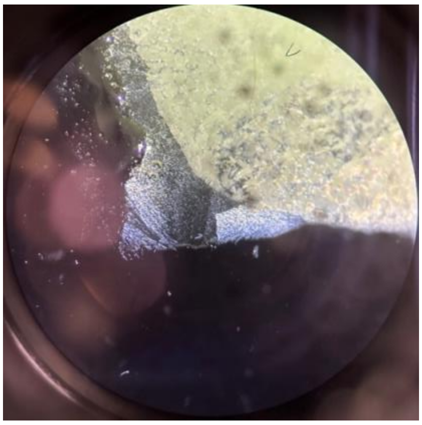

Figure S18: Crystals formed after adding $PrCl_3$ and $HTcO_4$ in equimolar ratio.

5.3.4.20 Attempted synthesis of $[Nd(TcO_4)(H_2O)_4Cl]Cl\cdot(H_2O)$

$$NdCl_3 + HTcO_{4(aq)} \rightarrow [Nd(TcO_4)(H_2O)_4Cl]Cl\cdot(H_2O)$$

500 µL of pertechnetic acid (0.04 M, 3.4 mg, $2.1\cdot10^{-2}$ mmol, 1 eq.) was added to $NdCl_3\cdot6H_2O$ (7.92 mg, $2.1\cdot10^{-2}$ mmol, 1 eq.). The product was obtained by evaporation in a desiccator as lilac crystals that were highly hygroscopic and too small for SC-XRD.

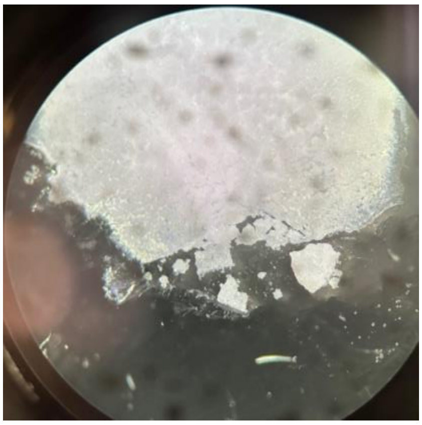

Figure S19: Crystals formed after adding $NdCl_3$ and $HTcO_4$ in equimolar ratio.

5.3.4.21 Synthesis of $[La(TcO_4)_2(H_2O)_5]Br\cdot(H_2O)_2$ (**16-LaTcBr**)

$$La_2O_3 + 6HBr_{(aq)} \rightarrow 2LaBr_3 + 3H_2O$$
$$LaBr_3 + HTcO_{4(aq)} \rightarrow [La(TcO_4)_2(H_2O)_5]Br\cdot(H_2O)_2$$

61.8 µL of HBr (1 M, $6.15\cdot10^{-2}$ mmol, 6 eq) was added to La_2O_3 (3.3 mg, $1.025\cdot10^{-2}$ mmol, 1 eq) and heated in a water bath (6 h, 100 °C). $LaBr_3\cdot xH_2O$ was obtained by evaporation in air as colourless crystals (7.5 mg). 500 µL of pertechnetic acid (0.04 M, 3.4 mg, $2.1\cdot10^{-2}$ mmol, 1 eq.) was added to $LaBr_3\cdot xH_2O$ (7.5 mg, 1 eq.). The product was obtained by evaporation in air as yellow crystals.

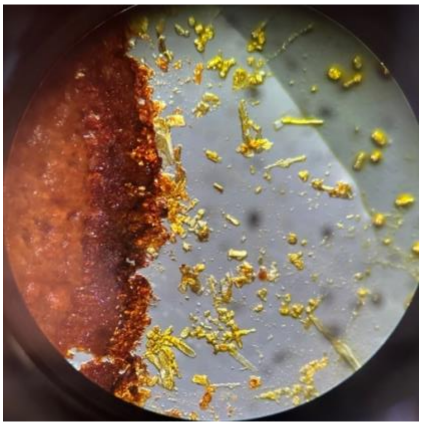

Figure S20: Crystals of **16-LaTcBr**.

5.3.5 Synthesis of Non-Lanthanoid REE Pertechnetates (Sc and Y)

5.3.5.1 Synthesis of $[Y(TcO_4)_3(H_2O)_3](H_2O)$ (**18-YTc**)

500 µL of pertechnetic acid (0.04 m, 3.4 mg, $2.1 \cdot 10^{-2}$ mmol, 3 eq.) were added to solid $YCl_3 \cdot 6\,H_2O$ (2.23 mg, $7.4 \cdot 10^{-3}$ mmol, 1 eq.). The solid immediately dissolved, giving a colourless solution. The product was obtained as colourless crystals after evaporation on air by using a heat lamp.

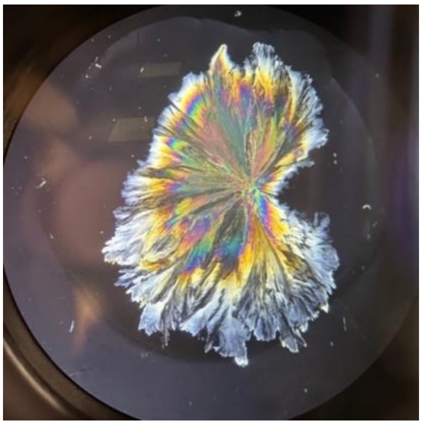

Figure S21: Crystals of **18-YTc**.

5.3.6 Synthesis of Lanthanoid Perrhenate

5.3.6.1 Attempted synthesis of $[Pm(ReO_4)_3(H_2O)_3]$

$$PmCl_3 + 3\ \text{“}HReO_4\text{”}_{(aq)} \rightarrow [Pm(ReO_4)_3(H_2O)_3]$$

2.7 µL of perrhenic acid (0.04 M, 30.8 µg, 0.116 µmol, 3 eq.) was added to $^{147}PmCl_3$ (~5.7 µg, $3.87 \cdot 10^{-2}$ µmol, 1 eq.). The resultant solution was added and evaporated 1 µL at a time on to a glass slide, resulting in colourless NH_4TcO_4 covered in brown-yellow impurities.

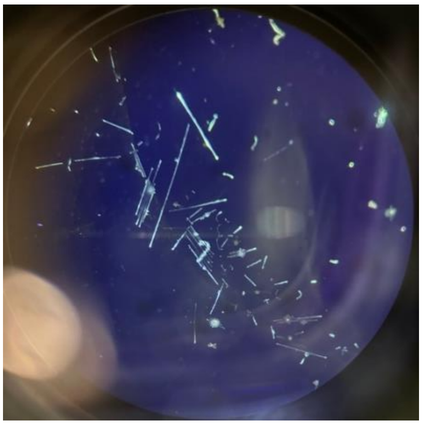

Figure S22: Colourless crystals of NH_4ReO_4.

5.4 Crystallographic Data

Table S1: Crystallographic data.

Short hand formula	**1-LaTc**	**2-CeTc**	**3-PrTc**
CSD number	**2321350**	**2321351**	**zenodo.org/ records/10488703**
Internal data code	**mo_cytc1fullabs**	**data_2**	**mo_CYTc16bfull**
Empirical formula	$H_6LaO_{15}Tc_3$	$CeH_2O_{13}Tc_3$	$H_2O_{13}PrTc_3$
Formula weight	681.69	646.87	644.93
Temperature/K	100.0	100.0	100.0
Crystal system	monoclinic	monoclinic	triclinic
Space group	$P2_1/c$	$P2_1/n$	$P1$
a/Å	7.5202(5)	13.7303(7)	6.2482(4)
b/Å	13.6538(9)	6.2763(3)	7.6685(4)
c/Å	12.7064(7)	13.8280(7)	11.4162(7)
α/°	90	90	90.184(2)
β/°	102.530(2)	112.322(2)	90.001(2)
γ/°	90	90	89.994(2)
Volume/$Å^3$	1273.61(14)	1102.34(10)	547.00(6)
Z	4	4	2
ρ_{calc}g/cm^3	3.555	3.898	3.916
μ/mm^{-1}	6.549	7.796	8.148
F(000)	1248.0	1172.0	588.0
Crystal size/mm^3	0.241 × 0.029 × 0.025	0.168 × 0.077 × 0.052	0.051 × 0.04 × 0.018
Radiation	MoK_α (λ = 0.71073)	MoK_α (λ = 0.71073)	MoKα (λ = 0.71073)
2Θ range for data collection/°	4.436 to 54.968	5.31 to 61.076	5.312 to 66.338
Index ranges	$-9 \leq h \leq 9$, $-17 \leq k \leq 17$, $-16 \leq l \leq 16$	$-19 \leq h \leq 19$, $-8 \leq k \leq 8$, $-19 \leq l \leq 19$	$-9 \leq h \leq 9$, $-11 \leq k \leq 11$, $-17 \leq l \leq 17$
Reflections collected	76091	29735	41157
Independent reflections	2922 [R_{int} = 0.0515, R_{sigma} = 0.0148]	3357 [R_{int} = 0.0550, R_{sigma} = 0.0297]	8347 [R_{int} = 0.0386, R_{sigma} = 0.0326]
Data/restraints/parameters	2922/0/196	3357/0/155	8347/515/381
Goodness-of-fit on F^2	1.167	1.213	1.129
Final R indexes [I>=2σ (I)]	R_1 = 0.0169, wR_2 = 0.0338	R_1 = 0.0292, wR_2 = 0.0595	R_1 = 0.0570, wR_2 = 0.1267
Final R indexes [all data]	R_1 = 0.0192, wR_2 = 0.0353	R_1 = 0.0372, wR_2 = 0.0652	R_1 = 0.0608, wR_2 = 0.1300
Largest diff. peak/hole / e $Å^{-3}$	0.51/-0.58	1.08/-1.32	6.62/-9.54
Flack parameter	---	---	0.49(3)

Table S2: Crystallographic data.

Short hand formula	**4-NdTc**	**5-SmTc**	**6-EuTc**
CSD number	**2321352**	**zenodo.org/ records/10488703**	**2321353**
Internal data code	**mo_yong_cytc19_0m**	**mo_CYTc8full**	**mo_cytc9fullabs077**
Empirical formula	$H_6NdO_{15}Tc_3$	$H_6O_{15}SmTc_3$	$EuH_6O_{15}Tc_3$
Formula weight	684.29	690.40	694.75
Temperature/K	100.0	100.0	100.0
Crystal system	triclinic	triclinic	triclinic
Space group	*P*-1	*P*-1	*P*-1
a/Å	7.1359(5)	7.4059(9)	7.1041(12)
b/Å	8.3216(6)	12.7413(13)	8.2847(14)
c/Å	11.9730(9)	13.5716(16)	11.9201(19)
α/°	90.585(3)	88.182(4)	90.450(7)
β/°	91.231(2)	89.936(5)	91.532(7)
γ/°	111.188(2)	76.794(4)	111.447(7)
Volume/Å^3	662.64(8)	1246.1(2)	652.63(19)
Z	2	4	2
ρ_{calc}g/cm^3	3.430	3.680	3.535
μ/mm^{-1}	6.988	7.977	7.922
F(000)	630.0	1268.0	636.0
Crystal size/mm^3	0.124 × 0.041 × 0.021	? × ? × ?	0.281 × 0.13 × 0.058
Radiation	MoK_α (λ = 0.71073)	MoKα (λ = 0.71073)	MoK_α (λ = 0.71073)
2Θ range for data collection/°	5.252 to 72.692	4.378 to 50.042	5.284 to 54.97
Index ranges	$-11 \leq h \leq 11$, $-13 \leq k \leq 13$, $-19 \leq l \leq 19$	$-8 \leq h \leq 8$, $-11 \leq k \leq 12$, $-15 \leq l \leq 14$	$-9 \leq h \leq 9$, $-10 \leq k \leq 10$, $-15 \leq l \leq 15$
Reflections collected	57878	10757	43829
Independent reflections	6421 [R_{int} = 0.0544, R_{sigma} = 0.0284]	1920 [R_{int} = 0.0496, R_{sigma} = 0.0509]	2997 [R_{int} = 0.0649, R_{sigma} = 0.0300]
Data/restraints/parameters	6421/0/196	1920/356/383	2997/2/179
Goodness-of-fit on F^2	1.064	1.119	1.127
Final R indexes [I>=2σ (I)]	R_1 = 0.0228, wR_2 = 0.0439	R_1 = 0.0446, wR_2 = 0.0919	R_1 = 0.0203, wR_2 = 0.0483
Final R indexes [all data]	R_1 = 0.0270, wR_2 = 0.0451	R_1 = 0.0533, wR_2 = 0.0963	R_1 = 0.0207, wR_2 = 0.0487
Largest diff. peak/hole / e Å^{-3}	1.12/-0.77	1.94/-1.34	0.84/-1.39

Table S3: Crystallographic data.

Short hand formula	**7a-GdTc**	**7b-GdTc**	**8-TbTc**
CSD number	**2321354**	**2321355**	**2321356**
Internal data code	**mo_cytc3needlefullabs**	**mo_cytc3fullabs077**	**mo_cytc10tbfull**
Empirical formula	$GdH_6O_{15}Tc_3$	$Gd_2H_{16}O_{32}Tc_6$	$H_6O_{15}TbTc_3$
Formula weight	700.03	1436.09	701.71
Temperature/K	100.0	100.0	100.0
Crystal system	triclinic	monoclinic	triclinic
Space group	P-1	$P2_1/c$	P-1
a/Å	7.0881(4)	11.5186(8)	7.0687(4)
b/Å	8.2638(6)	7.3521(5)	8.2410(6)
c/Å	11.8977(8)	15.9042(11)	11.8895(8)
α/°	90.510(3)	90	90.428(3)
β/°	91.524(2)	94.493(3)	91.703(3)
γ/°	111.484(2)	90	111.618(2)
Volume/Å^3	648.12(7)	1342.72(16)	643.47(7)
Z	2	2	2
ρ_{calc}g/cm^3	3.587	3.552	3.622
μ/mm^{-1}	8.255	7.979	8.657
F(000)	638.0	1316.0	640.0
Crystal size/mm^3	0.181 × 0.027 × 0.023	0.24 × 0.091 × 0.05	0.225 × 0.027 × 0.023
Radiation	MoK_α (λ = 0.71073)	MoK_α (λ = 0.71073)	MoK_α (λ = 0.71073)
2Θ range for data collection/°	5.298 to 57.41	5.138 to 54.962	5.318 to 61.998
Index ranges	$-9 \leq h \leq 9$, $-11 \leq k \leq 11$, $-16 \leq l \leq 16$	$-14 \leq h \leq 14$, $-9 \leq k \leq 9$, $-20 \leq l \leq 20$	$-10 \leq h \leq 10$, $-11 \leq k \leq 11$, $-17 \leq l \leq 17$
Reflections collected	27998	30487	31707
Independent reflections	3353 [R_{int} = 0.0524, R_{sigma} = 0.0289]	3063 [R_{int} = 0.0451, R_{sigma} = 0.0246]	4098 [R_{int} = 0.0780, R_{sigma} = 0.0426]
Data/restraints/parameters	3353/1/177	3063/7/189	4098/1/177
Goodness-of-fit on F^2	1.116	1.422	1.064
Final R indexes [I>=2σ (I)]	R_1 = 0.0202, wR_2 = 0.0382	R_1 = 0.0296, wR_2 = 0.0776	R_1 = 0.0254, wR_2 = 0.0495
Final R indexes [all data]	R_1 = 0.0238, wR_2 = 0.0404	R_1 = 0.0297, wR_2 = 0.0777	R_1 = 0.0314, wR_2 = 0.0537
Largest diff. peak/hole / e Å^{-3}	0.77/-1.09	1.04/-1.30	1.15/-1.42

Table S4: Crystallographic data.

Short hand formula	**9-DyTc**	**10-HoTc**	**11-ErTc**
CSD number	**2321357**	**2321358**	**2321359**
Internal data code	**mo_cytc11dyfull**	**mo_cytc15hofull**	**mo_cytc12erfull**
Empirical formula	$DyH_8O_{16}Tc_3$	$H_8HoO_{16}Tc_3$	$ErH_8O_{16}Tc_3$
Formula weight	723.29	725.72	728.05
Temperature/K	100.0	100.0	100.0
Crystal system	triclinic	triclinic	triclinic
Space group	*P*-1	*P*-1	*P*-1
a/Å	7.0285(4)	7.0267(5)	7.0066(7)
b/Å	8.6411(5)	8.6413(8)	8.6389(8)
c/Å	11.9459(8)	11.9210(11)	11.9026(12)
α/°	72.790(3)	72.925(4)	72.904(4)
β/°	82.942(2)	83.043(4)	83.103(4)
γ/°	78.627(2)	78.500(4)	78.437(4)
Volume/Å^3	677.81(7)	676.53(10)	673.21(12)
Z	2	2	2
ρ_{calc}g/cm^3	3.544	3.563	3.592
μ/mm^{-1}	8.523	8.864	9.265
F(000)	662.0	664.0	666.0
Crystal size/mm^3	0.107 × 0.081 × 0.051	0.192 × 0.072 × 0.07	0.127 × 0.086 × 0.059
Radiation	MoK_α (λ = 0.71073)	MoK_α (λ = 0.71073)	MoK_α (λ = 0.71073)
2Θ range for data collection/°	5.008 to 67.452	5.006 to 52.74	5.01 to 63.012
Index ranges	$-10 \leq h \leq 10$, $-13 \leq k \leq 13$, $-18 \leq l \leq 18$	$-8 \leq h \leq 8$, $-10 \leq k \leq 10$, $-14 \leq l \leq 14$	$-10 \leq h \leq 10$, $-12 \leq k \leq 12$, $-17 \leq l \leq 17$
Reflections collected	40849	30134	32437
Independent reflections	5405 [R_{int} = 0.0742, R_{sigma} = 0.0432]	2764 [R_{int} = 0.1126, R_{sigma} = 0.0471]	4498 [R_{int} = 0.0573, R_{sigma} = 0.0363]
Data/restraints/parameters	5405/0/187	2764/12/187	4498/0/187
Goodness-of-fit on F^2	1.132	1.145	1.080
Final R indexes [I>=2σ (I)]	R_1 = 0.0352, wR_2 = 0.0696	R_1 = 0.0495, wR_2 = 0.1210	R_1 = 0.0211, wR_2 = 0.0471
Final R indexes [all data]	R_1 = 0.0416, wR_2 = 0.0723	R_1 = 0.0607, wR_2 = 0.1297	R_1 = 0.0222, wR_2 = 0.0477
Largest diff. peak/hole / e Å^{-3}	2.01/-1.88	2.84/-2.09	0.89/-1.21

Table S5: Crystallographic data.

Short hand formula	12-TmTc	13-YbTc	14-LuTc
CSD number	**2321360**	**2321361**	**2321362**
Internal data code	**mo_cytc28_0m**	**mo_cytc13fullabs077**	**mo_cytc6lufull082**
Empirical formula	$H_8O_{16}Tc_3Tm$	$H_8O_{16}Tc_3Yb$	$H_8LuO_{16}Tc_3$
Formula weight	729.72	733.83	735.76
Temperature/K	100.0	100.0	100.0
Crystal system	triclinic	triclinic	triclinic
Space group	*P*-1	*P*-1	*P*-1
a/Å	7.0049(7)	7.0034(4)	6.9809(5)
b/Å	8.6322(10)	8.6175(5)	8.6153(7)
c/Å	11.9011(14)	11.8770(7)	11.8573(10)
α/°	72.882(4)	73.040(2)	73.100(4)
β/°	83.084(4)	83.257(2)	83.284(4)
γ/°	78.357(4)	78.221(2)	78.207(4)
Volume/Å^3	672.17(13)	669.90(7)	666.67(9)
Z	2	2	2
ρ_{calc}g/cm^3	3.592	3.638	3.665
μ/mm^{-1}	9.636	10.027	10.465
F(000)	668.0	670.0	672.0
Crystal size/mm^3	0.194 × 0.149 × 0.081	0.226 × 0.156 × 0.078	0.266 × 0.039 × 0.017
Radiation	MoK_α (λ = 0.71073)	MoK_α (λ = 0.71073)	MoKα (λ = 0.71073)
2Θ range for data collection/°	5.016 to 63.01	5.022 to 54.968	5.024 to 51.34
Index ranges	$-10 \leq h \leq 10$, $-12 \leq k \leq 12$, $-17 \leq l \leq 17$	$-9 \leq h \leq 9$, $-11 \leq k \leq 11$, $-15 \leq l \leq 15$	$-8 \leq h \leq 8$, $-10 \leq k \leq 10$, $-14 \leq l \leq 14$
Reflections collected	37562	24783	19768
Independent reflections	4410 [R_{int} = 0.0421, R_{sigma} = 0.0255]	3048 [R_{int} = 0.0551, R_{sigma} = 0.0346]	2538 [R_{int} = 0.1084, R_{sigma} = 0.0565]
Data/restraints/parameters	4410/0/187	3048/0/188	2538/6/187
Goodness-of-fit on F^2	1.132	1.107	1.118
Final R indexes [I>=2σ (I)]	R_1 = 0.0177, wR_2 = 0.0416	R_1 = 0.0212, wR_2 = 0.0487	R_1 = 0.0381, wR_2 = 0.0761
Final R indexes [all data]	R_1 = 0.0179, wR_2 = 0.0417	R_1 = 0.0213, wR_2 = 0.0488	R_1 = 0.0500, wR_2 = 0.0826
Largest diff. peak/hole / e Å^{-3}	0.87/-1.60	0.91/-1.08	1.61/-1.54

Table S6: Crystallographic data.

Short hand formula	**15-CeTcCl**	**16-LaTcBr**	**17-YTc**
CSD number	**---**	**---**	**2321333**
Internal data code	**mo_Yong_CYTc17_0m**	**mo_CYTc33b_0m**	**mo_cytc43_0m**
Empirical formula	$O_9H_{10}Cl_2TcCe$	$BrH_{14}LaO_{15}Tc_2$	$H_8O_{16}Tc_3Y$
Formula weight	463.10	668.93	646.97
Temperature/K	100.00	100.0	100
Crystal system	monoclinic	triclinic	triclinic
Space group	$P2_1/m$	*P*-1	*P*-1
a/Å	6.8671(11)	7.0198(4)	7.0284(4)
b/Å	6.9150(11)	8.5739(5)	8.6572(5)
c/Å	11.2230(17)	12.6452(8)	11.9284(7)
α/°	90	97.134(3)	72.956(2)
β/°	94.908(7)	93.410(3)	83.030(3)
γ/°	90	103.490(2)	78.427(3)
Volume/Å^3	530.98(14)	731.26(8)	678.30(7)
Z	2	2	2
ρ_{calc}g/cm^3	2.897	3.038	3.168
μ/mm^{-1}	6.055	7.531	7.308
F(000)	434	624.0	608
Crystal size/mm^3	0.193 × 0.138 × 0.083	0.27 × 0.099 × 0.09	0.183 × 0.063 × 0.054
Radiation	MoK_α (λ = 0.71073)	MoK_α (λ = 0.71073)	MoK_α (λ = 0.71073)
2Θ range for data collection/°	5.954 to 69.92	4.936 to 67.456	4.998 to 63.034
Index ranges	$-10 \le h \le 11$, $-11 \le k \le 11$, $-17 \le l \le 18$	$-10 \le h \le 10$, $-13 \le k \le 13$, $-19 \le l \le 19$	$-10 \le h \le 10$, $-12 \le k \le 12$, $-17 \le l \le 17$
Reflections collected	15918	47792	53146
Independent reflections	2468 [R_{int} = 0.0598, R_{sigma} = 0.0422]	5830 [R_{int} = 0.0637, R_{sigma} = 0.0339]	4527 [R_{int} = 0.0707, R_{sigma} = 0.0293]
Data/restraints/parameters	2468/1/77	5830/1/185	4527/0/187
Goodness-of-fit on F^2	1.083	1.131	1.059
Final R indexes [I>=2σ (I)]	R_1 = 0.0293, wR_2 = 0.0561	R_1 = 0.0379, wR_2 = 0.0932	R_1 = 0.0223, wR_2 = 0.0480
Final R indexes [all data]	R_1 = 0.0366, wR_2 = 0.0603	R_1 = 0.0427, wR_2 = 0.0965	R_1 = 0.0273, wR_2 = 0.0517
Largest diff. peak/hole / e Å^{-3}	1.37/-1.27	3.73/-1.13	1.45/-0.80

Table S7: Crystallographic data.

Short hand formula	**---**
CSD number	**---**
Internal data code	RGFCY_(NH4)2[TcCl6]
Empirical formula	$N_4H_{16}Tc_2Cl_{12}$
Formula weight	693.57
Temperature/K	100.00
Crystal system	cubic
Space group	Fm-3m
a/Å	9.8079(2)
b/Å	9.8079(2))
c/Å	9.8079(2)
α/°	90
β/°	90
γ/°	90
Volume/Å^3	943.47(6)
Z	2
ρ_{calc}g/cm^3	2.441
μ/mm^{-1}	3.151
F(000)	668.0
Crystal size/mm^3	0.052 × 0.035 × 0.031
Radiation	MoK_α (λ = 0.71073)
2Θ range for data collection/°	7.196 to 64.85
Index ranges	-14 ≤ h ≤ 14 -14 ≤ k ≤ 14, -14 ≤ l ≤ 12
Reflections collected	4201
Independent reflections	121 [R_{int} = 0.0431, R_{sigma} = 0.0128]
Data/restraints/parameters	121/1/7
Goodness-of-fit on F^2	1.097
Final R indexes [I>=2σ (I)]	R_1 = 0.0176, wR_2 = 0.0355
Final R indexes [all data]	R_1 = 0.0186, wR_2 = 0.0357
Largest diff. peak/hole / e Å^{-3}	0.41/-0.70

6. References

[1] D. I. Mendeleev, *Zh. Russ. Khim. Obshch.* **1869**, *1*, 60–77.

[2] H. G. J. Moseley, *Phil. Mag.* **1913**, *26*, 1024–1034.

[3] J. C. Hackney, *J. Chem. Educ.* **1951**, *28*, 186–190.

[4] E. G. Segrè, *A Mind in Motion: The Autobiography of Emilio Segrè*, University Of California Press, Berkeley, **1993**.

[5] C. Perrier, E. Segrè, *J. Chem. Phys.* **1937**, *5*, 712–716.

[6] C. Perrier, E. Segrè, *Nature* **1947**, *159*, 24.

[7] E. V. Johnstone, M. A. Yates, F. Poineau, A. P. Sattelberger, K. R. Czerwinski, *J. Chem. Edu.* **2017**, *94*, 320–326.

[8] A. H. Meena, Y. Arai, *Environ. Chem. Lett.* **2017**, *15*, 241–263.

[9] K. Schwochau, *Angew. Chem.* **1964**, *76*, 9–19.

[10] F. W. Aston, *J. Chem. Soc., Trans.* **1921**, *119*, 677–687.

[11] J. Mattauch, *Eur. Phys. J. A* **1934**, *91*, 361.

[12] J. Magill, G. Pfenning, J. Galy, *Karlsruher Nuklidkarte - Karlsruhe Chart of the Nuclides - 7th Edition*, OPOCE, Luxembourg (Luxembourg), **2006**.

[13] T. Kobayashi, K. Sueki, M. Ebihara, H. Nakahara, M. Imamura, A. Masuda, *Radiochim. Acta* **1993**, *63*, 29–32.

[14] K. Schwochau, *Angew. Chem., Int. Ed. Engl.* **1994**, *33*, 2258–2267.

[15] K. H. Lieser, *Table of Radioactive Isotopes* **1987**, *91*, 500–501.

[16] E. Deutsch, K. Libson, *Comments on Inorg. Chem.* **1984**, *3*, 83–103.

[17] K. Schwochau, *Technetium: Chemistry and Radiopharmaceutical Applications*, **2000**.

[18] F. Poineau, P. F. Weck, K. German, A. Maruk, G. Kirakosyan, W. Lukens, D. B. Rego, A. P. Sattelberger, K. R. Czerwinski, *Dalton Trans.* **2010**, *39*, 8616–8619.

[19] C. Soderquist, J. Weaver, H. Cho, B. McNamara, S. Sinkov, J. McCloy, *Inorg. Chem.* **2019**, *58*, 14015–14023.

[20] K. E. German, A. M. Fedoseev, M. S. Grigoriev, G. A. Kirakosyan, T. Dumas, C. Den Auwer, P. Moisy, K. V Lawler, P. M. Forster, F. Poineau, *Chem. Eur. J.* **2021**, *27*, 13624–13631.

[21] M. Zegke, D. Grödler, M. Roca Jungfer, A. Haseloer, M. Kreuter, J. M. Neudörfl, T. Sittel, C. M. James, J. Rothe, M. Altmaier, A. Klein, M. Breugst, U. Abram, E. Strub, M. S. Wickleder, *Angew. Chem. Int. Ed.* **2022**, *61*, e202113777.

[22] S. Chatterjee, V. E. Holfeltz, G. B. Hall, I. E. Johnson, E. D. Walter, S. Lee, B. Reinhart, W. W. Lukens, N. P. Machara, T. G. Levitskaia, *Anal. Chem.* **2020**, *92*, 13961–13970.

[23] S. Simner, F. Coutelot, H. Chang, J. Seaman, *MRS Adv.* **2017**, *2*, 717–722.

[24] M.-S. Lee, W. Um, G. Wang, A. A. Kruger, W. W. Lukens, R. Rousseau, V.-A. Glezakou, *Nat. Commun.* **2016**, *7*, 12067.

[25] D. M. Rodríguez, N. Mayordomo, D. Schild, S. Shams Aldin Azzam, V. Brendler, K. Müller, T. Stumpf, *Chemosphere* **2021**, *281*, 130904.

[26] N. Mayordomo, H. Foerstendorf, J. Lützenkirchen, K. Heim, S. Weiss, U. Alonso, T. Missana, K. Schmeide, N. Jordan, *Environ. Sci. Technol.* **2018**, *52*, 581–588.

[27] M. Shohel, J. Bustos, A. Roseborough, M. Nyman, *Chem. Eur. J.* **2024**, *30*, e202303218.
[28] E. Strub, D. Grödler, D. Zaratti, C. Yong, L. Dünnebier, S. Bazhenova, M. Roca Jungfer, M. Breugst, M. Zegke, *Chem. Eur. J.* **2024**, *30*, e202400131.
[29] J. Gadolin, *Kungl. Vetensk. Akad. Handl.* **1794**, *15*, 137–155.
[30] C. G. Mosander, *Phil. Mag. S3* **1843**, *23*, 241–254.
[31] D. I. Mendeleev, *J. Chem. Soc., Trans.* **1889**, *55*, 634.
[32] M. Laing, *Found. Chem.* **2005**, *7*, 203–233.
[33] J. A. Marinsky, L. E. Glendenin, C. D. Coryell, *J. Am. Chem. Soc.* **1947**, *69*, 2781–2785.
[34] P. F. Lang, B. C. Smith, *J. Chem. Educ.* **2010**, *87*, 875–881.
[35] S. G. Wang, W. H. E. Schwarz, *J. Phys. Chem.* **1995**, *99*, 11687–11695.
[36] S. T. Liddle, *Angew. Chem. Int. Ed.* **2015**, *54*, 8604–8641.
[37] K. Binnemans, C. Görller-Walrand, *Chem. Phys. Lett.* **1995**, *235*, 163–174.
[38] J. C. Krupa, *J. Alloys Compd.* **1995**, *225*, 1–10.
[39] G. H. Dieke, *Spectra and Energy Levels of Rare Earth Ions in Crystals*, John Wiley & Sons, New York, **1968**.
[40] S. A. Cotton, *C. R. Chim.* **2005**, *8*, 129–145.
[41] B. P. Hay, *Inorg. Chem.* **1991**, *30*, 2876–2884.
[42] K. De Jesus, R. Rodriguez, D. L. Baek, R. V Fox, S. Pashikanti, K. Sharma, *J. Mol. Liq.* **2021**, *336*, 116006.
[43] S. Cotton, *Lanthanide and Actinide Chemistry*, John Wiley & Sons, Chichester, **2006**.
[44] C. S. Dileep, P. Jagasia, P. S. Dhami, P. V Achuthan, A. Dakshinamoorthy, B. S. Tomar, S. K. Munshi, P. K. Dey, *Desalination* **2008**, *232*, 157–165.
[45] B. J. Mincher, N. C. Schmitt, M. E. Case, *Solvent Extr. Ion Exc.* **2011**, *29*, 247–259.
[46] K. L. Nash, *Solvent Extr. Ion Exc.* **2015**, *33*, 1–55.
[47] A. Bhattacharyya, P. K. Mohapatra, *Radiochim. Acta* **2019**, *107*, 931–949.
[48] A. V Gelis, G. F. Vandegrift, A. Bakel, D. L. Bowers, A. S. Hebden, C. Pereira, M. Regalbuto, **2009**, *Radiochim. Acta 97*, 231–232.
[49] A. Wilden, G. J. Lumetta, F. Sadowski, H. Schmidt, D. Schneider, M. Gerdes, J. D. Law, A. Geist, D. Bosbach, G. Modolo, *Solvent Extr. Ion Exc.* **2017**, *35*, 396–407.
[50] B. Brauner, *Nature* **1926**, *118*, 84–85.
[51] L. Rolla, L. Fernandes, *Z Anorg. Allg. Chem.* **1926**, *157*, 371–381.
[52] J. A. Harris, L. F. Yntema, B. S. Hopkins, *Nature* **1926**, *117*, 792–793.
[53] A. K. Lavrukhina, A. A. Pozdnyakov, *Analytical Chemistry of Technetium, Promethium, Astatine, and Francium*, Humphrey Science Publishers, Ann Arbor, **1970**.
[54] J. A. Marinsky, L. E. Glendenin, C. D. Coryell, *J. Am. Chem. Soc.* **1947**, *69*, 2781–2785.
[55] S. Cantrill, *Nat. Chem.* **2018**, *10*, 1270.
[56] P. P. Passler, B. M. Rode, *Chem. Phys. Lett.* **2015**, *642*, 12–16.
[57] D. Sheng, J. Liu, *Cast Irons Containing Rare Earths*, Tsinghua University Press, Beijing, **2000**.

[58] D. M. Driscoll, F. D. White, S. Pramanik, J. D. Einkauf, B. Ravel, D. Bykov, S. Roy, R. T. Mayes, L. H. Delmau, S. K. Cary, T. Dyke, A. Miller, M. Silveira, S. M. VanCleve, S. M. Davern, S. Jansone-Popova, I. Popovs, A. S. Ivanov, *Nature* **2024**, *629*, 819–823.
[59] G. E. Boyd, *J. Chem. Educ.* **1959**, *36*, 3.
[60] H. Flicker, J. J. Loferski, T. S. Elleman, *IEEE Trans. Electron Devices* **1964**, *11*, 2–8.
[61] R. B. Firestone, V. S. Shirley, C. M. Baglin, S. Y. F. Chu, J. Zipkin, *The 8th Edition of the Table of Isotopes*, Springer, Hungary, **1997**.
[62] K. Broderick, R. Lusk, J. Hinderer, J. Griswold, R. Boll, M. Garland, L. Heilbronn, S. Mirzadeh, *Appl. Radiat. Isot.* **2019**, *144*, 54–63.
[63] S. Ravi, K. M. Mathew, N. K. Seshadri, T. K. Subramanian, *J. Radioanal. Nucl. Chem.* **2001**, *250*, 565–568.
[64] M. T. Pekka, *Nuclear Gauge for Measuring a Characteristic of Moving Sheet Material and Alignment Compensation*, **2000**, US6133578A.
[65] E. G. Funk, J. W. Mihelich, C. F. Schwerdtfeger, *Phys. Rev.* **1960**, *120*, 1781–1789.
[66] S. I. Sukhoruchkin, Z. N. Soroko, *Nuclear Binding Energies and Atomic Mass*, Springer Berlin , Heidelberg, **2009**.
[67] B. Chen, M. He, H. Zhang, Z. Jiang, B. Hu, *Phys. Sci. Rev.* **2017**, *2*, 20160057.
[68] J. Ward, B. Bucher, K. Carney, M. Snow, *J Radioanal Nucl Chem* **2021**, *327*, 307–316.
[69] E. P. Horwitz, C. A. A. Bloomquist, *J.Inorg. Nucl. Chem.* **1975**, *37*, 425–434.
[70] C. Pin, J. S. Zalduegui, *Anal. Chim. Acta* **1997**, *339*, 79–89.
[71] L. M. Arrigo, J. Jiang, Z. S. Finch, J. M. Bowen, C. L. Beck, J. I. Friese, L. R. Greenwood, B. N. Seiner, *J. Radioanal. Nucl. Chem.* **2021**, *327*, 457–463.
[72] R. Trikha, B. K. Sharma, K. N. Sabharwal, K. Prabhu, *J. Sep. Sci.* **2015**, *38*, 3810–3814.
[73] D. Zaratti, Umsetzung von Pertechnetiumsäure Zu Pertechnetatsalzen Der 2. Und 12. Gruppe, Thesis, Universität zu Köln, **2022**.
[74] L. Dünnebier, Die Perrhenate Und Pertechnetate Der Übergangsmetalle, Thesis, Universität zu Köln, **2023**.
[75] C. Mujica, K. Peters, E.-M. Peters, H. G. von Schnering, *Z. Kristallogr. NCS* **1997**, *212*, 297–298.
[76] C. Mujica, D. Jimenez, R. Cardoso-Gil, *Z. Kristallogr. NCS* **2009**, *224*, 387–388.
[77] M. Shohel, A. K. Sockwell, A. E. Hixon, M. Nyman, *Inorg. Chem.* **2024**, *63*, 2044–2052.
[78] G. J. Reiß, *Acta Crystallogr. E* **2001**, *57*, i35–i37.
[79] C. Mujica, J. Llanos, V. Sánchez, W. Schnelle, R. Cardoso-Gil, *J. Alloys Compd.* **2004**, *364*, 89–92.
[80] C. Mujica, J. Llanos, K. Peters, E.-M. Peters, H. G. von Schnering, *Bol. Soc. Chil. Quím.* **2000**, *45*, 329–332.
[81] C. Mujica, J. Llanos, K. Peters, E.-M. Peters, H. G. von Schnering, *Chem. Inform* **1999**, *30*.
[82] S. Grupe, Perrhenate Mit Dreiwertigen Metallen, Universität zu Köln, **2002**.
[83] E. A. Decoteau, M. J. Polinski, *J. Solid State Chem.* **2022**, *306*, 122780.

[84] W. T. Carnall, P. R. Fields, K. Rajnak, *J. Chem. Phys.* **1968**, *49*, 4424–4442.
[85] C. Mujica, J. Llanos, V. Sánchez, P. Gómez-Romero, N. Casañ-Pastor, *J. Solid State Chem.* **2003**, *172*, 200–204.
[86] V. P. Mashonkin, M. B. Varfolomeev, V. V Ilyukhin, *Koord. Khim.* **1977**, *3*, 1248–1253.
[87] R. C. Elder, G. W. Estes, E. Deutsch, *Acta Crystallogr. B* **1979**, *35*, 136–137.
[88] M. Zegke, A. Raauf, J.-M. Neudörfl, E. Strub, *Z. Naturforsch. B* **2023**, *78*, 339–342.
[89] G. Goldstein, J. A. Dean, *J. Inorg. Nucl. Chem.* **1966**, *28*, 285–286.
[90] R. B. Firestone, V. S. Shirley, C. M. Baglin, S. Y. F. Chu, J. Zipkin, *The 8th Edition of the Table of Isotopes*, Springer, Hungary, **1997**.
[91] S. Rozas, J. López, R. Idoeta, M. Herranz, *J. Radioanal. Nucl. Chem.* **2022**, *331*, 3335–3341.
[92] J. Cosier, A. M. Glazer, *J. Appl. Crystallogr.* **1986**, *19*, 105–107.
[93] Bruker AXS Inc, *APEX4 Version 2021.4-0*, Madison, Wisconsin, USA, **2021**.
[94] G. M. Sheldrick, *Acta Crystallog. A* **2015**, *71*, 3–8.
[95] G. M. Sheldrick, *Acta Crystallogr. A* **2008**, *64*, 112–122.
[96] G. M. Sheldrick, *Acta Crystallogr. C* **2015**, *71*, 3–8.
[97] Bruker AXS Inc., *SADABS*, Madison, Wisconsin, USA, **2016**.
[98] C. F. Macrae, I. Sovago, S. J. Cottrell, P. T. A. Galek, P. McCabe, E. Pidcock, M. Platings, G. P. Shields, J. S. Stevens, M. Towler, P. A. Wood, *J. Appl. Crystallogr.* **2020**, *53*, 226–235.
[99] O. V Dolomanov, L. J. Bourhis, R. J. Gildea, J. A. K. Howard, H. Puschmann, *J. Appl. Crystallogr.* **2009**, *42*, 339–341.

7. Appendix

7.1 ICP-MS Results for Nd and Sm

Table S8: ICP-MS data for the separation of Nd and Sm using 0.75 M HCl. The main peaks are highlighted in bold.

Drop Count	Counts for ^{143}Nd / cps	Counts for ^{147}Sm / cps
11	2220.20954	1270.06948
12	34016.3555	245.0033
13	**516825.415**	190.00212
14	148745.724	70.00048
15	54568.9861	50.00044
16	52455.0397	70.0006
17	**337061.378**	55.00034
18	148300.306	1400.08661
19	92780.6242	210666.207
20	89853.332	1727123.88
21	91315.838	**3918293.14**
22	75082.2369	1929607.46
23	78154.9598	443438.255
24	70457.4633	298285.376
25	58106.07	256570.129
26	50595.4987	222942.067
27	49814.3208	208201.549
28	44111.9923	171750.75
29	39066.1877	146269.753
30	39064.0944	134416.825

Table S9: ICP-MS data for the separation of Nd and Sm using 0.70 M HCl. The main peaks are highlighted in bold.

Drop Count	Counts for ^{143}Nd / cps	Counts for ^{147}Sm / cps
15	66773.275	49437.7545
16	50251.1442	37651.7107
17	30968.4028	21678.89
18	4740.91346	3215.42856
19	10979.8528	7622.35113
20	9848.95348	7197.09263
21	555.01518	190.00252
22	3350.46779	70.0004
23	78174.2189	70.00048
24	212889.242	50.00028
25	**255542.753**	102.000768
26	149629.505	212.002672
27	103936.945	384.007792
28	84491.071	1394.0843
29	60056.2974	31291.2528
30	65203.0125	328040.609
31	63707.3192	**510257.447**
32	48128.7086	231136.832
33	35430.3392	106190.844
34	35833.4863	76381.1787
35	34647.1367	64745.625
36	29630.2272	61064.2431
37	22991.2432	42216.4353
38	20961.6622	33179.1352
39	13534.3887	24372.8414
40	13858.7389	24511.1438

Table S10: ICP-MS data for the repeated separation of Nd and Sm using 0.70 M HCl. The main peaks are highlighted in bold.

Drop Count	Counts for ^{143}Nd / cps	Counts for ^{147}Sm / cps
10	2040.17454	1830.14269
11	385.00698	550.01372
12	196956.447	410.00856
13	**1374832.89**	435.00878
14	160454.922	190690.75
15	84233.4492	**2538196.33**
16	77333.9947	1186693.03
17	49959.8444	372633.966
18	35370.1117	248999.108
19	26924.015	184213.685
20	21483.5395	95509.4404
21	17852.8254	68628.1989
22	20266.4824	61862.8844
23	14508.5216	34848.6375
24	8342.83562	20657.1309
25	15970.2966	31394.553
26	11590.407	27961.3771
27	5061.0533	14173.0772
28	6701.83119	18483.75
29	7037.01393	14528.5217
30	6466.69099	11785.5989
31	5796.36831	11019.9012
32	9908.99145	16561.0313
33	5191.09335	7857.49602
34	4725.91516	7227.11709
35	4725.91252	6761.84579
36	5041.03906	6706.82809
37	4265.75924	6306.6202
38	3465.49909	4335.7636
39	3280.46111	3535.51066
40	2805.32706	3060.40038

Table S11: ICP-MS data for the separation of Nd and Sm using 0.65 M HCl. The main peaks are highlighted in bold.

Drop Count	Counts for ^{143}Nd / cps	Counts for ^{147}Sm / cps
15	390.00808	55.00034
16	516808.635	25.00018
17	**1729007.76**	115.00102
18	218576.908	15.0001
19	67190.5116	25.0001
20	73697.3988	1970.15905
21	73566.4413	375.0077
22	56698.613	33605.2487
23	30652.6596	1000821.97
24	15064.1336	**3101756.37**
25	9653.78294	1757879.31
26	7537.29004	561994.737
27	5901.42347	411098.312
28	5371.16958	303039.493
29	4520.83636	166235.327
30	3865.61568	71786.0037

Table S12: ICP-MS data for the elution profile of Sm using 0.65 M HCl. The main peaks are highlighted in bold.

Drop Count	Counts for ^{147}Sm / cps
15	813.363655
16	6686.82192
17	3180.42182
18	2240.21378
19	2610.28103
20	7627.356
21	**131984.618**
22	66099.9211
23	**273498.226**
24	9168.39773
25	6451.69121
26	3215.42032
27	5166.08713
28	34898.8066
29	3705.56547
30	14673.7008

Table S13: ICP-MS data for the elution profile of Sm using 0.65 M HCl. The main peaks are highlighted in bold.

Drop Count	Counts for ^{147}Sm / cps
18	90.0018001
19	338.3418736
20	12501.50247
21	**6402653.893**
22	25257.25912
23	11540.38082
24	3575.523192
25	1900.152106
26	784.7139320

7.2 LSC Results for Purification of ^{147}Pm

Table S14: LSC data, Geiger-Müller counter for the purification of ^{147}Pm using 0.65 M HCl. The main peaks are highlighted in bold.

Drop Count	LSC counts for ^{147}Pm / cpm	Mass of ^{147}Pm from LSC counts / µg	Gamma Spectroscopy counts for ^{147}Pm / cps	Geiger-Müller counts for ^{147}Pm / cps
9	135108.45	0.551142	85.00	802
10	316505.93	1.28979	202.88	1370
11	422641.34	1.7234	269.18	2390
12	**494253.935**	**2.01722**	282.68	2560
13	204430.34	0.83224	140.63	1793
14	46998.36	0.191414	30.00	325

Table S15: LSC data, Geiger-Müller counter for the purification of ^{147}Pm using 0.65 M HCl. The main peaks are highlighted in bold.

Drop Count	LSC counts for ^{147}Pm / cpm	Mass of ^{147}Pm from LSC counts / µg	Gamma Spectroscopy counts for ^{147}Pm / cps	Geiger-Müller counts for ^{147}Pm / cps
7	12612.39	0.02537	9.97	116
8	283775.3	1.15763	225.00	1800
9	**594421.56**	**2.42435**	354.12	2485
10	417412.21	1.70268	342.67	2794
11	303187.62	1.2355	188.43	1894
12	60275.47	0.12254	37.32	290